Institute of Thermoelectricity, Academy of Sciences and Ministry of Education and Science of Ukraine

# Journal of THERMOELECTRICITY

International Research

Founded in December, 1993

published 6 times a year

*No. 1* *2016*

## Editorial Board



## International Editorial Board

Founders – National Academy of Sciences, Ukraine
Institute of Thermoelectricity of National Academy of Sciences and Ministry of Education and Science of Ukraine

Certificate of state registration № КВ 15496-4068 ПР

Editorial office manager O. Pugantseva



Approved for printing by the Academic Council of Institute of Thermoelectricity of the National Academy of Sciences and Ministry of Education and Science, Ukraine

Address of editorial office:
Ukraine, 58002, Chernivtsi, General Post Office, P.O. Box 86.
Phone: +(380-372) 90 31 65.
Fax: +(380-3722) 4 19 17.
E-mail: jt@inst.cv.ua
http://www.jt.inst.cv.ua

Signed for publication 25.03.16. Format 70×108/16. Offset paper №1. Offset printing.
Printer's sheet 11.5. Publisher's signature 9.2. Circulation 400 copies. Order 5.

Printed from the layout original made by "Journal of Thermoelectricity" editorial board in the printing house of "Bukrek" publishers,
10, Radischev Str., Chernivtsi, 58000, Ukraine

**CONTENTS**

*T. Kajikawa*

**T. Kajikawa[1], R. Funahashi[2]**

[1] Shonan Institute of Technology, 1-1-25,
Tsujidonishikaigan, Fujisawa,
Kanagawa 251-8511 Japan;
[2]National Inst. of Advanced Industrial Sci. & Tech

*R. Funahashi*

# RECENT ACTIVITY ON THERMOELECTRIC POWER GENERATION TECHNOLOGY IN JAPAN

*Thermoelectric power generation(TEPG) technology in Japan has been noticed as one of the innovative energy technologies in order to contribute to the establishment of comfortable society and individual life in the real world in the near future due to push-forward by globally environmental issues and serious energy problems (3E + S). Several R&D projects on TEPG technology in Japan have been actively ongoing such as 1) Thermal Management, Materials and Technology Research to utilize unused heat in the social environment, 2) Development of TEPG Application to a Gas Carburizing Furnace, 3) Development of Thermoelectric Generation Using Waste Heat in Steel Works, 4) Development of Tubular Thermoelectric Generator (TTEG), 5) Development of Solar Powered Desalination Using Thermoelectric Power Generation, 6) Practical Development of Rare-Metal-Free Thermoelectric Generator for Automotive Waste Heat Recovery, 7) Practical-use of Multilayer type Thermoelectric Generator for Self-powered Wireless Sensor Network Node supported by government and /or private enterprise funds. As the future prospects several aspects, such as advanced nano-structured TE materials, organic/hybrid TE materials, durability science, safety engineering including hazard analysis have been discussed aiming the smooth promotion of TEPG applications to the real world.*

**Key words:** thermoelectric power generation, nano-structured TE, thermoelectric generation.

## Introduction

Reflecting the Paris agreement for United Nations climate change framework convention No.21 (COP21) and Japan's No.5 Science & Technology basic plan (2016 – 2020), Japan has to be challenge to conquer the serious energy problems on so-called (3*E* + *S*) which stands for Energy security, Environmental preservation, Economic activation and Safety because of poor fossil energy resources, small country and keeping enormously gross domestic product and enhancement of safety consciousness to health and hazards [1]. Overall energy efficiency for total energy system in Japan has been around only 34 %. It means 66 % of supplied energy is rejected into the environment as low graded thermal energy. Therefore, it is strongly recognized to be more important that advanced thermal technologies on the basis of 3 *R* (Reduce, Reuse and Recycle) should be urgently established. In these circumstances TEPG technology has been noticed as one of the innovative energy technologies in order to contribute to the establishment of comfortable society and individual life in the world in the near future. Therefore, the government organizations such as Ministry of Economy, Trade and Industry (METI), Ministry of Education, Culture, Sports, Science and Technology (MEXT) and Ministry of the Environment (MOE), and various industrial fields such as

steel, chemical plant, information, energy etc. are going to pay attention to R&D on various kinds of TEPG applications. Many R&D projects on TEPG technology in Japan have been ongoing, such as:

1. Thermal Management, Materials and Technology Research to utilize unused heat in the social environment;
2. Development of TEPG Application to a Gas Carburizing Furnace;
3. Development of Thermoelectric Generation Using Waste Heat in SteelWorks;
4. Development of Tubular Thermoelectric Generator (TTEG);
5. Development of Solar Powered Desalination Using Thermoelectric Power Generation;
6. Practical Development of Rare-Metal-Free Thermoelectric Generator for Automotive Waste Heat Recovery;
7. Practical-use of Multilayer type Thermoelectric Generator for Self-powered Wireless Sensor Network Node, etc.

In this paper, the recent activity on thermoelectric technology in Japan is overviewed and the future prospects to commercialization of TEPG applications are also discussed.

## Several current topics on R&D activity in JAPAN.

### Thermal Management, Materials and Technology Research (TherMAT)

This is a 10-year fully government-supported R&D project aiming to provide new, highly efficient systems that can achieve significant reductions in energy consumption and finally promoting to realize the energy conservation in many aspects of the social systems [2]. TherMAT has been carried out under the leadership by H. Obara, National Institute of Advanced Industrial Science & Technology (AIST) since FY2013, which has 8 Major Development Field-Divisions such as:

1. Heat Storage Technology;
2. Heat Shielding Technology;
3. Heat Insulation Technology;
4. Thermoelectric Conversion Technology;
5. Waste Heat Recovery Technology;
6. Heat Pump Technology;
7. Heat Management Technology;
8. Basic Energy Technology.

The R&D budget in FY2015 was about 15.4 M $ in all including around 1.7 ~ 2.0 M $ for thermoelectric conversion technology division.

The goal of the thermoelectric conversion technology division is as follows: The final goal in 2023 is:

1. The establishment of TEPG module technology of $ZT = 4$ using inorganic material systems;
2. The establishment of TEPG module technology of $ZT = 2$ for organic materials systems including hybrid ones.

In order to achieve the final goal the intermediate goal is to achieve the advanced TEPG materials systems based on the inorganic materials of $ZT = 2$, and the organic materials of $ZT = 1$ by 2018.

Six domestic private companies, AIST and several universities have joined in TEPG group. The following 8 R&D sub-items on the TEPG project such as:

1. High Efficient thermoelectric materials and devices on the basis of nano- and/or layered-structured technology by AIST;
2. Thermoelectric device and materials based on conducting high polymer by AIST and Osaka Univ;
3. Thermoelectric device using carbon system such as CNT, graphite etc. by AIST, as shown by a sample of carbon nanotube based flexible thermoelectric devices fabricated by printing process in Fig. 1;

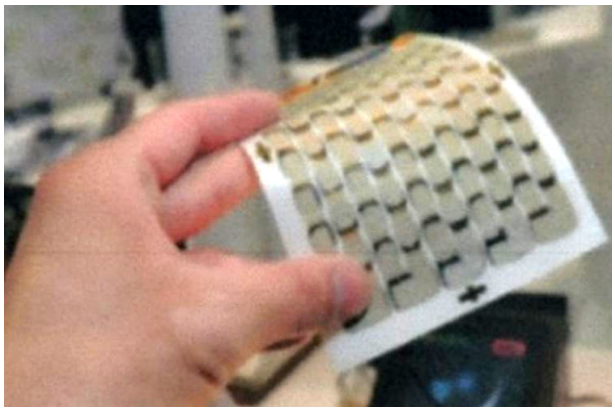

*Fig. 1. Carbon nanotube based flexible thermoelectric device.*

4. Thermoelectric device based on durable skutterudite materials establishing $ZT > 1.1$, i.e. 8 % in conversion efficiency by FURUKAWA, as shown by the experimental results on the durability of the skutterudite thermoelectric modules in Fig. 2;

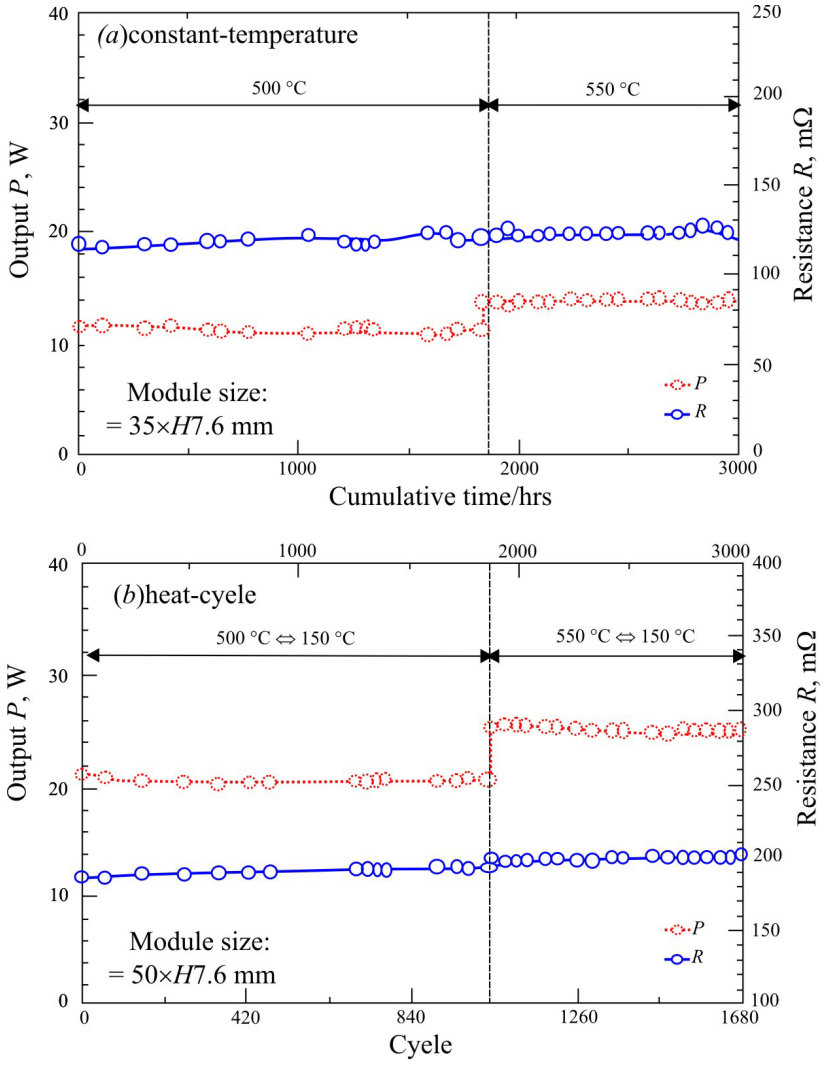


*Fig. 2. Durability test result for skutterudite thermoelectric modules for (a) Constant temperature mode and (b) Heat cycle mode.*

5. Waste heat recovery system of 5 – 10 kW class using thermoelectric power generating technology by HITACHI;
6. Flexible organic thermoelectric materials and devices controlling the orientation and distribution of CNT and developing the advanced hybrid of nano-particle technology by FUJIFILM;
7. High efficiency sintered Clathrate device in connection to electrode bonding technology for practical use by FURUKAWA DENKO;
8. Silicide thermoelectric materials, devices and optimal systems for automobile application by Yamaguchi University and Nippon Thermostat Inc.

**Development of thermoelectric power generation (TEPG) system using waste heat recovery from Steelmaking system**

The steel industry in Japan has achieved the significant reduction of energy consumption to produce high-quality steel and has been pursuing to establish a further more efficient process. It has been recognized that the waste heat recovery technologies in each section for steelworks is very important. Thermoelectric power generation system has been favorably paid attention from the viewpoints of reliability, compactness and environmental friendly way.

The demonstration experiment for 10 kW class TEPG system installed in the JFE's continuous casting line has been carried out aiming the commercialization of large-scale 100 kW class TEPG application base on the established Bismuth-Telluride TEPG module by KELK, as shown in Fig. 3.

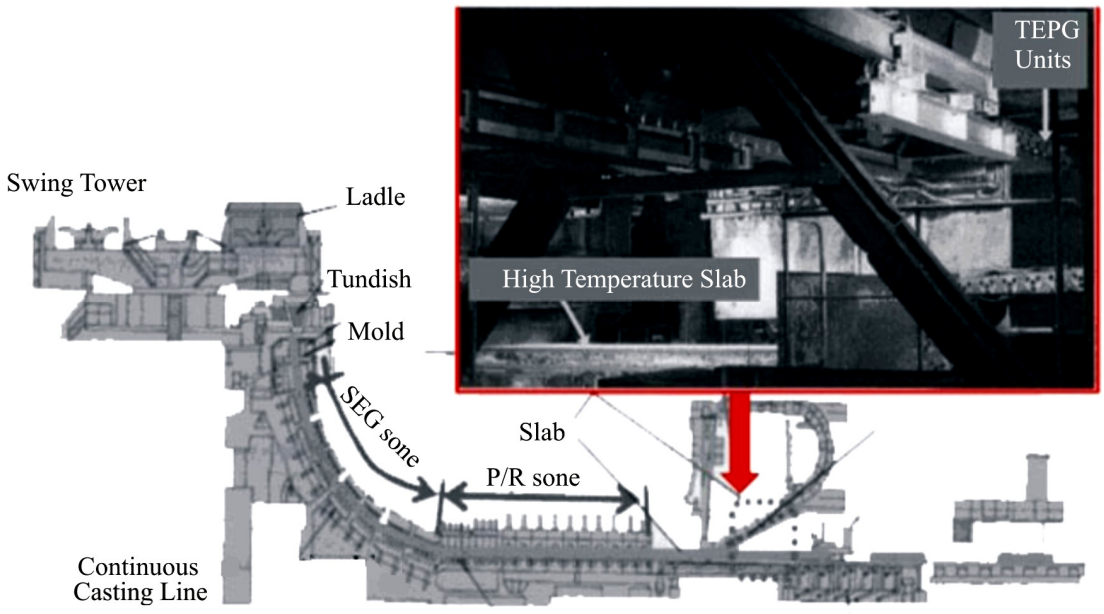


*Fig. 3. JFE's continuous casting line installed with TEPG units.*

This project has been achieved by the team of JFE, KELK and Hokkaido University partially supported by NEDO, and individual fund after finishing NEDO project [3]. The high temperature heat source is radiation heat from the slab flow, of which temperature is around 1073 K ~ 1273 K, while the low temperature is factory water of around room temperature. The overall TEPG system is 2 m wide and 4 m long in size consisting of 56 TEPG units, as shown in Fig. 4 in order to generate about 10 kW in D.C. electricity, and also has installed an emergency countermeasure apparatus.

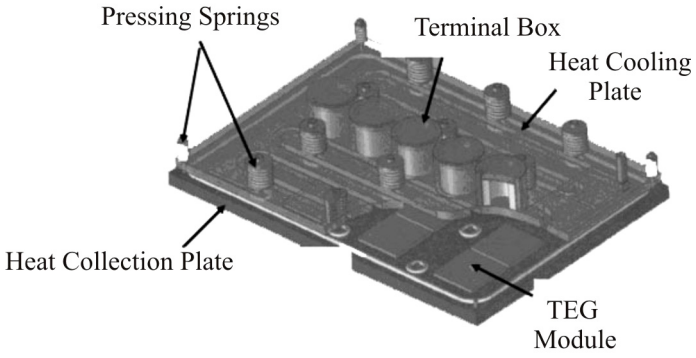


*Fig. 4. Components of TEG unit (Size:400 mm × 280 mm) constituted of 16 commercial high-efficiency TEG modules of 50 mm × 50 mm × 4.2 mm by KELK.*

The output power from this thermoelectric power generation system is about 9 kW (i.e., 1.7 kW/m$^2$ for module-base) at 1188 K in slab temperature for 1.7 m in slab width. The experimental results have been satisfactorily consistent with the estimated values from the system simulation analysis as shown in Fig. 5.

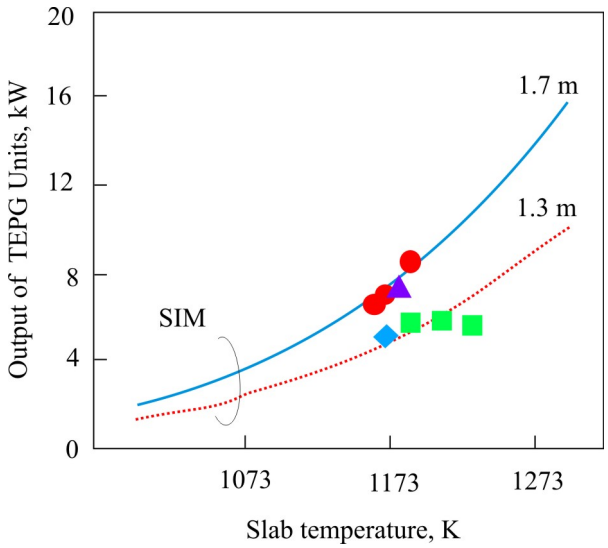


*Fig. 5. Experimental results of power output versus slab temperature for JFE's TEPG system in comparison with their simulations:*
*1. ● – slab width = 1.7 m, Experiment; 2. ▲ – slab width = 1.6 m, Experiment;*
*3. ◆ – slab width = 1.4 m, Experiment; 4. ■ – slab width = 1.3 m, Experiment;*
*5. ▬ – slab width = 1.7 m, Simulation; 6. ▪▪▪▪ – slab width = 1.3 m, Simulation.*

The power output will surely obtain greater values than the present ones in the future by development of the durable TEPG modules against temperature higher than the upper temperature limit for the *Bi – Te* modules. Because at the present stage the surface temperature for *Bi – Te* based TEPG modules is constrained to be lowered to avoid thermal degradation.

**R &D of solar powered desalination system using thermoelectric power generation**

The shortage of the supply of fresh water is one of the biggest social issues all over the world in the near future. It is urgently established the economical desalination system technology combined with renewable energy sources such as solar power without large amount of consumption of fossil fuel resources.

From the viewpoints of easy and continuous operation, maintenance-free, high quality of fresh water, the concept of a solar powered Multi-Effect Desalination and Reverse Osmosis (MED-RO) hybrid desalination system using thermoelectric power generation system has been proposed by TDS-conference constituted of several private companies and universities under the leadership of Prof. Y.Horita, Tokyo Institute of Technology (TITech) with international cooperation since 2010 [4]. The proposed system is composed of a concentrated solar thermal power plant with high temperature (around 850 K) thermal energy storage, novel TESG (Thermoelectric and Steam Generator), and two kinds of desalination systems (MED (Multi-Effect Desalination and RO (Reverse Osmosis)) as main sub-systems, as shown in Fig. 6. For the TESG the hot side of TEPG devices is heated by the high temperature molten salt from the thermal storage unit powered by a concentrating solar power unit and the cold side of TEPG devices is cooled by the large latent heat of continuously supplied water to produce low temperature steam which is used by the first stage of MED unit. All of the discharged thermal energy used to cool TEPG devices in the TESG system is effectively and steadily utilized in the system, while for TEPG systems as usual the water that cooled the cold side of TEPG devices is rejected from the system to the environment. It is clarified with the feasibility study for cost evaluation that this proposed desalination system has the good potentiality to be the most cost-competitive solution at least in the Middle and Near East area.

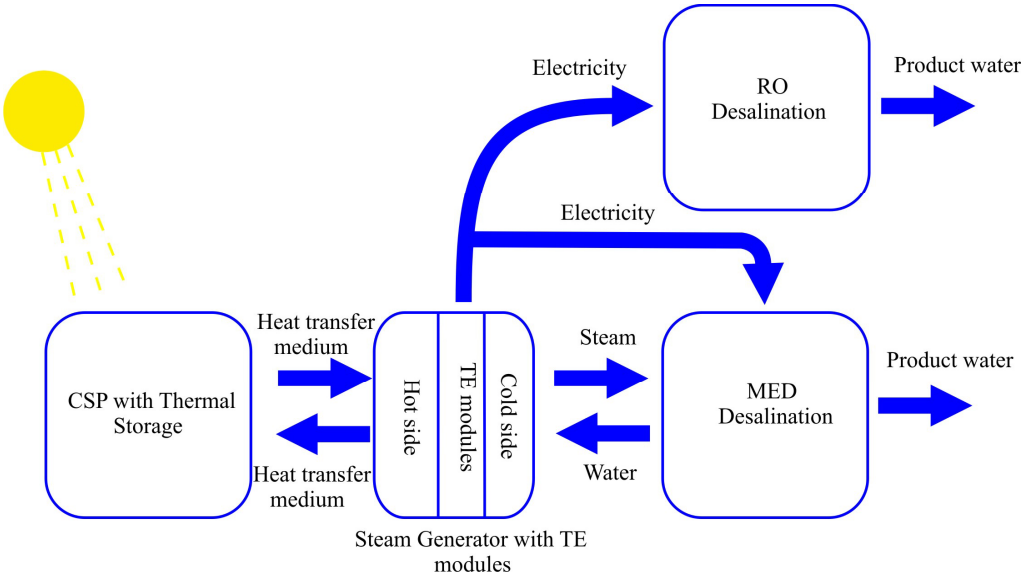


*Fig. 6. Concept of the solar powered desalination system using thermoelectric power generation.*

*Fig. 7. Proof-of-concept experimental facility.*

A small scale proof-of-concept experiment for TESG system as the most important key component has been carried out in order to confirm the system characteristics, such as static heat balance, dynamic mass balance response, which are needed for accurate design of the proto-type solar desalination system combined with TEPG system. The experimental facility is shown in Fig. 7.

**Practical-use of Multilayer type Thermoelectric Generator for Self-powered Wireless Sensor Network Node**

Murata Manufacturing Co., Ltd has developed TEPG device aiming to establish energy harvesting TEPG device for self-powered wireless sensor network node for practical use by its own fund applying the existing MLCC (Multi-layered Ceramic Capacitor) facilities to the TEPG device production [5]. Thermoelectric device consists of composite of $Ni_{0.9}Mo_{0.1}$ and $Ni_{1-x}Mo_x$ for *p*-type, and $(La_ySr_{1-y})TiO_3$ for *n*-type. For a couple of TE device *p*-type and *n*-type are directly bonded to each other without electrode metal. An insulator of the thin layer composed $(Yb, Zr)\ O_2$ is inserted between them. These materials were selected because of having the same performance of thermal expansion coefficient to reduce thermal stress among them. A sample of the TEPG device is shown in Fig. 8. The commercial proto-type TEPG-integrated wireless sensor node device has been installed, as shown in Fig. 9, and was attached at the steel pipe line in the factory as shown in Fig. 10.

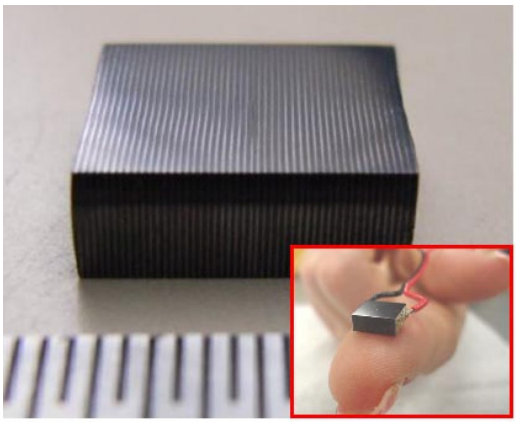

*Fig. 8. Sample of multilayered type TEPG module for energy harvesting TEPG device.*

*Fig. 9. Commercial proto-type TEPG-integrated wireless sensor node device.*


*Fig. 10. Installation of TEPG-integrated wireless sensor node device to a pipe.*

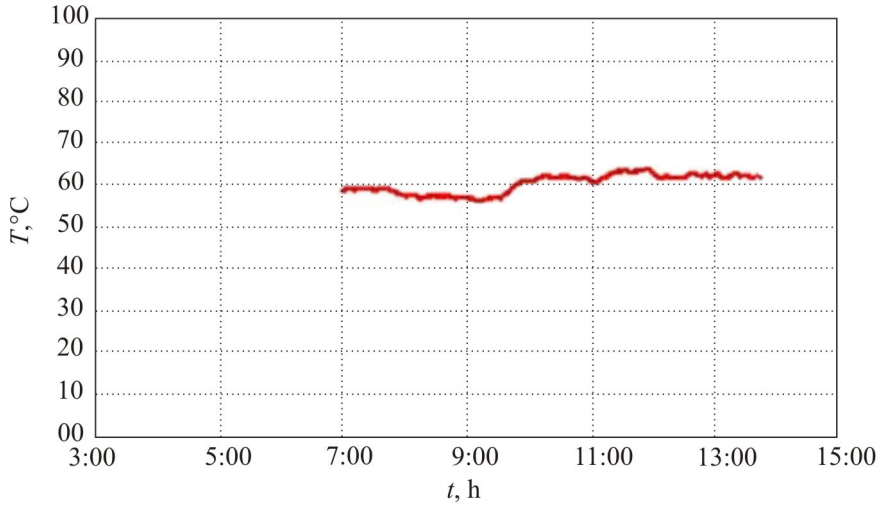


*Fig. 11. Demonstration result of the monitor of pipe temperature.*

The power characteristics for the thermoelectric device of 50 couples and 6.0 mm × 6.9 mm × 2.7 mm in size are as follows: the open circuit voltage and maximum power output are 52.3 mV and 105 μW at 10 K in temperature difference respectively. The demonstration run has been successfully carried out for over 12 months to monitor the temperature every 20 seconds, as shown in Fig. 11.

## Future prospects

We have been proceeding a lot of R&D works to mature TEPG technology for practical use as the following in parallel with the above-mentioned developments for academia and industry sector supported by METI, NEDO, MEXT, JST and/or private enterprise funds:

- Sophisticated nano-structured TE technology for enhancement of high *ZT* by bottom-up approach ($ZT > 4$);
- Development of advanced Organic/Hybrid TE materials;
- Progress of durability science, and safety engineering in terms of TEPG field;
- Establishment of international standardization for TEPG measurement.

The sophisticated nano-structured TE device approach is based on the fact that nano-structure for the *Mg* – doped *PbTe* could be found not to degrade the electrical properties such as the Seebeck coefficient and electrical conductivity, but to reduce of the lattice thermal conductivity independently by AIST [6]. Therefore, for the optimum nano-structured TE device of *Mg* – doped *PbTe* – 4 % *Na* the maximum value of *ZT* could be enhanced to be 1.8 at 810 K as compared with the maximum value of *ZT* of 1.1 at 710 K for non-doped one, as shown in Fig. 12.

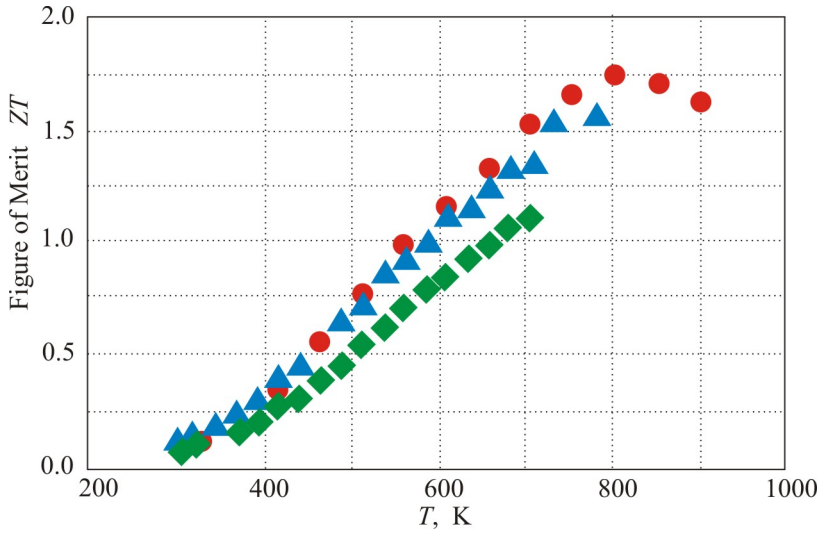


*Fig. 12. Effect of the enhancement of ZT due to the nano-structured processfor PbTe – 4 %Na system:*
*1. ● – Mg – doped PbTe – 4 % Na sintered;*
*2. ▲ – Mg – doped PbTe – 4 % Na melted;*
*3. ◆ – PbTe – 4 % Na melted.*

A sample of TE module made of eight couples of nano-structured *p*-type *Mg* – doped *PbTe* – 4 % *Na* sintered leg and *n*-type *PbTe* – 0.2 % $PbI_2$ sintered leg has been successfully fabricated to generate 3.55 W at 570 K in temperature difference (high temperature: 873 K, and low temperature: 303 K at the electrode respectively). It is recognized to be important that controlled nano-structure processing approaches should be established in the shape, size, density, components, and so on for all of thermoelectric material systems.

Polymer thermoelectrics have received a remarkable attention due to several advantages, such as low cost, easiness of assembly, light weight, and feasibility of efficient bottom-up approach to expand the TE application fields recently. Ternary organic-inorganic hybrid systems consisting of a conducting polymer (*Ni* – ethylenetetrathiolate: *Ni* – PETT), PVC (polyvinyl chloride) and CNT (Carbon nano-tube) have been researched to obtain notable experimental results of *ZT*: 0.28 at 340 K in comparison with the performance for PEDOT-PSS (poly 3, 4 – ethylenedioxythiophene-poly styrenesulfonate) film and PEDDOT-TSS/CNT film, as shown in Fig. 13 by Toshima's group [7, 8]. It can be said that recent experimental results and research on various kinds of organic thermoelectric materials including hybrid systems will be promising in the future.

Environmentally friendly thermoelectric materials are considered to be very important for the contribution of thermoelectric applications to the real world. There are many R&D works on *Te* – free TE materials such as Silicide, Oxide, Sulfide systems including Colusites [9], Heusler systems including Half-Heusler, Skutterudite, Clathrate, etc in Japan.

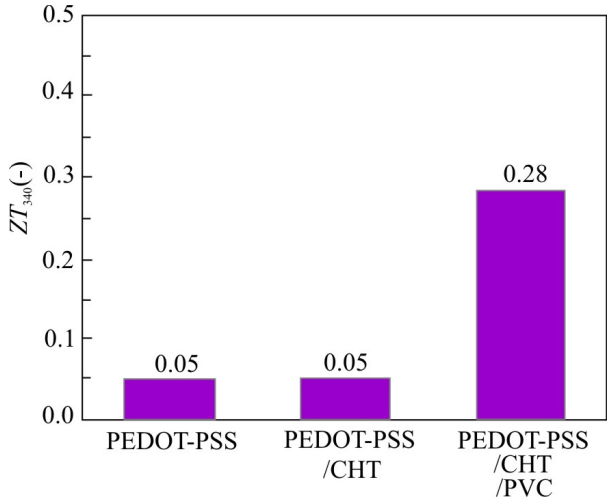


*Fig. 13. Effect of the performance enhancement of ZT for a ternary organic-inorganic hybrid system in comparison with PEDOT-PSS and PEDOT-PSS/CNT systems.*

In order to penetrate the thermoelectric power generation technology to the real world smoothly, it is inevitable to get the social acceptance in advance. It means that we have to show the evidence of risk management for TEPG systems in parallel with the development of durability science [10] and safety engineering in terms of TEPG field [11]. It is necessary to achieve the hazard analysis and include the countermeasure design in TEPG system even at the demonstration phase. For the hazard analysis the three kinds of hazard are classified due to functional stress for sub-systems and components, time dependence in operation and interface among components for three major sub-systems; main power generation system, power transmission-transformation, and heat sources & rejection systems. Practically, a 10 kW class TEPG demonstration plant using waste heat from steel works at JFE and TEPG units set up on each carburizing furnace at Awazu gear manufacturing plant, Komatsu Ltd., have been installed some emergency sub-units in order to protect the main system as the first priority and also TEPG systems from the serious troubles in operation. It can be emphasized to be important that market- oriented TEPG systems should be raised to the social life step by step.

Finally, it can be said that the human resource is the most important power for the establishment of a new technology such as thermoelectrics into the real world. The number of members of the Thermoelectrics Society of Japan (TSJ) is increasing year and year to be more than 500 in 2015. The activity of thermoelectric R&D in Japan has been kept to be high. For example, the number of the attendee was about 150 at International Conference on Organic and Hybrid Thermoelectrics (ICOT2016) held in Kyoto on January 2016.

## Concluding Remarks

On the one hand, several R&D efforts of the enhancement of TE performance for various TE material systems have been steadily progressed on and on. The distinguished experimental results for several TE materials such as sulfide, self-assembled and forced nano-structured TE materials, and hybrid organic TE materials have been presented year and year.

On the other hand, the demonstration run of the TEPG systems using *Bi – Te* based modules has been connected to the power grid to prove its reliability for 500 W class and 10 kW class systems. They have been able to give us the prospect the realization of the practical-use for TEPG

system over more than 100 kW class system. The TEPG-Integrated Wireless Sensor Node has been established for practical-use stage as the TEPG application to energy harvesting field.

TEPG systems have been approached to the advanced stage for practical TEPG system. For this stage the durability science, the safety engineering and various assessments will be highly required. It can be believed that a TEPG technology should be able to become the indispensable core technology in the near future to build the high-efficiency energy system in the world.

## Acknowledgements

We express our hearty gratitude to the following researchers for the sincere cooperation:
Dr. H. Obara (AIST), Prof. K. Koumoto (Nagoya Univ.), Dr. M. Mikami (AIST), Prof. H. Nishino (Nagoya Inst. of Tech.), Mr. N. Uchiyama (Atsumitec), Dr. H. Kaibe (KELK), Dr. H. Hachiuma (KELK), Dr. T. Kanno (Panasonic), Prof. Y. Horita (Tokyo Inst. of Tech.), Mr. A. Yamamoto (AIST), Prof. T. Iida (Tokyo Univ. of Science), and Dr. T. Nakamura (Murata Manufacturing Co., Ltd.)

## References

1. www8.cao.go.jp
2. www.thermat.jp
3. T.Kuroki, K.Kabeya, K.Makino, T.Kajihara, H.Kaibe, H.Hachiuma, H.Matsuno, and A.Fujibayashi, Thermoelectric Generation Using Waste Heat in Steel Works, *J. of Electronic Materials* **43** (6), 2405 – 2410 (2014).
4. Y.Saito, M.Inomata, T.Oono, T.Kannari, H.Hachiuma, R.Chu, Y.Horita, Solar Powered Desalination Using Thermoelectric Power Generation, *Proc. of the 3rd Joint SQU-JCCP Environment Symposium, Muscat, Oman, 2010.*
5. T.Nakamura, Fabrication of Multi-Layer Type Thermoelectric Modules using Multi-Layer Co-fired Ceramics (MLCC) Process and Application for Energy Harvesting, *Thermoelectric Power Generation System Technology*, 226 – 242, S$T Press, 2013.
6. M.Ohta, Matured but Novel *Pb – Te* Thermoelectric Material: Marvelous Performance due to the Nano-Structure Technology, *J. of Kinzoku Materials Science & Technology*, 86(3), 213 – 220(2016).
7. A.Yoshida, N.Toshima, Gold Nanoparticles and Gold Nanorod Embedded PEDOT:PSS Thin Films as Organic Thermoelectric Materials, *J. of Electronic Materials* 43(6), 1492 – 1497(2014).
8. N.Toshima, Thermoelectric Performance of Organic Materials Including Hybrid Systems, *J. of Kinzoku Materials Science & Technology* 86(3), 221 – 229 (2016).
9. K.Kim, K,Suekuni, H.Nishiate, M.Ohta, H.Tanaka, and T.Takabatake, High Thermoelectric Performance in Coulsites $Cu_{26-x}Zn_xV_2M_6S_{32}$($M = Ge$, $Sn$), *Extended Abstract of TSJ 2014, 27, 2014.*
10. K.Nagase, A.Yamamoto, Development of Durability Testing for Thermoelectric Power Generation Module, *J. of Kinzoku Materials Science & Technology*, 86 (3), 230 – 236 (2016).
11. T.Kajikawa, Present Status on Thermoelectric Power Generation Systems and their Safety, *J. of Japan Society for Safety Engineering* 53(6), 477 – 484 (2014).

Submitted 27.01.2016.

*A.V. Prybyla*

**A.V. Prybyla**

Institute of Thermoelectricity of the NAS
and MES of Ukraine, 1, Nauky str., Chernivtsi, 58029, Ukraine

# PHYSICAL MODELS OF PERSONAL AIR-CONDITIONERS *(Part One)*

*This paper is focused on the prospects of using personal air-conditioners that are capable of saving energy resources, reducing environment thermal pollution and improving living standards. With a view to determine possible development of rational variants of air-conditioners, they have been classified according to the method and purpose of air-conditioning. From the classification more than 20 new design opportunities of air-conditioners have been found. They can be useful in the development of mass and special-purpose air-conditioners. From the analysis of these opportunities follows the promising outlook for the use of thermoelectric cooling or heating in personal air-conditioners. Such applications are defined as a promising way of wide use of thermoelectricity.*

**Key words:** heat pump, thermoelectricity, air conditioning, physical model.

## Introduction

*General characterization of the problem.* There is a well-known tendency to saving energy resources for the improvement of the Earth ecological state, in particular, reduction of its thermal pollution. One of important trends in this saving is reduction of energy cost for creation of comfortable conditions for human vital activity [1]. Considerable is electric energy consumption for air-conditioning of dwellings, work places and public facilities (cinema theatres, theater halls, public eating places, etc). Energy demands for air-conditioning, especially in critical weather conditions (summer period) are so great that the power of existing electric grids cannot meet them in some cases. Total air-conditioning cost in recent decades has reached $\approx 800 \cdot 10^9$ kW·h per year and, according to forecasts, by 2100 it will have increased by a factor of 30 [2]. In the meantime, there is no need in air-conditioning of big spaces in dwellings, industrial enterprises. In fact, for creation of such conditions it is enough to provide air-conditioning of person himself, which allows reducing energy cost by a factor of tens and hundreds.

Moreover, according to medical investigations, in many cases there is no need in air-conditioning the entire human body. To assure comfortable conditions, it is enough to act with heat or cold on certain areas of the human body [4], for instance on the head under overheat conditions or on the extremities under supercooling conditions. Moreover, it can be expected that the use of air-conditioned garment will result in considerable reduction of cold-related diseases, and creation of appropriate temperature conditions should produce curative effect with various inflammatory processes, chronic diseases of joints and other organs of the human body.

Personal air-conditioning is efficient for electric energy saving not only at elevated ambient temperatures, but also at reduced temperatures. Such air-conditioners can reduce requirements to temperature conditions of human residence. According to estimates, the use of individual air-conditioners in heating mode can save $4 \cdot 10^{12}$ kW·h of thermal energy per year (from the world level

of energy consumption on space heating $40 \cdot 10^{12}$ kW·h per year) [3], which will correspond to reduction of energy consumption by about 10 %.

Personal air-conditioners allow improving the quality of life in general. This is due to the capabilities of such air-conditioners of maintaining comfortable conditions with a change of ambient temperature conditions (in wide limits) or with a change in the emission of heat from the human body depending on mechanical loads (from 100 W in a quiescent state to 1 kW, for instance, in the process of running or hard work) [5] by automatic change in person exposure to heat or cold.

The foregoing points to the importance and relevance of studies aimed at creating personal air-conditioners which, by the highest standards, can influence the conditions and life style of mankind. This will be due to transition from passive garment which has mainly performed the function of thermal insulation of the human body, to the use of active garment which responds to changes in the temperature conditions of human activity.

With regard to the above, it is important to consider methods than can achieve garment air-conditioning nowadays, and how these methods or combinations thereof can be used for solving this task. The latter comes down to studying physical models that can be used when creating such air-conditioners and their analysis with a view to find the most rational variants. Exactly this is the subject of research in this work. In so doing, of particular interest when creating optimal designs are air-conditioners which employ thermoelectric cooling and heating effects [6], which, according to investigations, at low powers of heat and cold can dominate over all other methods.

*Analysis of the literature.* Activities aimed at creating air-conditioned garment are already actively pursued in many countries worldwide [7 – 18]. The greatest acceptance nowadays has been gained by passive air-conditioning garment, the so-called thermal garment (thermal underwear) [19]. It retains heat (in terms of heat-insulating properties it is equivalent to two and more layers of traditional clothes) and removes humidity from the human body due to the use of synthetic textiles of complicated internal structure. As a rule, such garment is composed of three layers – the lower one absorbs and removes humidity; the middle one removes humidity outside and retains heat; the upper one protects from unfavourable weather conditions.

As to active air-conditioning, these are mainly special-purpose air-conditioners for creation of appropriate conditions that are related to professional activity under extreme temperature conditions.

In particular, works [7, 8] represent special garment for overheat protection of workers of hot shops which employs cold accumulators in the form of potassium acrylate copolymer [7] or dry ice [8]. In the former case for "charging" of accumulator the garment is soaked in water for several hours, accumulator substance absorbs the liquid which assures cooling within 8 hours, absorbing in this case up to 12.5 kJ/cm$^2$ per hour. Air-conditioner [8] using dry ice in garment inner lining proves cooling by circulation of cooled gas-like carbon dioxide in the space between internal jacket surface and the human body.

Works [9, 10] employ the method of human body cooling by ambient air blowing. Such air-conditioner has the form of overalls with channels for passing of air which is blown into garment by an electric fan.

Works [11 – 13] describe cooled garment for military men, sportsmen and doctors which is based on thermal energy absorption due to substance phase transition. Such garment is made as jackets, knee or elbow bandages, etc. having water-filled channels. Cooling in this case is done by water evaporation through special porous external surface of air-conditioner. The time of its continuous operation is up to 6 hours assuring temperature reduction to 15 °C from the ambient temperature (at relative air humidity 30 %).

Works [14, 15] provide insight into creation of air-conditioners heaters for supercooling protection. In particular, [14] describes a design of air heater in the form of a mask for miners working at extremely low temperatures, where air is heated by a resistive heater.

Of particular interest are works [16 – 18] which represent the results of development of thermoelectric air-conditioners. These are garment-embedded Peltier modules for garment cooling or heating depending on the electric current direction.

All above mentioned garment air-conditioning methods offer their specific advantages and, at the same time, have considerable shortcomings. Therefore, it is important to consider all modern methods used for individual air-conditioning of the human body, and to determine how these methods or combinations thereof can be used for creation of new efficient personal air-conditioners.

*The purpose of this work* is determination of possible modifications of personal air-conditioners, their classification and analysis for further enhancement of their quality with regard to specific operating conditions.

## Classification of personal air-conditioners

In this paper, personal air-conditioners are classified according to function, the type of heat and cold source, the object of cooling or heating and garment purpose (Fig. 1).

According to function, personal air-conditioners are recognized that are used only for cooling, only for heating or for cooling and heating, as the need may be. Each of these air-conditioners differs in the type of heat or cold source.

According to the object of cooling or heating, personal air-conditioners can be classified as such that provide air-conditioning of the entire human body (overalls with individual air-conditioner) or its areas – head (air-conditioned headwear), body (air-conditioned vest), elbow or knee joints (air-conditioned bandage), loin (air-conditioned belt), abdomen (air-conditioned plate fixed on the belly), hands (air-conditioned gloves), feet (air-conditioned footwear).

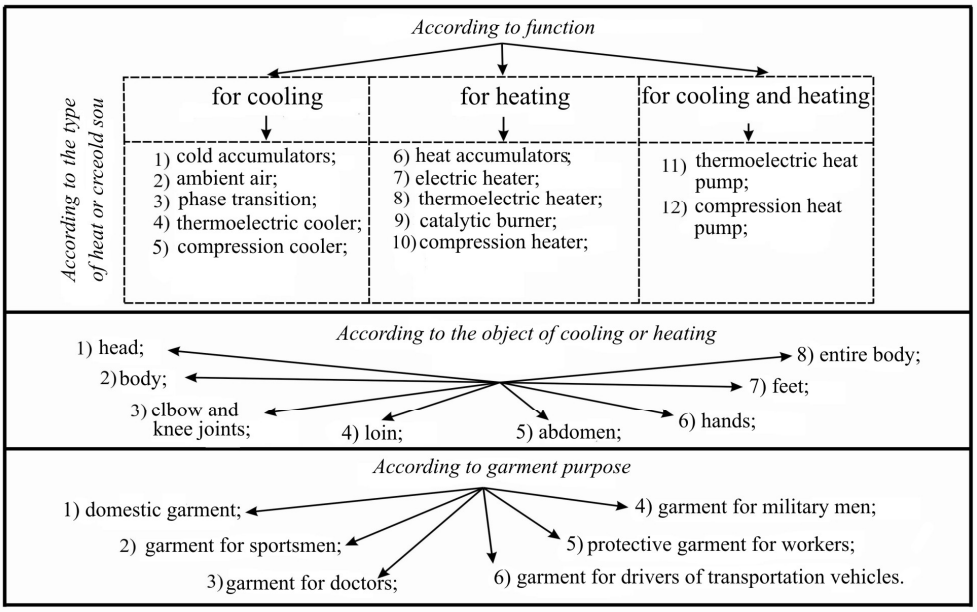


*Fig. 1. Classification of personal air-conditioners for garment.*

Depending on the spheres of application of air-conditioned garment they are classified as air-conditioners for domestic garment (creation of comfortable conditions in everyday life and on

holidays), for sportsmen (garment abstracting heat during extreme physical loads), for doctors (for instance, protective garment for surgeons during long-term surgical interventions or operations in garment protecting against harmful radiation), for drivers of transportation vehicles (pilots, cosmonauts, drivers of automobiles and motorcycles), for military men (for instance, air-conditioner for armour vests that will assure comfortable conditions for combat mission performance under various climatic conditions), for workers (for instance, garment for protection against long-term exposure to elevated temperatures at metallurgical plants or, on the contrary, for protection of workers against low temperatures in the North).

The key attribute which distinguishes one air-conditioner from another is the type of heat or cold sources. They primarily govern the operating efficiency of air-conditioners. So, let us consider classification of personal air-conditioners by the types of heat and cold sources.

## Classification of physical models of personal air-conditioners

Analysis of the literature testifies that the problem of creation of personal air-conditioners that would combine the basic advantages of known methods of heat and cold production is still poorly understood. We first discuss all possible combinations of heat and cold sources which provide air-conditioning. This is an exhaustive list of physical models of air-conditioners. Their modifications are given in Table. Here: 1 – heat or cold accumulators (12 in particular, using substance phase transition); 2 – ambient air; 3 – electric heater; 4 – catalytic heater; 5 – compression heat pump; 6 – thermoelectric heat pump.

*Table*

*Modifications of physical models of personal air-conditioners*

| | 1 | 2 | 3 | 4 | 5 | 6 | 1.2 |
|---|---|---|---|---|---|---|---|
| 1.3 | 1.4 | 1.5 | 1.6 | 2.3 | 2.4 | 2.5 | 2.6 |
| 3.4 | 3.5 | 3.6 | 4.5 | 4.6 | 5.6 | 1.2.3 | 1.2.4 |
| 1.2.5 | 1.2.6 | 1.3.4 | 1.3.5 | 1.3.6 | 1.4.5 | 1.4.6 | 1.5.6 |
| 2.3.4 | 2.3.5 | 2.3.6 | 2.4.5 | 2.4.6 | 2.5.6 | 3.4.5 | 3.4.6 |
| 3.5.6 | 4.5.6 | 1.2.3.4 | 1.2.3.5 | 1.2.3.6 | 1.2.4.5 | 1.2.4.6 | 1.2.5.6 |
| 1.3.4.5 | 1.3.4.6 | 1.3.5.6 | 1.4.5.6 | 2.3.4.5 | 2.3.4.6 | 2.3.5.6 | 2.4.5.6 |
| 3.4.5.6 | 1.2.3.4.5 | 1.2.3.4.6 | 1.2.3.5.6 | 1.2.4.5.6 | 1.3.4.5.6 | 2.3.4.5.6 | 1.2.3.4.5.6 |

- already in use;
- promising;
- use is unreasonable.

The Table comprises known modifications of air-conditioners (13 physical models, preferably the simplest, with one type of heat or cold source), as well as those which are unreasonable to be used now (28 models). Nevertheless, it enables us to single out new physical models of air-conditioners that can be promising for practical use.

We first discuss physical models of known air-conditioners. They are numbered according to Table.

## Physical models of known personal air-conditioners

### Physical models with heat or cold accumulators

One of the simplest methods of cooling or heating is the use of cold or heat accumulators, respectively [7, 8]. The operating principle of such air-conditioners is based on the use of high heat capacity substances which gradually release or absorb human heat flux.

Physical models of personal air-conditioner with heat or cold accumulator are represented in Fig. 2.

In cooling mode (Fig. 2*a*) heat accumulator absorbs the amount of heat equal to:

$$Q_{accum.} = V \cdot \rho \cdot C \cdot (T_2 - T_1) \cdot t, \tag{1}$$

where $Q_{accum.}$ is thermal energy absorbed by heat accumulator (J), $V$ is volume of heat accumulator ($m^3$), $\rho$ is its density ($kg/m^3$), $C$ is specific heat capacity ($W/kg \cdot K$), $(T_2 - T_1)$ is the difference between final $T_2$ and initial $T_1$ temperatures of heat accumulator substance, $t$ is time of accumulator discharge (sec) from temperature $T_1$ to $T_2$.

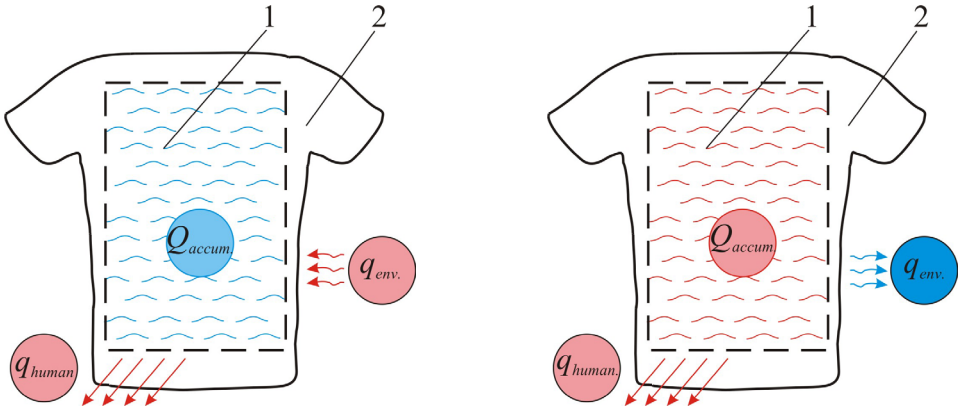


*Fig. 2. Physical model of personal air-conditioner with heat or cold accumulator:*
*1 is vessel with heat accumulator, 2 is air-conditioned garment,*
*a) cooling mode, b) heating mode.*

In this case heat balance equation will be of the form:

$$Q_{accum.} = (q_{human.} + q_{env.}) \cdot t, \tag{2}$$

where $q_{human.}$ is heat release from human body (W), $q_{env.}$ is power of heat release from the environment (W), for instance, thermal radiation from heated objects, $t$ is time of accumulator discharge (sec) from temperature $T_2$ to $T_1$.

In heating mode (Fig. 2*b*), heat balance equation will be of the form:

$$Q_{accum.} = (q_{env.} - q_{human.}) \cdot t. \tag{3}$$

From (2), (3) it is clear that normal heat exchange from human body can be assured within time $t$ which depends on the parameters of heat accumulator and power of heat release from human body $q_{human.}$ and environment $q_{env.}$

The disadvantage of such air-conditioning circuit is the need for permanent replacement ("charging") of accumulator which makes impossible its long-term use.

A variety of air-conditioners using heat accumulators are coolers with substance phase transition [11 – 13]. The working substance here (liquid, dry ice) is evaporated, absorbing therewith thermal energy. Such air-conditioning scheme is more efficient than the previous variant, but it has its weak points, namely the absence of possibility of garment heating, strong dependence on ambient conditions, in particular, humidity and air temperature.

Thermal energy $Q_{ph.tr.}$ (J), removed to environment by such air-conditioner will be equal to:

$$Q_{ph.tr.} = L \cdot V \cdot \rho, \tag{4}$$

where $L$ is specific heat of evaporation (J/kg), $V$ is the volume of substance which is evaporated ($m^3$), $\rho$ is its density ($kg/m^3$).

In this case heat balance equation will be of the form:

$$Q_{accum.} = (q_{human.} + q_{env.}) \cdot t, \tag{5}$$

where $t$ is time of full evaporation of substance.

As is seen from (5), an essential deficiency of such air-conditioner model is the need for permanent replacement of working substance which renders impossible its long-term use.

**Physical model using thermal energy of ambient air**

A common method employed only for cooling of human body is the use of heat exchange with the environment [9, 10] (Fig. 3). In this case the prerequisite for human body cooling is that the ambient temperature must be lower than the body temperature. Moreover, such air-conditioning scheme involves the electric fan which consumes certain power $W_{fan.}$, and, accordingly, its power supply.

Thermal power $q_{air.}(W)$ removed to the environment by such air-conditioner will be equal to:

$$q_{air.}(W_{fan.}, T_1) = G(W_{fan.}) \cdot \rho \cdot C \cdot (T_2 - T_1), \tag{6}$$

where $G$ is air flow rate ($m^3$/sec) which is a function of fan power $W_{fan.}$, $\rho$ is air density ($kg/m^3$), $C$ is specific heat of air (W/kg·K), $(T_2 - T_1)$ is the difference between air-conditioner outlet temperature $T_2$ and inlet temperature $T_1$.

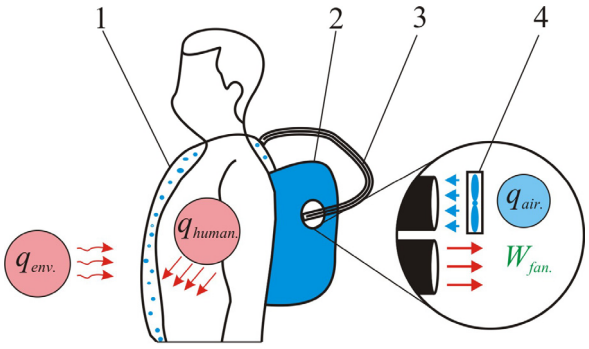


*Fig. 3. Physical model of personal air-conditioner using heat-exchange with the environment: 1 – garment with air passage channels, 2 – air-conditioner unit comprising an electric fan 4 with power supply, 3 – channels for air change.*

Heat balance equation in this case can be written as follows:

$$q_{air.} = q_{human.} + q_{env.}. \tag{7}$$

The shortcomings of this air conditioning method are low efficiency, absence of the possibility of heating, strong dependence on the environmental conditions, the need for electric power supply.

**Physical model using the Joule effect**

A simple method of garment heating is the use of electric resistive heaters [14, 15] (Fig. 4). Such air-conditioner comprises a garment-embedded heater in the form of current-carrying conductor and an electric power supply with control unit. Despite its simplicity, such air-conditioner has its weak points, namely absence of the possibility of cooling and the need for permanent charge of power supply (electric accumulator).

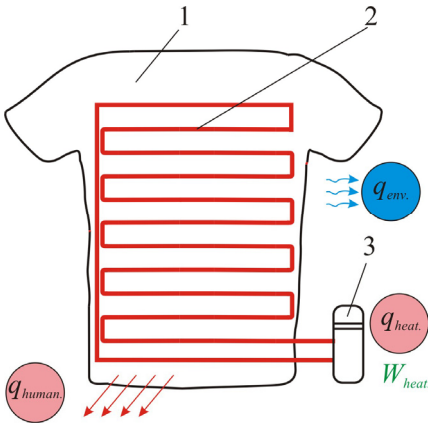


*Fig. 4. Physical model of personal air-conditioner using the Joule effect:*
*1 – air - conditioned garment, 2 – electric heater, 3 – power supply.*

Thermal power $q_{heat.}$ (W) release by such heater will be equal to:

$$q_{heat.} = I^2 \cdot r, \tag{8}$$

where $I$ is current strength (A), $r$ is electric resistance of the heater (Ω).

Heat balance equation will be of the form:

$$q_{heat.} = q_{env.} - q_{human}. \tag{9}$$

The efficiency of such heater is close to unity, as long as almost all spent electric power $W_{human.}$ is converted into thermal flux $q_{human}$.

**Physical model with catalytic fuel combustion**

Another method of garment heating is the use of gas catalytic combustion in a burner [20]. The operating principle of such air-conditioner-heater lies in heat release with flameless oxidation (combustion) of gas mixture in the presence of a catalyst. The air heated in this way gets through the system of channels into garment, heating it. Gas combustion products are removed to the environment.

Thermal energy $Q_{g.f.}$ (*J*) released with fuel combustion will be equal to:

$$Q_{c.n.} = g \cdot m, \tag{10}$$

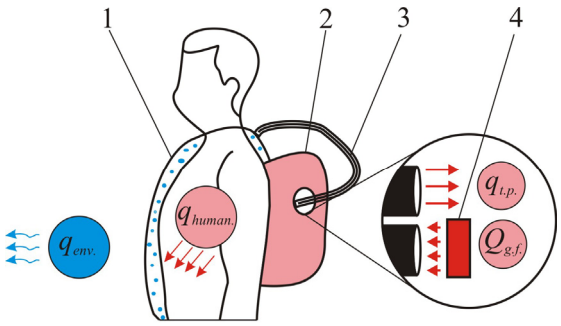


*Fig. 5. Physical model of personal air-conditioner with catalytic gas combustion: 1 – garment with heated air passage channels 3, 2 – container with burner 4.*

where $g$ is specific heat of fuel combustion (J/kg), $m$ is fuel weight (kg).

Heat balance equation will be of the form:

$$Q_{g.f.} = (q_{env.} - q_{human.} + q_{t.p.}) \cdot t\,, \tag{11}$$

where $q_{t.p.}$ is thermal power (W) which is released to environment with fuel combustion products and spent air.

This method of garment air-conditioning offers the advantages of a relatively low need for heat source (petrol, spirit), its weak point is absence of the possibility of garment cooling.

**Physical model with compression heat pump**

The operation of compression heat pumps is based on a refrigeration cycle [21]. A simple vapour cycle of mechanical refrigerating machine is realized by means of four members forming a closed cooling loop, namely compressor, condenser, throttle valve and evaporator or cooler (Fig. 6). Vapor from the evaporator comes to compressor and is compressed, owing to which its temperature is rising. On leaving the compressor, vapour that has high temperature and pressure comes to condenser where it is cooled and condensed. Liquid from the condenser passes through throttle valve. As long as boiling (saturation) temperature for this pressure proves to be lower than liquid temperature, it starts to boil violently; in the process, part of the liquid is evaporated and the temperature of the rest is lowered to equilibrium saturation temperature (the heat of the liquid is spent on its conversion to vapour). In this way, the necessary garment areas are cooled or heated. The disadvantages of this air-conditioning method include the demand for charging of compressor electric power supply (storage battery), the presence of coolant (specifically, freone, which is rather toxic), weight-size parameters, as well as noisy work.

Thermal power $q_{cool.}$ (W) taken off on the cold side of compressor cooler (cooling capacity) is determined by the relation:

$$q_{cool.} = q_{heat.} - W_{compr}\,, \tag{12}$$

where $q_{heat.}$ is thermal power (W) removed from the hot side to the environment, $W_{compr.}$ is electric power (W) spent by compressor.

To provide for heat balance in cooling mode:

$$q_{cool.} = q_{env.} + q_{human}\,. \tag{13}$$

In heating mode (13) will be rewritten as:

$$q_{heat.} = q_{env.} - q_{human.}\,. \tag{14}$$

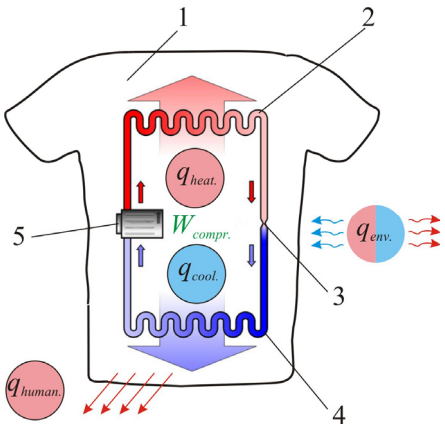


*Fig. 6. Physical model of personal air-conditioner with compression heat pump: 1 – garment, 2 – evaporator, 3 – throttle valve, 4 – condenser, 5 – compressor.*

It is worth mentioning that despite their disadvantages, compression heat pumps have high value of energy conversion efficiency factor (coefficient of performance at a level of 3).

**Physical model with thermoelectric heat pump**

A convenient method of garment cooling or heating is the use of thermoelectric heat pumps based on the Peltier effect [16 – 18] (Fig. 7). Depending on the electric current direction such air-conditioner can be used both for cooling and heating.

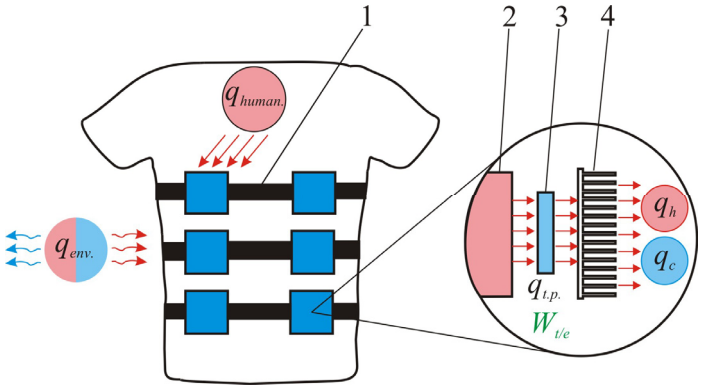


*Fig. 7. Physical model of personal air-conditioner with thermoelectric heat pump: 1 – garment with fastener system, 2 – member assuring thermal contact of thermoelectric energy converter 3 to garment, 4 – air heat exchanger.*

In cooling mode, thermal power $q_c$ (W) absorbed on the cold side of thermoelectric converter is equal to:

$$q_c = \Pi \cdot I - \frac{1}{2} \cdot I^2 \cdot r - \mathrm{K} \cdot \Delta T \,, \tag{15}$$

where $\Pi$ is the Peltier coefficient (V), $\mathrm{K}$ is full thermal conductivity (W/K), $\Delta T$ is temperature difference on thermoelectric converter (K).

Heat balance is given below:

$$q_c = q_{env.} + q_{human.} \,. \tag{16}$$

For heating mode, thermal power $q_h$ (W) released on the hot side of thermoelectric converter is equal to:

$$q_h = \Pi \cdot I + \frac{1}{2} \cdot I^2 \cdot r - \mathrm{K} \cdot \Delta T \,. \tag{17}$$

Heat balance in heating mode is given below:

$$q_h = q_{env.} - q_{human} \,. \tag{18}$$

This air-conditioning method offers the advantages of high efficiency, reliability, low weight-size parameters, environmental friendliness (absence of harmful coolants) and noise-free operation. The shortcoming includes the demand for permanent charging of electric accumulators.

**Model 1.2**

Fig. 8 represents a physical model of personal air-conditioner which is a combination of the above models using thermal energy of the ambient air (item 2) and heat accumulators (item 1).

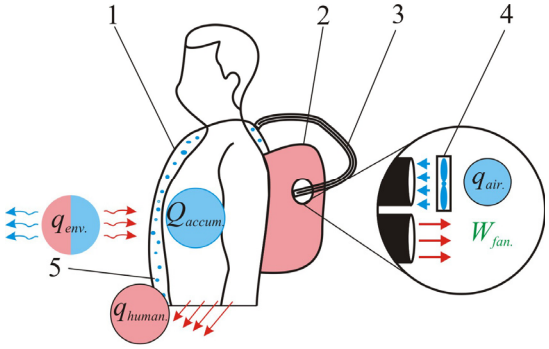


*Fig. 8. 1 – garment with air passage channels 3, 2 – container with a fan 4, 5 – vessel with heat accumulator.*

This method of garment air-conditioning offers the advantage of increased cooling efficiency due to the use of two sources of cold. Its shortcomings include absence of the possibility of garment heating and the demand for permanent charging of fan electric supply and replacement of heat accumulator (water, dry ice, etc).

**Model 1.3**

Fig. 9 represents a physical model of personal air-conditioner which is a combination of models using the Joule effect (item 3) and heat accumulators (item 1).

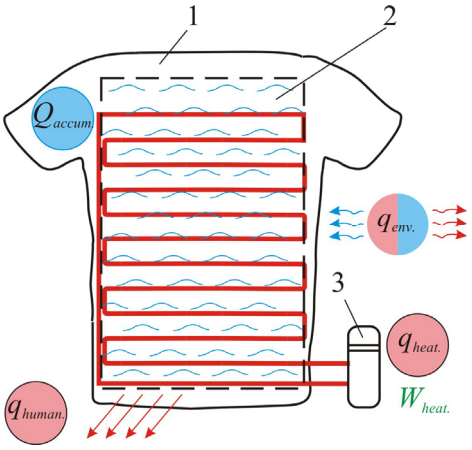


*Fig. 9. 1 – air-conditioned garment, 2 – vessel with heat accumulator, 3 – electric heater.*

The advantages of this garment air-conditioning method include both cooling (by thermal energy absorption at substance phase transition) and heating (by heat release at current flow through conductor) capabilities. The shortcoming is the demand for permanent charging of heater electric supply and replacement of heat accumulator (water, dry ice, etc).

**Model 2.3**

Another physical model of personal air-conditioner which already finds practical implementation is depicted in Fig. 10. It combines the models using thermal energy of ambient air (item 2) and thermal action of the Joule effect (item 3).

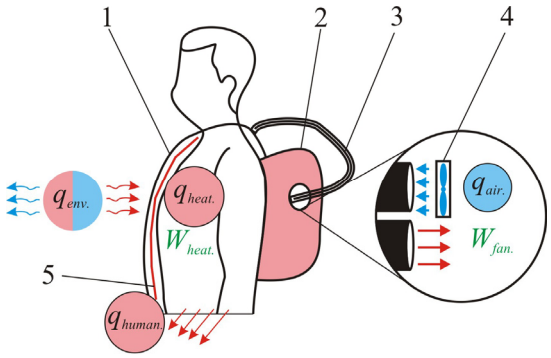


*Fig. 10. 1 – garment with air passage channels 3,*
*2 – container with a fan 4, 5 – electric heater.*

The advantages of this garment air-conditioning method include both cooling (by absorption of thermal energy at blowing of human body with a lower temperature ambient air), and heating (by heat release at current flow through conductor) capabilities. The shortcoming is the demand for permanent charging of heater and fan electric supply.

**Model 2.4**

Fig. 11 represents a physical model of personal air-conditioner which combines the use of thermal energy of ambient air (item 2) and thermal action with catalytic fuel combustion (item 4).

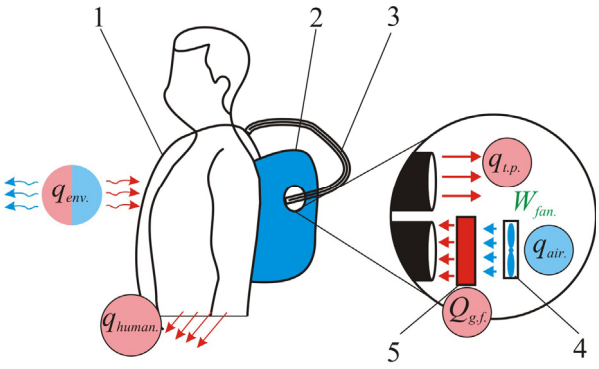


*Fig. 11. 1 – garment with air passage channels 3,*
*2 – container with a fan 4 and gas burner 5.*

The advantage of this air-conditioner is both cooling (by absorption of thermal energy at blowing of human body with a lower temperature ambient air) and heating (thermal energy release at catalytic fuel combustion) capabilities. The shortcomings include the demand for permanent charging of fan electric supply and replacement of fuel in catalytic heater).

**Model 2.5**

Fig. 12 represents a physical model which combines the use of thermal energy of ambient air (item 2) and compression heat pump (item 5).

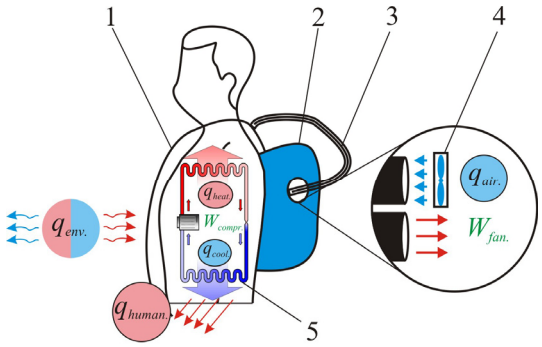


*Fig. 12. 1 – garment with air passage channels 3,*
*2 – container with a fan 4, 5 – compression heat pump.*

This model offers the advantages of both cooling (by operation of compression heat pump and absorption of thermal energy at blowing of human body with a lower temperature ambient air) and heating (thermal energy release with a reverse cycle of compression heat pump) capabilities. Its shortcomings include the demand for permanent charging of the fan and compressor power supply, the presence of harmful coolants (for instance, freon).

**Model 2.6**

Fig. 13 represents a physical model of personal air-conditioner which combines the use of thermal energy of ambient air (item 2) and thermoelectric heat pump (item 5).

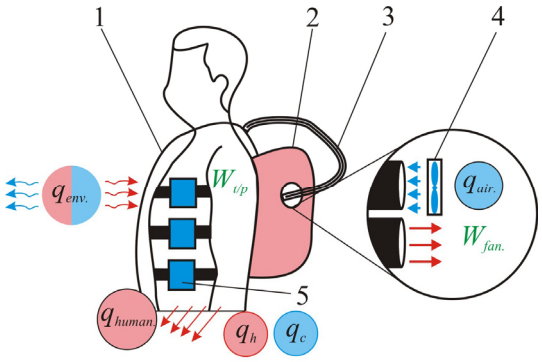


*Fig. 13. 1 – garment with air passage channels 3,*
*2 – container with a fan 4, 5 – thermoelectric heat pump.*

The advantages of this garment air-conditioning method include both cooling (by using thermoelectric heat pump and by absorption of thermal energy at blowing of the human body with a lower temperature ambient air) and heating (thermal energy release at thermoelectric heating) capabilities. The shortcomings include the demand for permanent charging of the fan and thermoelectric power converters electric supply.

## New physical models of personal air-conditioners

As is shown in Table 1, 23 physical models of personal air-conditioners have been selected that

hold promise for further studies. These models are combinations of known methods of heat and cold production that have been discussed in the previous section. Consider them in more detail.

**Model 1.4**

Fig. 14 represents a physical model of personal air-conditioner which combines catalytic heater (item 4) with heat accumulator (item 1). This model allows enhancing the functionality of garment air-conditioning, namely to provide for garment cooling (by thermal energy absorption at phase transition of substance contained in a vessel with heat accumulator) or heating (heating of air that gets into garment channels due to catalytic combustion of gas). Its shortcoming is the demand for permanent replacement of heat accumulator and fuel in the heater.

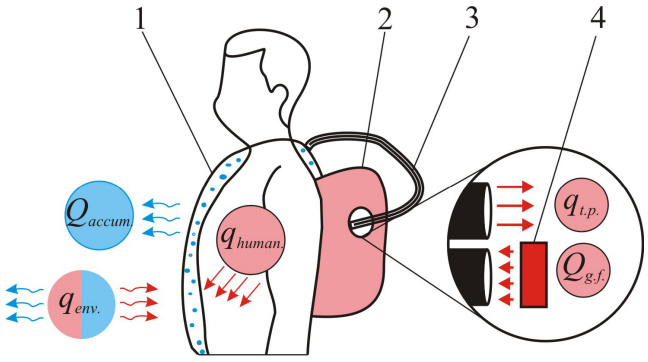


*Fig. 14: 1 – vessel with heat accumulator, 2 – container with gas burner 4, 3 – heated air passage channels.*

**Model 1.5**

Fig. 15 represents a physical model of personal air-conditioner which combines compression heat pump (item 5) with heat accumulator (item 1). The use of such air-conditioning method makes it possible to increase garment cooling efficiency through combination of mechanical cooling by compression refrigeration machine with cooling by substance phase transition. Another advantage of this garment air-conditioning method is the possibility of its use in heating mode (through the reverse cycle of compression refrigeration machine). Its shortcoming is the need for permanent charging of compressor power supply, the demand for heat accumulator replacement and the presence of harmful coolants.

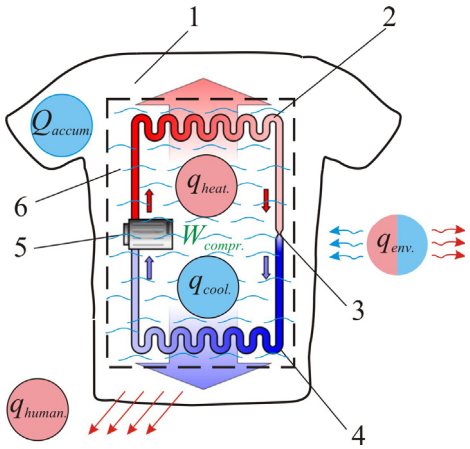


*Fig. 15: 1 – garment, 2 – evaporator, 3 – throttle valve, 4 – condenser, 5 – compressor, 6 – vessel with heat accumulator.*

**Model 1.6**

Fig. 16 represents a physical model which combines thermoelectric heat pump (item 6) with heat accumulator (item 1). Its use allows increasing garment cooling efficiency through combination of the Peltier thermoelectric effect with cooling by substance phase transition. It can be also used in heating mode due to thermoelectric power converters. Its shortcoming is the need for permanent charging of thermoelectric modules power supply and the demand for heat accumulator replacement.

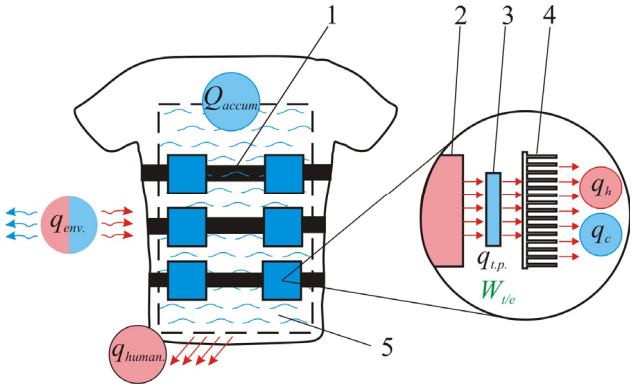


*Fig. 16: 1 – garment with fastener system, 2 – member providing for thermal contact of thermoelectric energy converter 3 to garment, 4 – air heat exchanger, 5 – vessel with heat accumulator.*

**Model 3.5**

Fig. 17 represents a physical model of personal air-conditioner which combines compression heat pump (item 5) with electric heater (item 3). The advantages of this garment air-conditioning method include both cooling (mechanical cooling by compression refrigeration machine) and heating (compression heat pump and the Joule effect in current-carrying conductor) capabilities; efficiency increase in heating mode due to the use of two heating modes. The shortcomings include the need for permanent charging of compressor and heater power supply, the presence of harmful coolants.

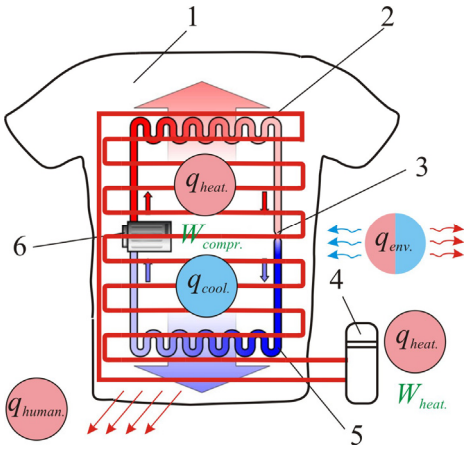


*Fig. 17: 1 – garment, 2 – evaporator, 3 – throttle valve, 4 – condenser, 5 – compressor, 6 – electric heater.*

**Model 3.6**

Fig. 18 represents a physical model which combines thermoelectric heat pump (item 6) with electric heater (item 3). The advantages of this model include both cooling (thermoelectric Peltier effect) and heating (thermoelectric heat pump and the Joule effect in current-carrying conductor)

capabilities; efficiency increase in heating mode due to the use of two heating methods. The shortcoming is the need for permanent charging of thermoelectric converters and heater power supply.

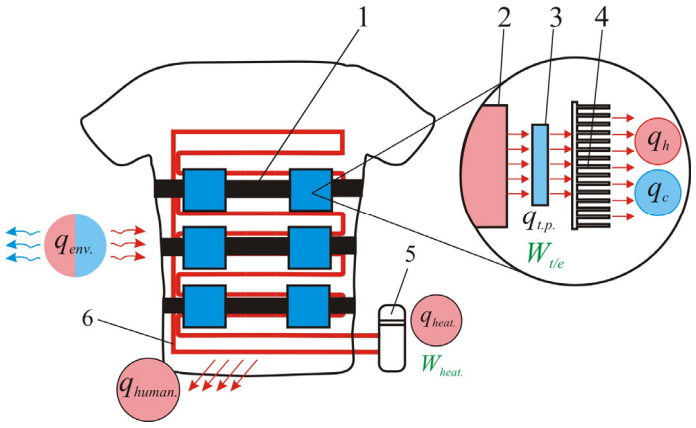


*Fig. 18: 1 – garment with fastener system, 2 – member providing for thermal contact of thermoelectric energy converter 3 to garment, 4 – air heat exchanger, 5 – electric heater.*

**Model 4.5**

Fig. 19 represents a physical model of personal air-conditioner (item 5) with a catalytic heater (item 4). The advantages of this model include cooling (mechanical cooling by compression refrigeration machine) and heating (compression heat pump and catalytic fuel combustion) capabilities; efficiency increase in heating mode due to the use of two heating methods. The shortcomings include the need for permanent charging of compressor power supply, the demand for fuel replacement in the heater and the presence of harmful coolants.

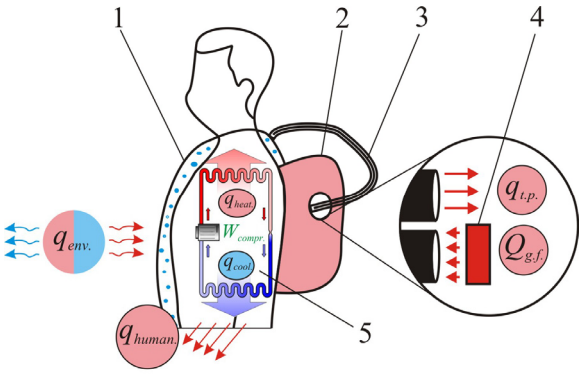


*Fig. 19: 1 – garment, 2 – container with gas burner 4, 3 – heated air passage channels, 5 – compression heat pump.*

**Model 4.6**

Fig. 20 represents a physical model which combines thermoelectric heat pump (item 6) with a catalytic burner (item 4). The advantages of this model include both cooling (cooling due to the Peltier effect) and heating(heat release due to catalytic fuel combustion, thermoelectric heating due to the Peltier effect) capabilities; efficiency increase in heating mode due to the use of two heating methods. The shortcomings include the need for permanent charging of thermoelectric converters power supply, the demand for replacement of fuel in the heater.

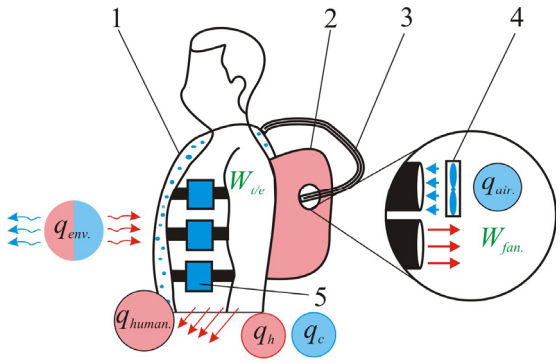


*Fig. 20: 1 – garment with channels 3, 2 – unit with a catalytic burner 4, 5 – thermoelectric heat pump.*

**Model 1.2.3**

Fig. 21 represents a physical model of personal air-conditioner which combines ambient air blowing (item 2), heat accumulator (item 1) with electric heater (item 3). Its advantages include cooling (heat absorption at substance phase transition, blowing with lower temperature ambient air) and heating (heat release according to the Joule effect in current-carrying conductor) capabilities. The shortcomings include the need for permanent charging of heater and fan power supply and the demand for heat accumulator replacement.

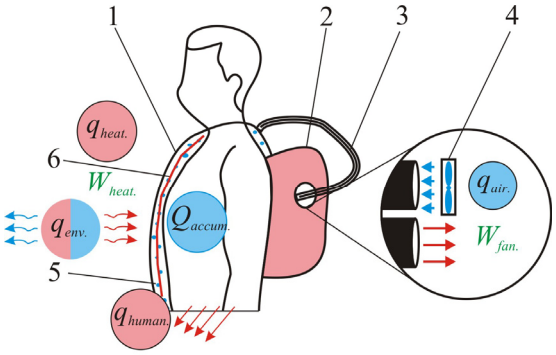


*Fig. 21: 1 – garment with air passage channels 3, 2 – air-conditioning unit comprising an electric fan 4 with power supply, 5 – vessel with heat accumulator, 6 – electric heater.*

**Model 1.2.4**

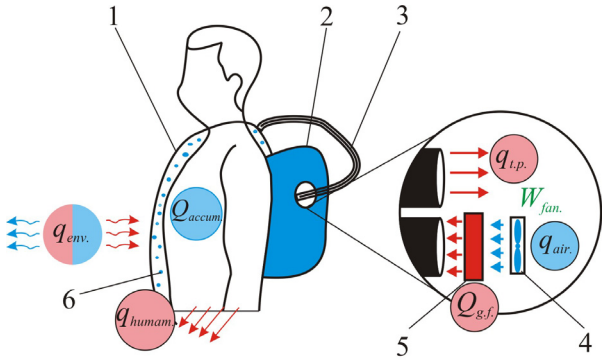


*Fig. 22: 1 – garment with air passage channels 3, 2 – air-conditioning unit comprising an electric fan 4, 5 – catalytic burner, 6 – vessel with heat accumulator.*

Fig. 22 represents a physical model of personal air-conditioner which combines ambient air blowing (item 2), heat accumulator (item 1) with a catalytic burner (item 4). The advantages of this garment air-conditioning method include cooling (heat absorption at substance phase transition, blowing with lower temperature ambient air) and heating (heat release due to catalytic fuel combustion combined with forced fanning) capabilities. The shortcomings include the need for permanent replacement of heat accumulator and fuel in the heater and the demand for electric fan power supply.

**Model 1.2.5**

Fig. 23 represents a physical model which combines compression heat pump (item 5), heat accumulator (item 1) and ambient air blowing (item 2). Its advantages include both cooling (mechanical cooling by compression refrigeration machine combined with ambient air blowing) and heating (compression heat pump) capabilities; efficiency increase in cooling mode due to the use of two methods of heat extraction. The shortcomings include the need for permanent charging of compressor power supply, the demand for heat accumulator replacement and the presence of harmful coolants.

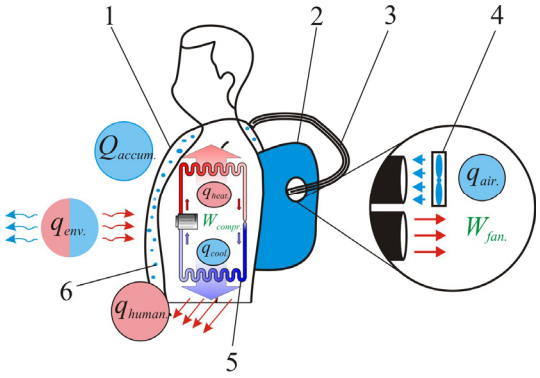


*Fig. 23: 1 – garment with air passage channels 3, 2 – unit comprising an electric fan 4, 5 – compression heat pump, 6 – vessel with heat accumulator.*

**Model 1.2.6**

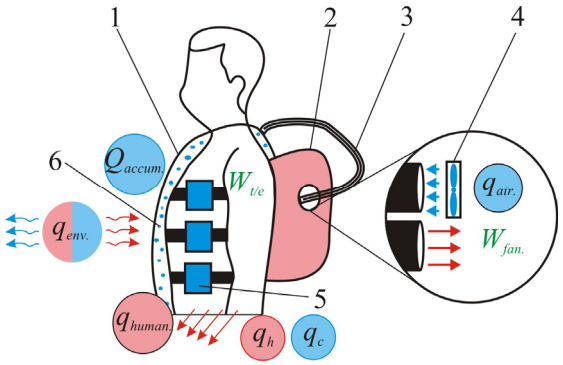


*Fig. 24: 1 – garment with air passage channels 3, 2 – unit comprising an electric fan 4, 5 – compression heat pump, 6 – vessel with heat accumulator.*

Fig. 24 represents a physical model which combines thermoelectric heat pump (item 6), heat accumulator (item 1) and ambient air blowing (item 2). Its advantages include both cooling (cooling due to the Peltier effect combined with ambient air blowing) and heating (thermoelectric heating) capabilities; efficiency increase in cooling mode due to the use of two methods of heat extraction.

The shortcomings include the need for permanent charging of thermoelectric converters power supply and the demand for heat accumulator replacement.

**Model 1.3.5**

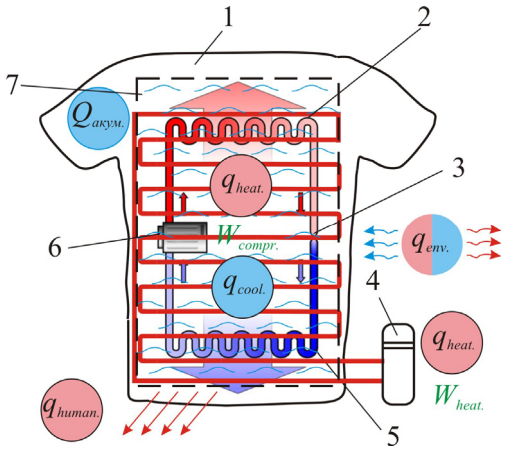


*Fig. 25: 1 – garment, 2 – evaporator, 3 – throttle, 4 – electric heater, 5 – condenser, 6 – compressor, 7 – heat accumulator.*

Fig. 25 represents a physical model which combines compression heat pump (item 5), heat accumulator (item 1) and electric heater (item 3). The advantages of this method include both cooling (mechanical cooling by compression refrigeration machine combined with heat absorption at substance phase transition) and heating (compression heat pump and electric heater) capabilities; efficiency increase in cooling and heating modes due to the use of two cooling or heating methods. The shortcomings include the need for permanent charging of compressor and heater power supply, the demand for heat accumulator replacement and the presence of harmful coolants.

**Model 1.3.6**

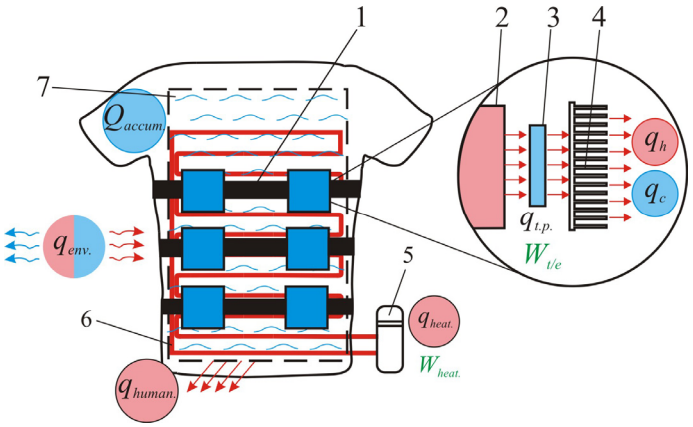


*Fig. 26: 1 – garment with fastener system, 2 – member providing for thermal contact of thermoelectric energy converter 3 to garment, 4 – air heat exchanger, 6 – electric heater with power supply 5, 7 – vessel with heat accumulator.*

Fig. 26 represents a physical model which combines thermoelectric heat pump (item 6), heat accumulator (item 1) and electric heater (item 3). The advantages of this garment air-conditioning method include both cooling (cooling due to the Peltier effect combined with heat absorption at substance phase transition) and heating (the Peltier effect and electric heater) capabilities; efficiency

increase in cooling and heating modes due to the use of two cooling or heating modes. The shortcomings include the need for permanent charging of thermoelectric converters and heater power supply, the demand for heat accumulator replacement.

**Model 1.4.5**

Fig. 27 represents a physical model which combines compression heat pump (item 5), heat accumulator (item 1) and a catalytic heater (item 4). Its advantages include both cooling (mechanical cooling by compression refrigeration machine combined with heat absorption at substance phase transition) and heating (heat release due to catalytic fuel combustion, heating by compression heat pump) capabilities; efficiency increase in cooling and heating modes due to the use of two cooling or heating modes. The shortcomings include the need for permanent charging of compressor power supply, the demand for replacement of heat accumulator and fuel in the heater, the presence of harmful coolants.

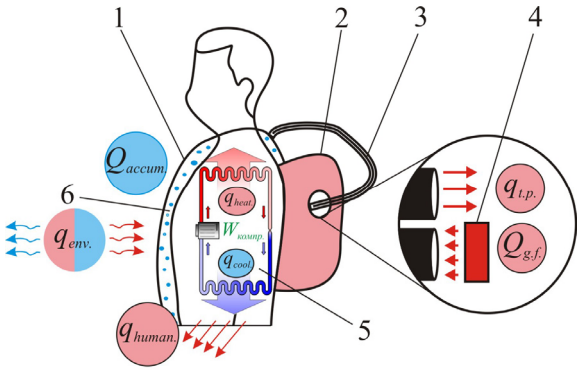


*Fig. 27: 1 – garment with air passage channels 3, 2 – unit comprising a catalytic burner 4 with power supply, 5 – compression heat pump, 6 – vessel with heat accumulator.*

**Model 1.4.6**

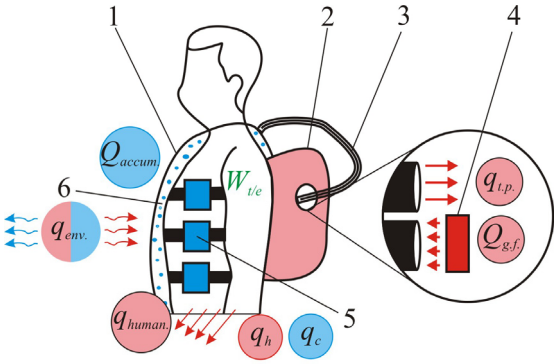


*Fig. 28: 1 – garment with channels 3, 2 – unit with a catalytic burner 4, 5 – thermoelectric heat pump, 6 – vessel with heat accumulator.*

Fig. 28 represents a physical model which combines thermoelectric heat pump (item 6), heat accumulator (item 1) with a catalytic burner (item 4). Its advantages include both cooling (cooling due to the Peltier effect combined with heat absorption at substance phase transition) and heating (heat release due to catalytic fuel combustion, thermoelectric heating due to the Peltier effect) capabilities; efficiency increase in cooling and heating modes due to the use of two cooling or heating modes. The shortcomings include the need for permanent charging of compressor power supply, the demand for replacement of heat accumulator and fuel in the heater, the presence of harmful coolants.

**Model 2.3.5**

Fig. 29 represents a physical model which combines compression heat pump (item 5), electric heater (item 3) with ambient air blowing (item 2). Its advantages include both cooling (mechanical cooling by compression refrigeration machine combined with cooled ambient air blowing) and heating (by compression heat pump combined with heat release in current-carrying conductor due to the Joule effect) capabilities; efficiency increase in cooling and heating modes due to the use of two cooling or heating modes. The shortcomings include the need for permanent charging of compressor and heater power supply, the presence of harmful coolants.

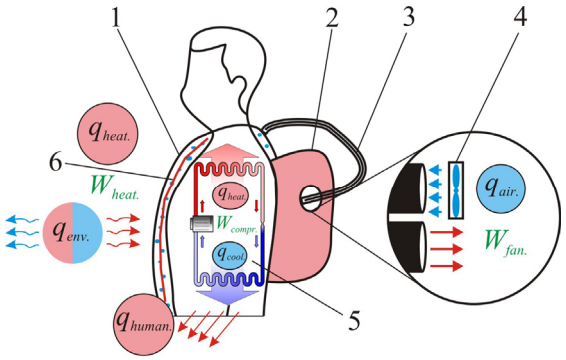


*Fig. 29: 1 – garment with air passage channels 3, 2 – unit comprising an electric fan 4 with power supply, 5 – compression heat pump, 6 – electric heater.*

**Model 2.3.6**

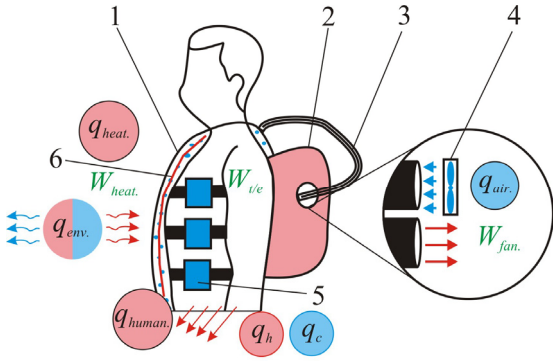


*Fig. 30: 1 – garment with channels 3, 2 – unit comprising and electric fan 4 with power supply, 5 – thermoelectric heat pump, 6 – electric heater.*

Fig. 30 represents a physical model which combines thermoelectric heat pump (item 6), electric heater (item 3) with ambient air blowing (item 2). Its advantages include both cooling (cooling due to the Peltier effect combined with cooled ambient air blowing) and heating (heating due to the Peltier effect combined with heat release in current-carrying conductor due to the Joule effect) capabilities; efficiency increase in cooling and heating modes due to the use of two cooling or heating modes. The shortcomings include the need for permanent charging of thermoelectric converters and heater power supply.

**Model 2.4.5**

Fig. 31 represents a physical model which combines compression heat pump (item 5), a catalytic burner (item 4) with ambient air blowing (item 2). Its advantages include both cooling (mechanical

cooling by compression refrigeration machine combined with cooled ambient air blowing) and heating (by compression heat pump combined with heat release due to catalytic fuel combustion) capabilities; efficiency increase in cooling and heating modes due to the use of two cooling or heating modes. The shortcomings include the need for permanent charging of compressor and heater power supply, the demand for fuel replacement in the burner, the presence of harmful coolants.

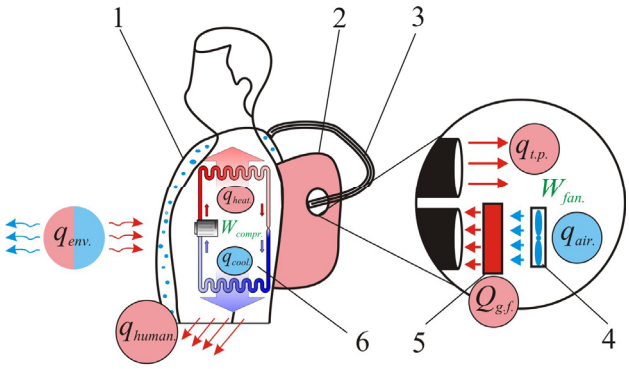


*Fig. 31: 1 – garment with air passage channels 3, 2 – unit comprising an electric fan 4 with power supply, 5 – catalytic heater, 6 – compression heat pump.*

**Model 2.4.6**

Fig. 32 represents a physical model which combines thermoelectric heat pump (item 6), a catalytic burner (item 4) with ambient air blowing (item 2). Its advantages include both cooling (due to the Peltier effect combined with cooled ambient air blowing) and heating (by compression heat pump combined with heat release due to catalytic fuel combustion) capabilities; efficiency increase in cooling and heating modes due to the use of two cooling or heating modes. The shortcomings include the need for permanent charging of thermoelectric converters and heater power supply, the demand for fuel replacement in the burner.

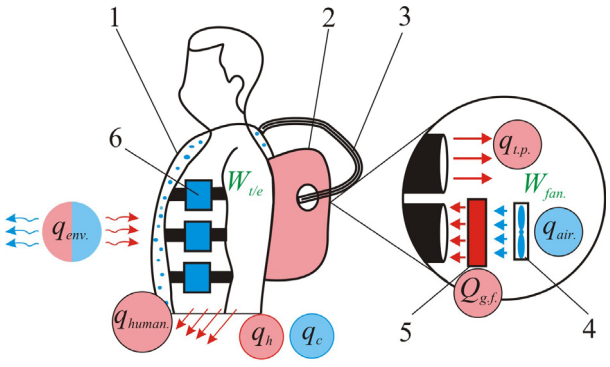


*Fig. 32: 1 – garment with air passage channels 3, 2 – unit comprising an electric fan 4 with power supply, 5 – catalytic heater, 6 – thermoelectric heat pump.*

**Model 1.2.3.5**

Fig. 33 represents a physical model which combines compression heat pump (item 5), electric heater (item 3), heat accumulator (item 1) with ambient air blowing (item 2). Its advantages include both cooling (mechanical cooling by compression refrigeration machine combined with cooled ambient air blowing and substance phase transition) and heating (by compression heat pump combined with heat release in current-carrying conductor due to the Joule effect) capabilities;

efficiency increase in cooling and heating modes due to the use of two cooling or heating modes. The shortcomings include the need for permanent charging of compressor and heater power supply, the demand for heat accumulator replacement, the presence of harmful coolants.

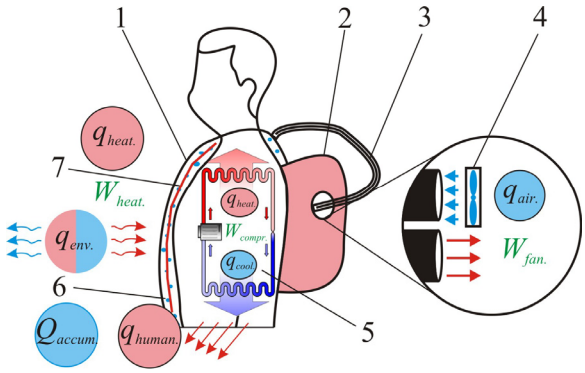


*Fig. 33: 1 – garment with air passage channels 3, 2 – unit comprising an electric fan 4 with power supply, 5 – compression heat pump, 6 – vessel with heat accumulator, 7 – electric heater.*

**Model 1.2.3.6**

Fig. 34 represents a physical model which combines thermoelectric heat pump (item 6), electric heater (item 3), heat accumulator (item 1) with ambient air blowing (item 2). Its advantages include both cooling (cooling due to the Peltier effect combined with cooled air blowing and substance phase transition) and heating (heating to to the Peltier effect combined with heatv release in current-carrying conductor) capabilities; efficiency increase in cooling and heating modes due to the use of two cooling or heating modes. The shortcomings include the need for permanent charging of thermoelectric converters and heater power supply, the demand for replacement of heat accumulator, the presence of harmful coolants.

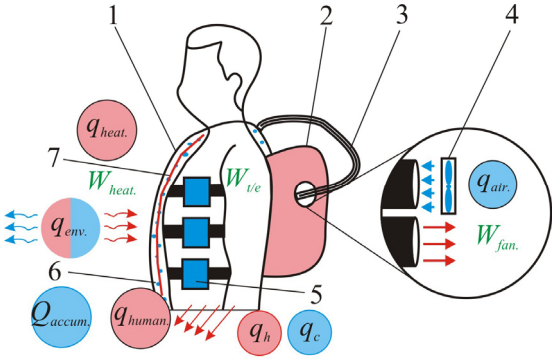


*Fig. 34: 1 – garment with air passage channels 3, 2 – unit comprising and electric fan 4 with power supply, 5 – thermoelectric haet pump, 6 – vessel with heat accumulator, 7 – electric heater.*

**Model 1.2.4.5**

Fig. 35 represents a physical model which combines compression heat pump (item 5), a catalytic burner (item 4), heat accumulator (item 1) with ambient air blowing (item 2). Its advantages include both cooling (mechanical cooling by compression refrigeration machine combined with cooled air blowing and substance phase transition) and heating (by compression heat pump combined with heat release due to catalytic fuel combustion) capabilities; efficiency increase in cooling and

heating modes due to the use of two cooling or heating modes. The shortcomings include the need for permanent charging of compressor power supply, the demand for replacement of heat accumulator and fuel in the heater, the presence of harmful coolants.

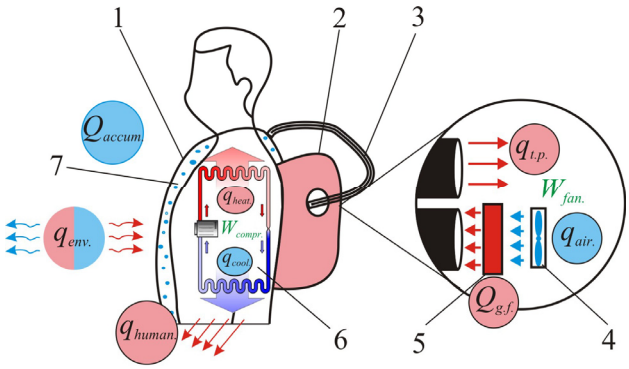


*Fig. 35: 1 – garment with air passage channels 3, 2 – unit comprising an electric fan 4 with power supply, 5 – catalytic heater, 6 – compression heat pump, 7 – vessel with heat accumulator.*

**Model 1.2.4.6**

Fig. 36 represents a physical model which combines thermoelectric heat pump (item 6), catalytic burner (item 4), heat accumulator (item 1) with ambient air blowing (item 2). Its advantages include both cooling (cooling due to the Peltier effect combined with cooled ambient air blowing and substance phase transition) and heating (heating due to the Peltier effect combined with heat release due to catalytic fuel combustion) capabilities; efficiency increase in cooling and heating modes due to the use of two cooling or heating modes. The shortcomings include the need for permanent charging of thermoelectric converters power supply, the demand for replacement of heat accumulator and fuel in the heater.

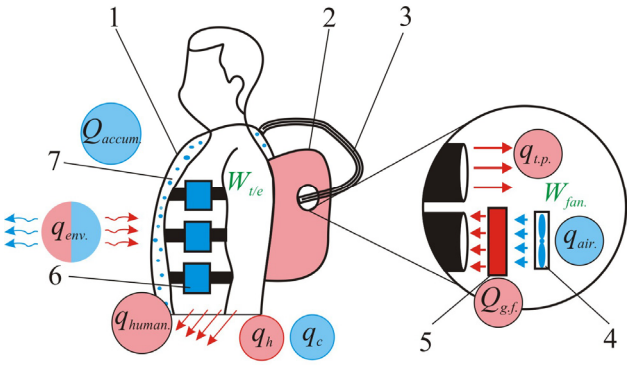


*Fig. 36: 1 – garment with channels 3, 2 – unit comprising and electric fan 4 with power supply, 5 – catalytic heater, 6 – thermoelectric heat pump, 7 – vessel with heat accumulator.*

The analysis of the above described physical models of personal air-conditioners for garment has proved their advantages which makes promising their further study. The results of investigations of such air-conditioners will be presented in the second part of this work.

## Conclusions

1. The features of physical models of personal air-condioners for garment have been analyzed and their detailed classification has been developed.

2. 63 variants of physical models of personal air-conditioners for garment have been proposed, of which only 12 have been studied to date.
3. Analysis of physical models of air-conditioners for garment has enabled us to single out 23 combinations of models that are promising for investigation and practical implementation.

## References

1. Review of the World Market of Air-Conditioning Systems in 2011 – 2012, *Kholodilny Business* 9, (2012).
2. Yu.Dubchak, Sales Growth of Air-Condioners as a Factor of Global Warming *http: //techhome.kiev.ua/articles* (2016).
3. I.E.Shkradyuk, V.A.Chuprov, Technological Pattern of World Power Engineering up to 2050, *Smart Power Toolkit, Greenpeace* (2010).
4. R.R.Kobylianskyi, I.A.Moskalyk, Computer Simulation of Local Thermal Effect on the Biological Tissue, *J.Thermoelectricity* 6, 59 – 68 (2015).
5. N.K.Vitte, *Human Heat Exchange and its Hygienic Significance* (Kyiv: Gosmedizdat, 1956), 148 p.
6. L.I.Anatychuk, K.Misava, N.Sudzuki, Ya.Takai, and Yu.Yu.Rozver, Thermoelectric Air-Conditioner for Rooms, *J.Thermoelectricity* 1, 54 – 56 (2003).
7. *Patent of Ukraine 66389*, InCl 2011.01. Garment for Overheat Protection, /L.V.Moroz, Publ.26.12.11, Bul. № 24.
8. *Pat. US 3950789*, Dry Ice Cooling Jacket / Stephan A. Konz, Jerry R. Duncan. Pub. Date: Apr. 20, 1976.
9. *Pat. CN 203633537 U*, Fan Type Cooling Human Body Air Conditioning Clothes / Tian Weiguo.- Pub. Date: June, 11, 2014.
10. *Pat. US 20060191270 A1,* Air Conditioning System for a Garment / Ray Warren, Pub. Date: Aug, 31, 2006.
11. *Pat. US 20140137596 A1*, Cooling Element / Vincent Dijkema, Erland Bakkers, Pub. Date: May, 22, 2014.
12. *Pat. US 20020073481 A1,* Cooling Garment / Christopher Creagan, Charles Bolian, Irwin Singer, Pub. Date: June, 20, 2002.
13. http://www.inuteq.com.
14. K.-Ch.Noutel, Systems of Working Clothes for Extremely Cold Working Conditions, *Mining Information-Analytical Bulletin* 2 (2002).
15. *Pat. US3524965 A,* Electric Heating Element for Apparel / Stanley Arron, Pub. Date: Aug. 18, 1970.
16. *Pat. US 2002/0156509 A1,* Thermal Control Suit, John A. Baker, Pub. Date: Oct. 24, 2002.
17. *Pat. US 2010/0107657 A1,* Appparel with Heating and Cooling Capabilities, Kranthi K. Vistakula.- Pub. Date: May. 6, 2010.
18. http://dhamainnovations.com.
19. Layered Clothing. (2015, April 11). In Wikipedia, The Free Encyclopedia. Retrieved 16:25, June 27, 2015, from https://en.wikipedia.org/w/index.php title=Layered_clothing&oldid=714783304.
20. A.Nishino, Recent Progress in High-Temperature Catalytic Combustion, *Catal. Today* 10, 107 (1991).
21. Heat Pump (2015, June 21). In Wikipedia, The Free Encyclopedia. Retrieved 16:55, June 27, 2015, from https: //en.wikipedia.org/w/index.php title=Heat_pump&oldid=726328458.

Submitted 19.02.2016.

*R.G. Cherkez*

**R.G. Cherkez**

Yu. Fedkovych Chernivtsi National University,
2, Kotsyubinsky str., Chernivtsi, 58012 Ukraine

# ON THE SIMULATION OF PERMEABLE THERMOELEMENTS

*The results of theoretical research on permeable thermoelements are presented. In Comsol Multiphysics application software package a 3D model of thermoelement is created with regard to temperature dependences of material parameters, the availability of connecting buses, heat spreaders and contact resistances. A method of mathematical optimal control theory and computer design for solving multi-factor optimization problems in a 1D model is described. Computer programs are created to determine design and thermophysical parameters affording maximal values to thermodynamic characteristics of energy conversion. Computer calculations of optimal parameters of permeable thermoelements for various materials based on Bi – Te – Se – Sb are performed. Calculated data point to possible improvement of thermoelectric energy conversion efficiency by a factor of 1.2 – 1.5 as compared to conventional thermoelements.*

**Key words:** permeable thermoelement, energy characteristics, optimization, design.

## Introduction

A promising direction for efficiency increase of thermoelectric energy conversion is the use of physical models of thermoelements wherein heat exchange with the heat source and heat sink occurs not only through the junctions of legs, as in conventional thermoelements, but also in the bulk of the legs material [1, 2]. The variants of such models include permeable thermoelements having channels for pumping liquid or gas heat carrier [3]. The availability of heat exchange in the bulk of the leg increases the intensity of heat transfer, leads to redistribution of temperature fields, potentials and thermal flows, thus affecting the energy characteristics of thermoelement. Having control over thermophysical parameters (heat carrier pumping speed, heat exchange intensity, electric current density, etc.) one can create such operating conditions whereby energy conversion efficiency will be improved.

The first theoretical investigations of permeable thermoelements for gas flows [4 – 6] showed the promising outlook for their creation, since they predict coefficient of performance improvement by 30 – 40 % [7] on air cooling and generator efficiency increase by 20 – 30 % [8] when using low-grade thermal energy of gases. However, such investigations were performed for the simplest model of permeable thermoelement in a one-dimensional approximation without regard to temperature dependences of material parameters, connecting heat spreaders, etc.

Therefore, for a more correct solution of such problems in [9] we pioneered the use of mathematical optimal control theory and studied permeable thermoelements in a 1-D model of semiconductors with regard to their temperature dependences for the homogeneous and functionally graded materials (FGM). This made it possible to create theory of permeable thermoelements of FGM and show the possibilities of energy characteristics improvement in electric energy generation and heat carrier cooling modes by a factor of 1.2 – 1.5.

Creation of a 3-D model of permeable thermoelement is complicated by the necessity to solve a conjugate problem of heat, electro- and mass exchange in solid-heat carrier system. This problem was solved in Comsol Multiphysics application software package for permeable plane thermoelement [10]. However, parameter optimization to find maximum values of energy characteristics in such 3-D cases is difficult. The present paper describes peculiarities of methods for solving problems in 3-D and 1-D cases for different models of permeable thermoelements.

## Physical model, mathematical description and the results of problem solution

For the inhomogeneous isotropic permeable thermoelectric medium (Fig. 1) where there is a steady-state flow of heat, charged particles and energy caused by the presence of temperature gradients $\nabla T$ and electrochemical potential $\nabla\zeta$, exchange and energy conversion processes are described by the fundamental laws of energy and electric charge conversion.

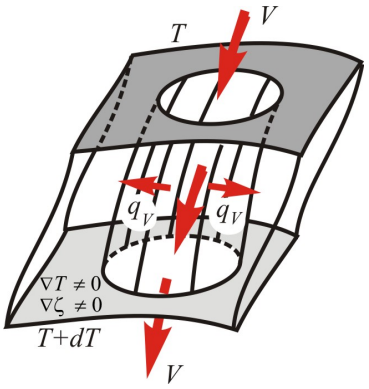


*Fig. 1. Permeable thermoelectric medium.*

In the steady-state case the distribution of temperature $T$ in thermoelectric material is determined by a system of differential equations in partial derivatives

$$\left.\begin{aligned}&\nabla(\kappa\nabla T)+\frac{\vec{\boldsymbol{i}}^{\,2}}{\sigma}-T\frac{\partial\alpha}{\partial T}(\vec{\boldsymbol{i}}\nabla T)-T(\vec{\boldsymbol{i}}\nabla\big|_{T=const}\,\alpha)=0,\\&\nabla(-\sigma\nabla\zeta-\sigma\alpha\nabla T)=0,\end{aligned}\right\} \qquad 1)$$

where $\vec{\boldsymbol{q}}=-\kappa\nabla T+\alpha T\vec{\boldsymbol{i}}$ is heat flux density vector; $\vec{\boldsymbol{i}}=-\sigma\nabla\zeta-\sigma\alpha T$ is current density vector; $\alpha$ is the Seebeck coefficient, $\sigma$ is electric conductivity coefficient; $\kappa$ is thermal conductivity coefficient .

The presence of heat exchange between thermoelectric material and heat carrier necessitates solving (1) conjugate to equations of continuity, motion and thermal conductivity for heat that can be written as follows:

$$\left.\begin{aligned}&\mathrm{div}(\rho_t\vec{\boldsymbol{V}})=0,\\&\rho_t\vec{\boldsymbol{F}}-\nabla p+\mu\nabla^2\vec{\boldsymbol{V}}+\frac{1}{3}\mu\vec{\nabla}(\mathrm{div}(\vec{\boldsymbol{V}}))=0,\\&\rho_t\vec{\boldsymbol{F}}\vec{\boldsymbol{V}}+\mathrm{div}(\Lambda\vec{\boldsymbol{V}})+\mathrm{div}(\kappa_t\nabla t)+\rho_t q_V=0,\end{aligned}\right\} \qquad (2)$$

where $\rho_t$ is heat carrier density; $\vec{\boldsymbol{V}}$ is heat carrier velocity; $\vec{\boldsymbol{F}}$ is mass force; $\rho$ is pressure; $\Lambda$ is stress tensor; $\kappa_t$ is heat carrier thermal conductivity; $q_V$ are internal heat sources; $U$ is internal energy.

To solve such a problem, it is reasonable to use specially developed application software programs of the type Femlab, ANSYS, COMSOL Multiphysics.

A 3-D simulation of generator thermoelement with a lateral heat exchange was performed in [10] on the basis of COMSOL Multiphysics program.

The obtained distribution of temperatures in the leg material based on $Bi-Te$ and in heat carrier (Fig. 2*a*), the distribution of heat carrier velocity (Fig. 2*b*) and potential distribution allow determination of thermodynamic conversion characteristics.

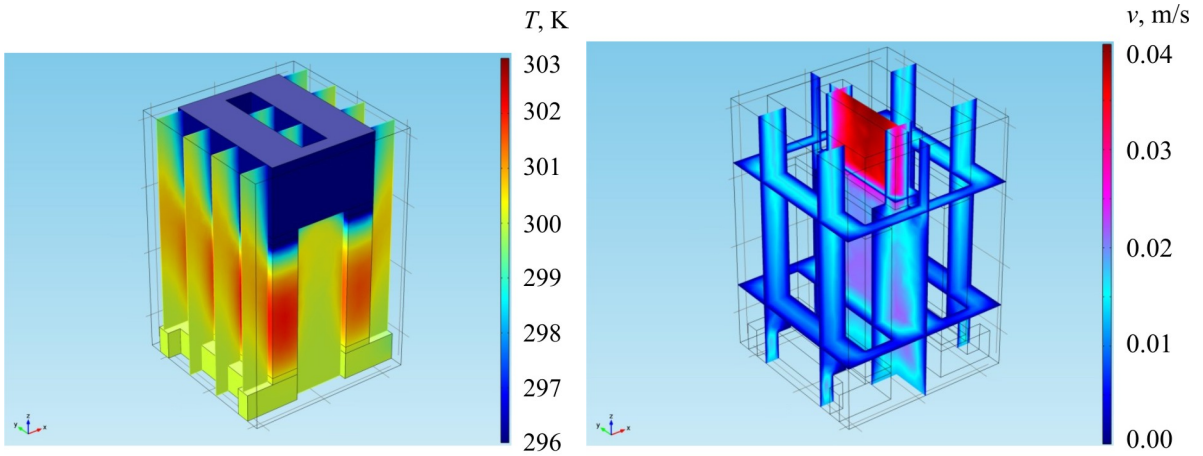


*Fig. 2. Temperature distribution in thermoelement and heat carrier (a), velocity field distribution in heat carrier (b).*

The calculated results point to the fact that with the use of lateral heat exchange large efficiency values are attained when heat exchange takes place at 0.5 of the leg height, and the other part is thermally insulated. The data is also obtained for other thermoelement designs and heat carrier temperature which varies in the range of 700 – 1100 K. The data suggests that the use of lateral heat exchange can yield efficiency increase by 20 – 30 % and electric power increase by 40 – 50 %.

The calculated results indicate a need to solve a multi-parameter optimization problem on finding optimal conditions for thermoelement operation and maximum values of its energy characteristics. However, to perform such multi-parameter optimization for a 3-D model is extremely difficult. The use of a 1-D model makes it possible to perform multi-parameter optimization of the energy characteristics of thermoelements, determine for them such operating conditions which enable one to attain maximum values of energy conversion efficiency.

In a 1-D case the energy characteristics of permeable thermoelement are determined on the basis of solving a system of differential equations for heat carrier and leg material of *n*- and *p*-types given below:

$$\left.\begin{aligned} &\frac{dT}{dx}=-\frac{\alpha j}{\kappa}T-\frac{q}{\kappa},\\ &\frac{dq}{dx}=\frac{\alpha^2 j}{\kappa}T+\frac{\alpha j}{\kappa}q+i^2\rho-\frac{\alpha_T P_K N_K l^2}{(S-S_K)j}(T-t),\\ &\frac{dt}{dx}=\frac{\alpha_T P_K N_K l}{Vc_p S_K}(T-t). \end{aligned}\right\} \qquad (3)$$

where $T,\ t$ is temperature of leg material and heat carrier at point $x$; $j=il$ is reduced electric current density; $l$ is height of thermoelement legs; $i$ is electric current density; $q=\frac{1}{j}\left(\alpha jT-\kappa\frac{dT}{dx}\right)$ is reduced

specific heat flux; $x=\frac{x}{l}$ is dimensionless coordinate; $S_K$ is cross-section area of all channels; $S$ is cross-section of the leg together with the channels; $P_k$ is channel perimeter; $N_K$ is the number of channels in the leg; $V$ is mass velocity of heat carrier in channels; $\alpha_T$ is coefficient of heat exchange in a channel.

For solving optimization problem to find the optimal operating conditions of thermoelement, the works employ Pontryagin's maximum principle of mathematical optimal control theory which yields the necessary optimality conditions:

1) optimal values of specific current density in thermoelement legs $j$ must meet the equalities

$$-\left[\frac{\partial J}{\partial j}\right]_{n,p}+\sum_{n,p}\int_0^1\left[\psi_1\frac{\partial f_1}{\partial j}+\psi_2\frac{\partial f_2}{\partial j}+\psi_3\frac{\partial f_3}{\partial j}\right]_{n,p}dx=0, \tag{4}$$

where $J$ is functional characterizing the efficiency of energy conversion process (efficiency for generators, coefficient of performance for cooling, etc); $\left(f_1,f_2,f_3\right)_{n,p}$ are the right-hand sides of equations (1), $\psi=\left(\psi_1,\psi_2,\psi_3\right)_{n,p}$ is vector function of pulses [12] found from the solution of auxiliary system of differential equations

$$\left.\begin{aligned}
&\frac{d\psi_1}{dx}=\frac{\alpha j}{\kappa}R_1\psi_1-\left(\frac{\alpha j}{\kappa}R_2-\frac{\alpha_e l}{(S-S_{\hat{E}})j}\right)\psi_2+\frac{\alpha_T P_K^1 N_K}{Gc_p}\psi_3,\\
&\frac{d\psi_2}{dx}=\frac{j}{\kappa}\psi_1-\frac{\alpha j}{\kappa}\psi_2,\\
&\frac{d\psi_3}{dx}=\frac{\alpha_T P_K^1 N_K l}{(S-S_{\hat{E}})j}\psi_2-\frac{\alpha_T P_K^1 N_K}{Gc_p}\psi_3,
\end{aligned}\right\}_{n,p} \tag{5}$$

where

$$\left.\begin{aligned}
&R_1=1+\frac{d\ln\alpha}{dT}T-\frac{d\ln\kappa}{dT}\left(T+\frac{q}{\alpha}\right),\\
&R_2=R_1+\frac{\kappa}{\alpha^2\sigma}\frac{d\ln\sigma}{dT}+\frac{d\ln\kappa}{dT}\left(T+\frac{q}{\alpha}\right)
\end{aligned}\right\}_{n,p}$$

2) optimal values of required parameters $\omega_i=(\omega_1,\ldots,\omega_r)$, are found from the system of integral-differential equations

$$-\left[\frac{\partial J}{\partial\omega_i}\right]_{n,p}+\sum_{n,p}\int_0^1\left[\psi_1\frac{\partial f_1}{\partial\omega_i}+\psi_2\frac{\partial f_2}{\partial\omega_i}+\psi_3\frac{\partial f_3}{\partial\omega_i}\right]_{n,p}dx=0,\cdot\cdot i=1,\ldots,r. \tag{6}$$

Based on the above ratios, with the use of successive approximations methods, numerical methods of solving the systems of differential equations (3) and (5), the Newton method of solving the systems of integral differential equations (6), computer program for design of permeable thermoelement has been developed [10].

The results of such calculations of permeable generator thermoelement of *Bi – Te – Se – Sb* based materials under optimal operating conditions are given in Fig. 3.

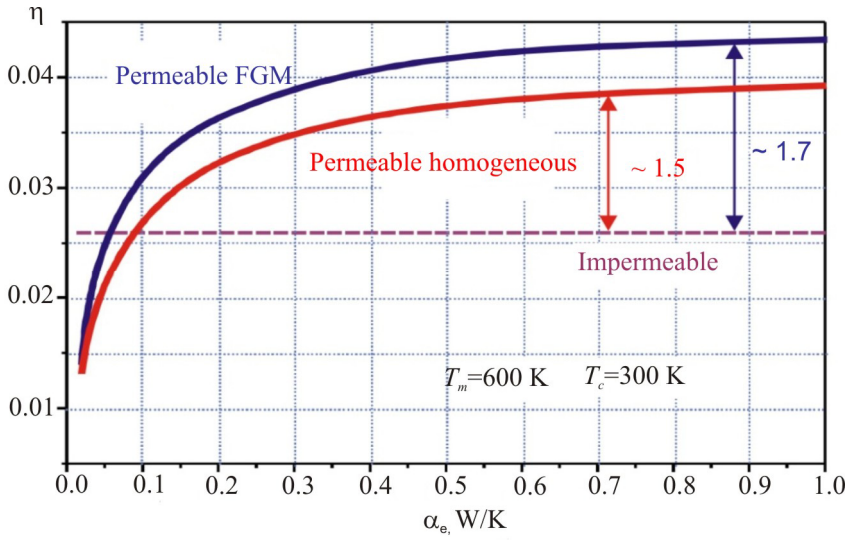


*Fig. 3. Thermoelements efficiency versus the effective heat exchange coefficient.*

As is evident, the efficiency of energy conversion with the use of permeable thermoelements made of homogeneous and functionally-graded materials can be increased by a factor of 1.2 – 1.5 as compared to impermeable thermoelements.

## Conclusions

A physical model and method for calculation and design of permeable thermoelement where heat carrier is pumped through the legs of semiconductor material is described. A comparison between the results of calculation of a 3-D model and a one-dimensional thermoelement model (1-D) shows that a 1-D model with regard to the bulk thermoelectric effects realistically describes the processes of thermal and electric conductivity in thermoelectric medium.

For *Bi – Te – Se – Sb* based materials the effect of design parameters (channel diameter and their number, leg height and the number of segments) on the energy characteristics under optimal operating conditions in terms of thermoelement efficiency is calculated. The rational values of these parameters are determined which make it possible to establish the necessary material science requirements for creation of thermoelement.

Comparison to conventional thermoelements in terms of thermodynamic efficiency of energy conversion has shown the possibility of efficiency increase by a factor of 1.2 – 1.5.

## References

1. L.I.Anatychuk, *Thermoelectricity, Vol.1, Physics of Thermoelectricity* (Chernivtsi, 1998), 388p.
2. D.T.Crane, J.W. LaGrandeur, F.Harris, L.E.Bell, Performance Results of a High Power Density Thermoelectric Generator: Beyond the Couple, *Proceedings of the International Conference on Thermoelectrics (Corvallis, OR, August 2008).*
3. Method for Efficiency Increase of Thermoelectric Generator (Cooler): The USSR Certificate of Authorship 144883 / Zorin I.V.: Filed 24.06.1961.
4. G.K.Kotyrlo, G.M.Schegolev, *Thermal Circuits of Thermoelectric Devices* (Kyiv: Naukova Dumka, 1973), 107 p.
5. L.I.Anatychuk, R.G.Cherkez, Permeable Thermoelement in Electric Energy Generation Mode, *J.Thermoelectricity* 2, 35 – 46 (2003).

6. L.I.Anatychuk and R.G.Cherkez, Energy Potential of Permeable Segmented Thermoelements in Cooling Mode, *Journal of Electronic Materials* 41(6), 1115 – 1119 (2012).
7. R.Cherkez, Theoretical Studies on the Efficiency of Air Conditioner Based on Permeable Thermoelectric Converter, *Applied Thermal Engineering* 38, 7 – 13 (2012).
8. L.I.Anatychuk, R.G.Cherkez, Permeable Segmented Thermoelement in Electric Power Generation Mode, *J.Thermoelectricity* №3, 5 – 12 (2010).
9. L.I.Anatychuk, R.G.Cherkez, Permeable Planar Cooling Thermoelement, *J. Thermoelectricity* 3, 5 – 12 (2008).
10. R.G.Cherkez, Energy Characteristics of Thermoelement with a Developed Lateral Heat Exchange, *J.Thermoelectricity* 3, 59 – 68 (2012).
11. L.I.Anatychuk, R.G.Cherkez, D.D.Demyanyuk, and N.R. Bukharayeva, Research on the Energy Characteristics of Permeable Planar Thermoelement, J.Thermoelectricity 2, 84 –88 (2012).
12. L.S.Pontryagin, V.G.Boltyansky, R.V.Gamkrelidze, and E.F.Mischenko, *Mathematical Theory of Optimal Processes* (Moscow: Nauka, 1976), 392 p.

Submitted 22.01.2016.

*A.I. Anukhin*

**A.I. Anukhin, V.V. Razinkov**

Institute of Thermoelectricity of the NAS and MES
of Ukraine, 1, Nauky str., Chernivtsi,
58029, Ukraine

*V.V. Razinkov*

# CRYSTALLIZATIONS OF SOLID SOLUTIONS OF BISMUTH AND ANTIMONY TELLURIDES BY ZONE MELTING AND NORMAL CRYSTALLIZATION

*This paper presents the results of mathematical simulation of normal crystallization and zone melting of solid solutions of bismuth and antimony tellurides. Components distribution along the ingot length for the cases of zone recrystallization and zone leveling is given.*

**Key words:** thermoelectric materials, solid solutions of bismuth and antimony tellurides, zone melting, crystallization.

## Introduction

The main *p*-type thermoelectric materials used for creation of thermoelectric cooling devices are based on the alloys of bismuth and antimony tellurides [1]. The highest thermoelectric figure of merit is attained by solid solutions as the most homogeneous materials among the alloys [2]. The solid solutions of bismuth and antimony tellurides are obtained from the melt by normal crystallization or zone melting that can also include zone leveling. Prediction of components distribution along the ingots and, hence, description of the distribution of their electrophysical properties seems to be a challenging task, since crystallization proceeds in multi-component systems with components distribution factors depending on chemical composition and the temperature of the melt. In the present paper, on the basis of mathematical model, iteration method is used to determine components distribution at crystallization of solid solutions of bismuth and antimony tellurides by zone melting and normal crystallization.

## The basic concepts of the model

The solid solutions of bismuth and antimony tellurides possess a narrow homogeneity region near the stoichiometric composition, in which case the factor of antimony telluride distribution in bismuth telluride depends on the concentration of $Te - Sb$ in the melt and the melt temperature [2]. Mathematical description of mass exchange process in the solid solutions is a complicated problem which has not been solved yet. Here, for the mathematical description of components distribution at crystallization in $Bi - Sb - Te$ system the iteration method is used. As a first approximation, the equality to zero of tellurium distribution factor in $(Bi, Sb)_2Te_3$ solid solutions is assumed [2], in which case the system is viewed as binary – $(Bi, Sb)_2Te_3 - Te$. As a second approximation, the dependence of antimony telluride distribution factor on the concentration of tellurium in the melt in $(Bi, Sb)_2Te_3 - Te$ binary system is viewed as linear, since antimony telluride distribution factor depends on components concentration. As a third approximation, tellurium solubility in $(Bi, Sb)_2Te_3$ solid solution is taken into account.

In the most general case of crystallization from the melt (irrespective of crystallization method) a differential equation for the description of concentration of superstoichiometric tellurium in Pfann's assumptions with an arbitrary ingot section is given below [4]:

$$\frac{dC}{dV}+\frac{C(\frac{dV_{liquid}}{dV}+k)}{V_{liquid}}=\frac{C_0(\frac{dV_{liquid}}{dV}+1)k}{V_{liquid}} \quad , \tag{1}$$

where $C$ is component concentration in solid phase, $C_o$ is initial component concentration, $k$ is component distribution factor, $V_{liquid}$ is melt volume, $V$ is crystallized part volume.

The boundary conditions for equation (1):

$$C(0) = kC_o,$$

$$V_{liquid}(0) = 0. \tag{2}$$

Let us consider mass exchange processes for both crystallizations individually. For normal crystallization $\frac{dV_{liquid}}{dV}=-1$. In the approximation of equality to zero of tellurium distribution factor for normal crystallization Eq. (1) is of the form:

$$\frac{dC}{dV}-\frac{C}{V_{liquid}}=0\,. \tag{3}$$

The concentration of superstoichiometric tellurium in the melt with regard to the boundary conditions (2) is given by equation:

$$C=\frac{C_0}{1-G}\,, \tag{4}$$

where $G$ is specific part of solid phase in the ingot which is determined by coordinate $X$ of crystallization front from the beginning of the ingot

$$C=\frac{C_0}{1-X}\,. \tag{5}$$

For the case of zone recrystallization $\frac{dV_{liquid}}{dV}=0$ and Eq. (1) takes on the form:

$$\frac{dC}{dV}=\frac{C_0}{V_{liquid}}\,. \tag{6}$$

The distribution of superstoichiometric tellurium concentration in the zone melt is determined from Eq. (6):

$$C=C_0(1+\frac{X}{V_{liquid}}). \tag{7}$$

The value of melt volume $V_{liquid}$ for the case of constant ingot section is advisable to be replaced by the length of molten zone $l$. As a result, we get a change in the concentration of superstoichiometric tellurium along the length of zone recrystallized ingot which is determined by the width of molten zone. At zone leveling the concentration of superstoichiometric tellurium in the melt is not changed and remains constant during the entire back pass of the zone and is equal to:

$$C = C_0(1 + \frac{L}{l}), \tag{8}$$

where $L$ is the length of zone forward pass along the ingot.

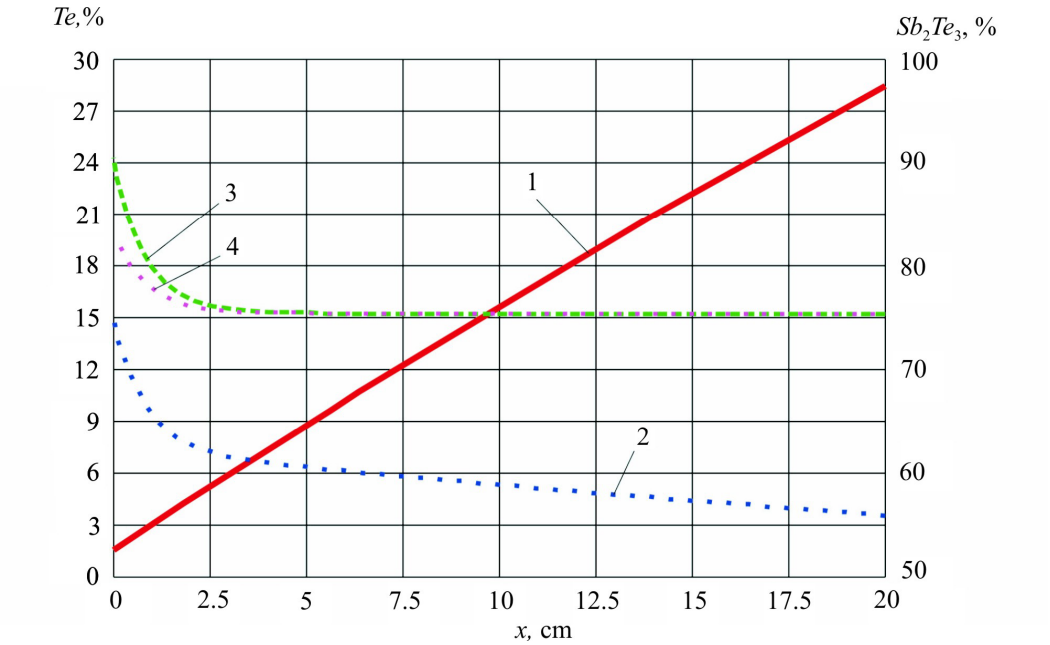


*Fig. 1. Estimated change in components concentration along the ingot length: 1 – superstoichiometric tellurium $C_{Te\_liquid}(x)$, 2 – antimony telluride $C_{TeSb\_liquid}(x)$ in the melt in the first pass of the zone, 3 – antimony telluride in the solid phase $C_{TeSb\_solid}(x)$ in the first pass of the zone, 4 – antimony telluride in the solid phase $C_{TeSb\_back\_solid}(x)$ in the back pass of the zone.*

The result of integration of material balance equation is represented in Fig. 1.

For the case of zone recrystallization the dependences of distribution factors have been obtained under the following assumptions:

- antimony telluride distribution factor $k_{Sb_2Te_3}$ is linearly dependent on the concentration of stoichiometric tellurium $C_{Te}$ / $k_{Sb_2Te_3} = k_0 + \alpha * C_{Te}$, where α = 0.05;
- superstoichiometric tellurium distribution factor is equal to 0.01;
- the concentration of antimony telluride is equal to 75 % (the most common compositions);
- antimony telluride distribution factor for stoichiometric compositions is equal to 1.02 [3];
- the ingot length is assumed to be equal to 20 cm;
- the initial concentration of superstoichiometric tellurium is assumed to be equal to 1.5 %.

It follows from the plots that concentrations of components and their change in the zone melt do not affect the distribution of antimony telluride at zone leveling. Therefore, the concentration of dissolved tellurium will be determined only by the achieved value of superstoichiometric concentration in the zone melt at the end of the ingot. With a single zone pass along the ingot, the concentration of tellurium will linearly increase in the zone melt.

## Discussion of the results

As a first approximation, the result of solving the problem of components distribution in the first zone pass is a linear change in the concentration of superstoichiometric tellurium in the zone melt when moving along the ingot (Fig. 1, dependence 1). At the same time, at normal crystallization

the concentration of superstoichiometric tellurium in the zone melt changes inversely proportional to crystallization front coordinate from the beginning of the ingot. This result is important, since it enables one to determine of which composition (with respect to tellurium) the solid solution was crystallized at zone melting. The latter is a simple method of controlling the chemical composition of the zone melt. For instance, changing ingot length, one can easily change melt composition, since in the back pass of zone leveling the concentration of tellurium in the zone will be constant and depend only on three values, namely the initial concentration of tellurium $C_{Te}$ in the charge, ingot length $L$ and molten zone length $l$. The value $\frac{L}{l}$ can be assumed as a technological parameter of ingot growth process.

The linear dependence of the concentration of superstoichiometric tellurium on the zone coordinate enables one to get "property-chemical composition" diagrams for a specific crosscut of zone recrystallized ingot along its length. As it follows from the numerical solution of differential material balance equation, antimony telluride concentration in the solid phase remains equal to its concentration in the charge, except for the initial part of the ingot. Therefore, after zone recrystallization the ratio between the concentrations of bismuth and antimony tellurides remains unchanged. In the initial part of the ingot the concentration of antimony telluride is higher than in the charge, and it must be taken into account in the construction of diagrams.

## Conclusions

1. At zone melting, the concentration of superstoichiometric tellurium in the zone melt is linearly increased in proportion to crystallization front coordinate from the beginning of the ingot.
2. At zone leveling, the concentration of superstoichiometric tellurium in the melt is constant and equal to concentration achieved at the end of the first zone pass.
3. With a normal crystallization, the concentration of superstoichiometric tellurium in the melt is changed inversely proportional to crystallization front coordinate from the beginning of the ingot.
4. In the solid phase the concentration of antimony telluride remains constant along the ingot length, except for its initial part, both at zone melting and at zone leveling.
5. Linear change in the concentration of superstoichiometric tellurium in the zone and constancy of antimony telluride concentration along the ingot length must be taken into account in the construction of "property-composition" diagrams for different crosscuts of solid solutions of bismuth and antimony tellurides.

## References

1. L.I.Anatychuk, Current Status and Some Prospects of Thermoelectricity, *J.Thermoelectricity* 2, 7 – 20 (2007).
2. A.F.Ioffe, L.S.Stilbans, E.K.Iordanishvili, and G.S.Stavitskaya, *Thermoelectric Cooling* (Moscow-Leningrad: AN SSSR Publ., 1956), 110 p.
3. W.M.Yin and A. Amith, *Bi – Sb* Alloys for Magneto-Thermoelectric and Peltier Cooling, *Solid-State Electronics* 15, 1141 – 1165 (1972).
4. V.N.Vigdorovich, *Zone Recrystallization Improvement* (Moscow: Metallurgiya, 1974), 200 p.

Submitted 04.02.2016.

*V.Ya. Mykhailovsky*

**V.Ya. Mykhailovsky, M.V. Maksimuk**

Institute of Thermoelectricity of the NAS
and MES of Ukraine,
1, Nauky Str., Chernivtsi, 58029, Ukraine

*M.V. Maksimuk*

# COMPUTER DESIGN OF THERMOELECTRIC AUTOMOBILE STARTING PRE-HEATER OPERATED WITH DIESEL FUEL

*The results of computer design of a 70 – 90 W thermoelectric automobile heater operated with diesel fuel for start heating of engine under low ambient temperatures are presented.*
**Key words:** computer design, physical model, starting pre-heater, thermoelectric generator.

## Introduction

The specific feature of diesel internal combustion engine is that compression stroke parameters (pressure and temperature) determine the reliability of fuel self-ignition. For a reliable start-up of diesel engine the temperature of the end of the compression stroke must exceed the temperature of fuel self-ignition. At engine start-up under low ambient temperatures the temperature of the end of the compression stroke is reduced for a number of reasons. Thus, reduction of engine crankshaft speed leads to a reduction of average piston speed. As a result, the time allotted for compression process is increased. Low temperature of engine cylinder walls is responsible for higher intensity of heat exchange between the air and cylinder walls, which leads to increased heat loss in the process of diesel fuel compression. Moreover, the temperature of the end of the compression stroke is reduced due to cold air coming to cylinders.

Under low ambient temperatures the reduction of compression temperature is affected by the non-uniform piston speed. In this case not only the time of heat exchange between “air charge” and cylinder walls is increased, but there is also maximum temperature difference between them, so heat loss due to heat exchange becomes greater. Due to reduced piston speed and insufficiently firm adherence of piston rings to cylinder walls, there is a loss of air flowing in the gaps between the piston and cylinder. So, in addition to reduced temperature of the end of the compression stroke, there is also an additional pressure reduction.

Low air temperature also has a negative effect on the quality of fuel spraying by engine nozzles, which also complicates start-up of internal combustion engine. It is primarily related to increase in diesel fuel viscosity, increase in its surface tension forces and, as a result, formation of waxes. Inferior quality of fuel spraying, low temperature and pressure values under compression increase the time of fuel ignition, complicating start-up of diesel engine. Sometimes a combination of these factors does not guarantee at all the conditions for diesel fuel self-ignition and engine start-up becomes impossible [1].

So far, the most efficient method for pre-heating of diesel engines and their reliable start-up is autonomous start heating. Such heaters are suitable practically for all types of transport means, so they are used in the cars and trucks, as well as in the buses, planes, yachts and motor boats. Moreover, the use of such equipment provides for a reduction of toxic discharge with automobile

exhaust gases by a factor of 5, increase in engine service life by 50 – 60 thousand km and saving of 90 –150 l of fuel during only one winter season [2].

However, one of the main constraining factors for a wide practical application of such equipment is the need for electric energy to power components of starting pre-heaters, such as a fuel pump, a fan for air delivery to combustion chamber, a circulating pump for pumping of liquid heat carrier. For instance, in operation of liquid heater of thermal power 4 kW and electric power consumption 37 – 40 W, and together with a standard fan of automobile heating system – 60 W, a storage battery of capacity 60 A·h in as few as 4.5 hours loses 50 % of capacity. To prevent from a "deep" discharge of storage battery by strong frosts it is recommended not only to switch off completely the function of interior heating, but also to refuse from using additional equipment installed in the car (audio- and video complexes, GPS-navigators, signaling systems). As practice shows, drivers who drive a car for less than 30 min throughout the day (home-office-home) and operate the heater prior to each engine start -up for 20 – 30 min, will not avoid weekly recharging of storage battery [3].

Note that so far none of known models of starting pre-heaters have solved the problem of battery discharge. Most common methods of heating cold automobile engine without the use of storage battery energy include electric heating and heating by means of thermal accumulators. However, in this case a driver is constantly confined to external power supply.

As shown in [4], said problem is solved by means of thermoelectric generator. As well as start heating process becomes fully autonomous, without the use of storage battery electric energy, the excess energy of thermal generator can be used for recharging storage battery and power supply to other automobile equipment.

In [5], analysis of technical specifications of starting pre-heaters for various kinds of transport means is made and electrical parameters of thermal generators necessary for the autonomous operation of such heaters are determined. Thus, total electric power of thermal generator for starting pre-heaters of transport means with engine displacement to 4 l must be 70 – 90 W; for transport means with engine displacement 4 – 10 l and over 10 l – 130 – 150 W, 230 – 250 W, respectively. Besides, such electric powers of thermal generator will allow power supply to a standard fan heater of transport means and storage battery recharging.

Therefore, *the purpose* of the work is to design a 70 – 90 W thermoelectric automobile starting pre-heater operated with diesel fuel for start heating of engine under conditions of low ambient temperatures.

## Design selection of thermoelectric starting pre-heater

Fig. 1. shows a schematic of automobile starting pre-heater with thermoelectric power supply. Structurally, such thermoelectric pre-heater is composed of the hot heat exchanger 1 accommodating in its internal space the source of heat 2 for flame combustion of liquid or gas fuel and air delivery fan 3 for fuel combustion. Fuel delivery to the source of heat is done by fuel pump 4. On the external surface of the hot heat exchanger there are thermoelectric modules 5 the heat from which is removed by liquid heat exchangers 6.

Liquid heat exchangers are combined into one hydraulic loop connected to engine cooling system with connecting pipes 7. Circulation of liquid heat carrier in the "heater-engine" loop is done by pump 8. Combustion products are removed to the environment by exhaust pipe 9. Start-up and operation control of all pre-heater devices (fan, fuel and circulating pumps) is done by electronic unit 10.

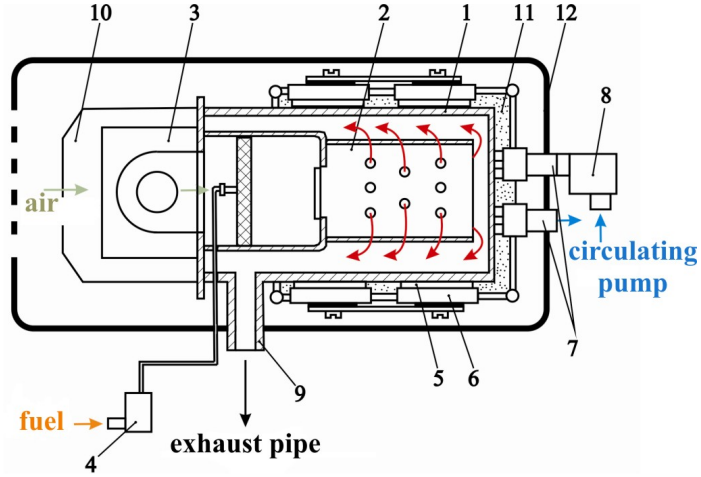


*Fig. 1. Schematic of automobile starting pre-heater with thermoelectric power supply: 1 – hot heat exchanger; 2 – source of heat; 3 – fan; 4 – fuel pump; 5 – thermoelectric module; 6 – cold heat exchanger; 7 – inlet and outlet connecting pipes; 8 – circulating pump; 9 – exhaust pipe; 10 – electronic unit; 11 – thermal insulation; 12 – case [6].*

Free space between the hot and cold heat exchangers is filled with thermal insulation 11. Automobile heater with a fan, electronic unit, heat exchangers and thermoelectric modules is placed in case 12.

The heater works as follows. Thermal energy from fuel combustion heats the hot heat exchanger, passes through thermoelectric converter and is removed by liquid heat carrier circulating in the heat exchanger of the heater and engine cooling system. Due to temperature difference between the hot and cold sides the thermal converter generates electric current. Thermal energy removed by heat carrier from the thermal converter is used for engine warm-up and heating of car interior.

As a source of heat, use was made of a diesel burner of maximum thermal power 4 kW of liquid starting pre-heater “Thermo Top Evo 4” (Webasto). The schematic and appearance of the burner is presented in Fig. 2.

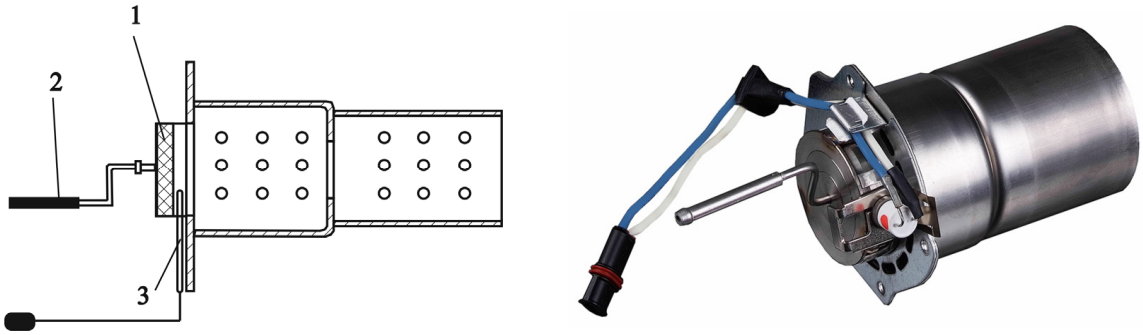


*a)* *b)*

*Fig. 2. Schematic (a ) and appearance (b) of diesel burner Ersatzbrenner D TT-C MB (Webasto): 1 – evaporator; 2 – fuel pipe; 3 – starting electrode [7].*

The most rational shape of the hot heat exchanger in terms of efficient heat exchange with the source of heat is a cylinder pipe with one end closed and the other end accommodating a diesel burner. The external surface of the heat exchanger has the form of planes where thermoelectric modules are arranged.

The thermoelectric converter is composed of thermoelectric modules based on bismuth telluride of the type “ALTEC-1061” which on arrival of the necessary amount of heat to the hot side and on achievement of optimal operating temperatures assure generation of the assigned electric

power. Fig. 3 shows a three-dimensional graphical image of the dependence of electric power $P'$ and efficiency $\eta'$ on the hot side $T_h$ and cold side $T_c$ temperature of thermoelectric module "ALTEC-1061".

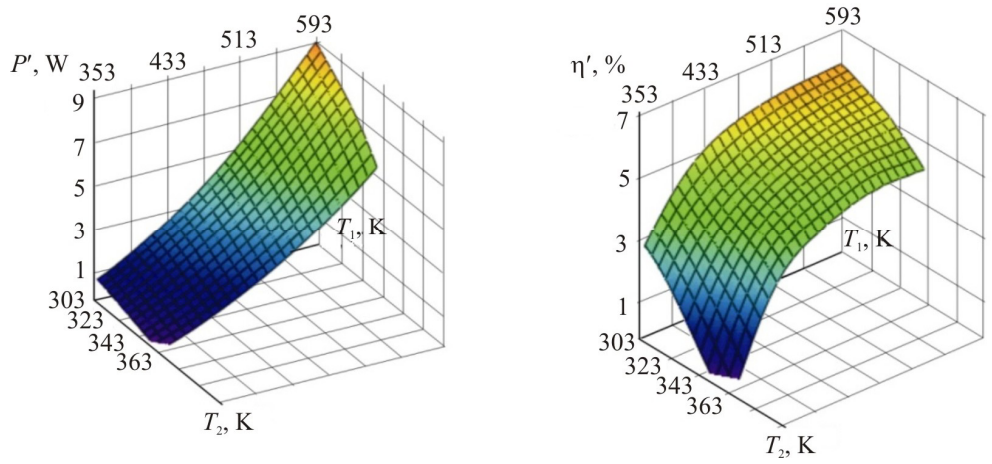


*a)* *b)*

*Fig. 3. Dependence of electric power $P'$ (a) and efficiency $\eta'$ (b) on the hot side Th and cold side Tc temperature of thermoelectric module "ALTEC-1061" [8].*

From the analysis of data presented in Fig. 3 it follows that to provide the output electric power of the heater 90 – 70 W, it is necessary to have 12 modules "ALTEC-1061". From these considerations, the most efficient design of the hot heat exchanger is a regular hexahedron, with 2 thermoelectric modules arranged on each side thereof. In so doing, the hot side temperature of modules must be 330 – 280 °C, the cold side – 30 – 70 °C.

For diesel fuel delivery use was made of a pulse fuel pump (Fig. 4) of liquid starting pre-heater "Thermo Top E" (Webasto). The experimentally found dependence of fuel combustion $g_n$ and thermal power $Q$ of diesel burner on pulse period $t$ of fuel pump is given in Fig. 5. From the data given in Fig. 5 it is seen that the heat source maximum power 4 kW is achieved with a pulse period of fuel pump 0.5 s. In so doing, fuel consumption is ~ 350 g/h.

*Fig. 4. Appearance of fuel pump BTL.DP30.02.12V DAEMPFLER E-TEIL (Webasto) [7].*

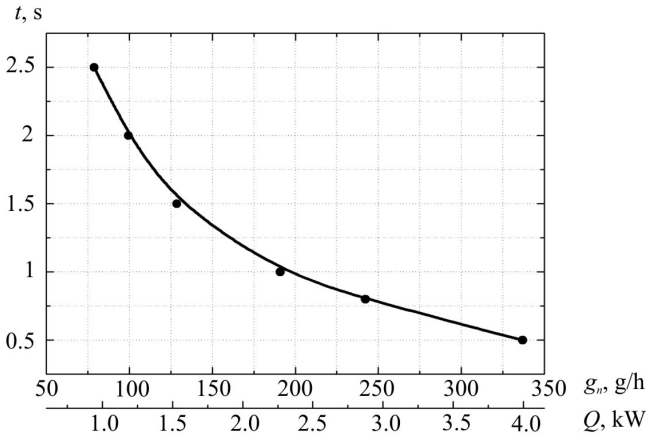


*Fig. 5. Dependence of fuel consumption $g_n$ and thermal power Q on pulse period t of fuel pump.*

Taking into account that the efficiency of thermoelectric generators using single-stage modules based on bismuth telluride is 3 – 3.5 % [9], to assure the output electric power of the heater 90 – 70 W, it is necessary to spend ~ 2.3 – 2.5 kW of heat which corresponds to fuel consumption 180 – 220 g/h.

As a circulating pump, the liquid pump (Fig. 6) of staring pre-heater "Thermo Top C" (Webasto) was used. This type of the pump is specially designed for pumping of heat carrier in transport means with engine displacement 2.5 – 4 l. Fig. 7 shows the experimentally determined dependence of liquid fuel consumption $q_T$ on the supply voltage $U$ of the pump.

*Fig. 6. Appearance of liquid pump 12V U4847 TT C/E (Webasto) [7].*

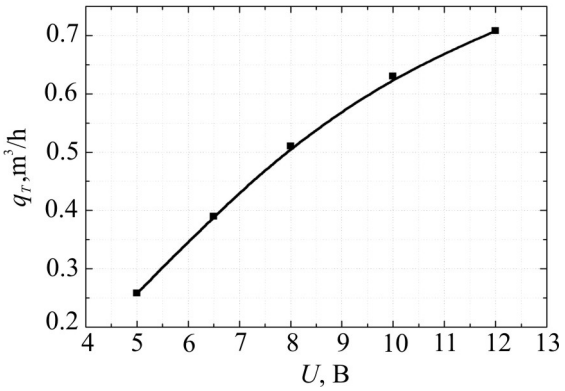


*Fig. 7. Dependence of liquid heat carrier consumption $q_T$ on the supply voltage U of the pump.*

Fuel pump starts pumping heat carrier at supply voltage 5 V with consumption 0.25 $m^3$/h. At a voltage of 12 V heat carrier consumption is maximum – 0.7 $m^3$/h.

## Physical model of thermoelectric starting pre-heater and its description

A physical model of thermoelectric automobile starting pre-heater is presented in Fig. 8.

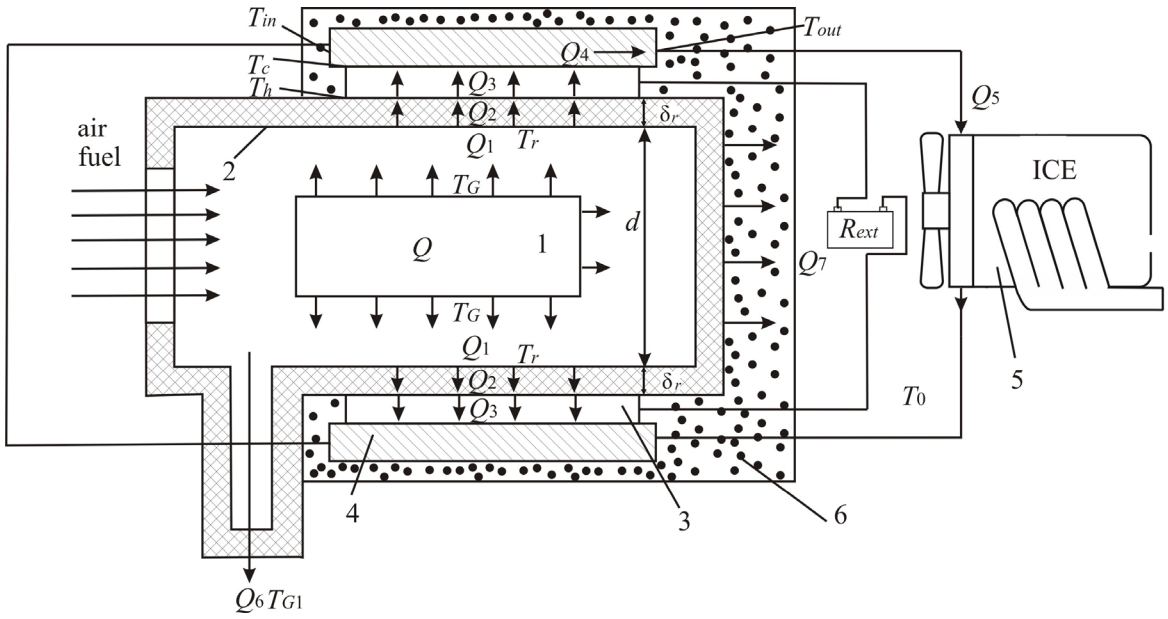


*Fig. 8. Physical model of thermoelectric automobile heater:*
*1 – heat source; 2 – hot heat exchanger; 3 – thermopile;*
*4 – cold heat exchanger; 5 – automobile engine; 6 – thermal insulation.*

The source of heat 1 in thermoelectric automobile heater is chemical reaction of diesel fuel flame combustion resulting in the release of thermal power $Q$.

$$Q = g_n G_n, \tag{1}$$

where $G_n$ is calorific power of diesel fuel; $g_n$ is diesel fuel consumption.

Heat $Q_1$ coming from the heat source to the hot heat exchanger 2 is transferred due to convection and radiation:

$$Q_1 = \alpha \cdot (T_G - T_r) \cdot S_R + \varepsilon \cdot \sigma_0 \cdot \left( \varepsilon_G \cdot \left( \frac{T_G}{100} \right)^4 - A_r \cdot \left( \frac{T_r}{100} \right)^4 \right) \cdot S_R, \tag{2}$$

where $\alpha$ is convective coefficient of heat transfer from the hot gas to heat-absorbing surface of the hot heat exchanger;

$T_G$ is average gas temperature in the hot heat exchanger;

$T_r$ is average temperature of the heat-absorbing surface of the hot heat exchanger;

$S_R$ is the area of the heat-absorbing surface of the hot heat exchanger;

$\varepsilon = (\varepsilon_r + 1)/2$ is effective emissivity factor of the "hot gas-heat-absorbing surface" system of the hot heat exchanger;

$\varepsilon_r$ is emissivity factor of the heat-absorbing surface of the hot heat exchanger;

$\sigma_0$ is Stephan-Boltzmann constant;

$\varepsilon_G$ is gas emissivity factor;

$A_r$ is absorbing ability of the heat-absorbing surface of the hot heat exchanger.

Heat $Q_2$ is transferred due to thermal conductivity from the heat-absorbing surface of the hot exchanger to the hot side of thermopile 3:

$$Q_2 = \frac{S_r \cdot \lambda_r}{\delta_r} \cdot (T_r - T_h), \tag{3}$$

$S_r$ is the area of the heat-releasing surface of the hot heat exchanger;

$\lambda_r$ is thermal conductivity of heat exchanger material;

$\delta_r$ is thickness of heat exchanger base;

$T_h$ is temperature of the thermopile hot side.

Useful heat $Q_3$ coming to thermoelectric modules was calculated from the power $P'$ of one module with determined hot side $T_h$ and cold side $T_c$ temperatures of thermopile, its efficiency $\eta'$ and the number of modules $n$:

$$Q_3(T_h, T_x) = n \cdot \frac{P'(T_h, T_c)}{\eta'(T_h, T_c)}. \tag{4}$$

Heat $Q_4$ is removed from the cold side of thermopile by heat carrier flow circulating in the cold liquid heat exchanger 4:

$$Q_4 = g_T \cdot c_{pT} \cdot (T_{in} - T_{out}), \tag{5}$$

where $g_T$ is heat carrier consumption $c_{pT}$ is heat carrier heat capacity $T_{in}$, $T_{out}$ are heat carrier temperatures at inlet to and outlet of thermopile cooling system, respectively.

As long as cold liquid heat exchangers are combined into one hydraulic loop with engine cooling system 5, the heat removed by heat carrier from the modules is spent on start heating of engine:

$$Q_5 = c_{eng} \cdot m_{eng} \cdot (T_{out} - T_0), \tag{6}$$

where $c_{eng}$, $m_{eng}$ are heat capacity and mass of automobile engine, respectively; $T_0$ is ambient temperature.

Basic heat losses:

1) $Q_6$ – with reaction products (water $H_2O$, carbon dioxide $CO_2$ and nitrogen $N_2$):

$$Q_6 = C_c \cdot m_c \cdot (T_{G1} - T_0), \tag{7}$$

where $C_c$ is average heat capacity of reaction products, $m_c$ is mass of reaction products, $T_{G1}$ is temperature of reaction products.

2) $Q_7$ – on thermal insulation :

$$Q_7 = \frac{\lambda S_{ph}}{L}(T_B - T_0), \tag{8}$$

where λ is thermal conductivity of insulating material; $S_{ph}$ is the area of the hot heat exchanger surface which is not occupied by thermopile; $L$ is thickness of thermal insulation layer.

Thus, heat balance equation for the selected model of thermoelectric automobile heater can be written as:

$$\begin{cases} Q = Q_1 + Q_6, \\ Q_1 = Q_2 + Q_7, \\ Q_2 = P + Q_4. \end{cases} \tag{9}$$

Solving the system of heat balance equations (9) enables one to determine the basic energy and design parameters of thermoelectric automobile heater.

Computer design of thermoelectric automobile heater was conducted in two stages aimed at determining:

– gas temperature $T_G$ in the hot heat exchanger and the effective area of heat-absorbing surface of the hot heat exchanger $S_R$ to assure on the hot side of the thermopile the temperature $T_h$ = 330 – 280 °C.

– thermal power $Q_5$ removed by heat carrier to estimate the warm-up rate of automobile engine.

## Calculation of hot gas temperature

The process of heating gases in the hot heat exchanger that formed due to diesel fuel combustion is described by equation:

$$Q = C_p \cdot (T_G - T_o), \tag{10}$$

where $C_p$ is total heat capacity of gases that formed due to diesel fuel combustion:

$$C_p = C_p(CO_2) + C_p(H_2O) + C_p(N_2) + C_p(air), \tag{11}$$

where $C_p(CO_2)$, $C_p(H_2O)$, $C_p(N_2)$, $C_p(air)$ is heat capacity of carbon dioxide, water, nitrogen and air.

Gas heat capacity is given by:

$$C_p = (\frac{i}{2} + 1) \cdot R \cdot \frac{M}{\mu}, \tag{12}$$

where $i$ is the number of degrees of freedom of gas, $R$ is the Mendeleyev-Klapeyron constant, $M$ is the weight of gas, μ is molar weight of gas.

The weights of $CO_2$ and $H_2O$ are defined by the ratio:

$$M(CO_2) = \frac{0.87 \cdot g_n \cdot \mu(CO_2)}{\mu(C)}, \tag{13}$$

$$M(H_2O) = \frac{0.13 \cdot g_n \cdot \mu(H_2O)}{\mu(H_2)}, \tag{14}$$

where coefficients 0.87 and 0.13 determine the content of $C$ and $H$ in diesel fuel; μ ($CO_2$), μ ($C$), μ ($H_2O$) and μ ($H_2$) are molar weights of carbon dioxide, carbon, water and hydrogen, respectively.

The weight of nitrogen is calculated through the weight of oxygen necessary for diesel fuel combustion:

$$M(N_2) = 4 \cdot M(O_2), \tag{15}$$

where

$$M(O_2) = \frac{0.87 \cdot g_n \cdot \mu(O_2)}{\mu(C)} + \frac{0.13 \cdot g_n \cdot \mu(O_2)}{2 \cdot \mu(H_2)}, \tag{16}$$

where $M(O_2)$ is the weight of oxygen necessary to form $CO_2$ and $H_2O$.

The weight of air that formed as a result of fuel combustion:

$$M(air) = 5 \cdot (\kappa - 1) \cdot M(O_2), \tag{17}$$

where $\kappa > 1$ is the excess coefficient that determines the amount of excess air that must be spent on complete fuel combustion. Ideally, $\kappa = 1$, however, in real conditions, using only the stoichiometric amount of oxygen, complete combustion cannot be achieved.

We substitute (13) – (17) into (10), equate (10) and (1) and get a ratio for the determination of $\kappa$:

$$\kappa = \frac{\frac{G_n}{T_G - T_0} - 18.53}{16.85} + 1. \tag{18}$$

Coefficients 18.53 and 16.85 determine the content of carbon dioxide, water, nitrogen and air that formed as a result of complete combustion of diesel fuel and were derived with regard to specific values of $i$, μ of gases and $R$.

On the other hand, the velocity of air delivery $v$ to heat exchanger is determined from the ratios:

$$v = \frac{g_{air}}{\rho_{T_o} \cdot S_R}, \tag{19}$$

$$g_{air} = 5 \cdot \kappa \cdot M(O_2), \tag{20}$$

where $g_{air}$ is air consumption, $\rho_{T_o}$ is air density at given ambient temperature.

Substituting (16) and (18) into (19) we obtain a dependence of velocity $v$ on the temperature of hot gases $T_G$ in the heat exchanger:

$$v = 5 \cdot \left[ \frac{\frac{G_n}{T_G - T_0} - 18.53}{16.85} + 1 \right] \cdot \frac{3.36 \cdot g_n}{\rho_{T0} \cdot \pi \cdot d^2 / 4}, \qquad (21)$$

where 3.36 is coefficient that determines the amount of oxygen required for complete combustion of diesel fuel.

The Mathcad application software package was used to determine the inverse dependence of hot gas temperature $T_G$ on air velocity $v$ (Fig. 9) at $G_n = 42.7$ MJ/kg, $T_0 = 0$ °C, $g_n = 220$ g/h, $\rho_{T_o} = 1.29$ kg/m$^3$ and combustion chamber diameter $d = 70$ mm.

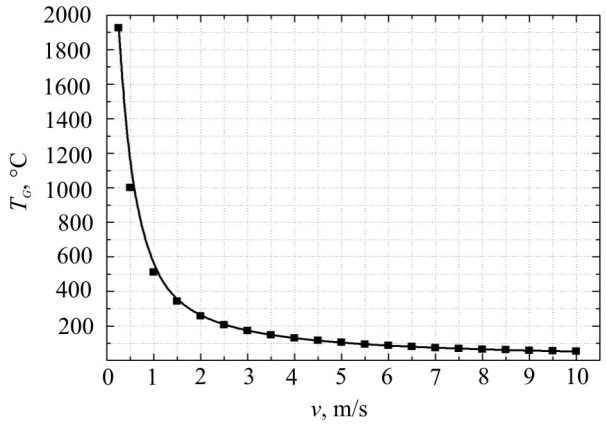


*Fig. 9. Dependence of hot gas temperature $T_G$ in the heat exchanger on air velocity v.*

From the analysis of data given in Fig. 9 it follows that for further calculations of the hot exchanger design it is not reasonable to use $T_G < 300$ and $T_G > 500$ °C: in the former case it is impossible to achieve the necessary hot side temperatures of module, in the latter case the rise in temperature leads to increase in the heat exchanger dimensions due to possible overheating of thermopile.

## Calculation of the hot heat exchanger

To determine a dependence of module hot side temperature $T_h$ on the area of the heat-absorbing surface, we used hot gas temperature $T_G$ = 500 – 300 °C which corresponds to air velocities 1 – 2 m/s.

Design was made with the use of "Comsol Multiphysics" software [10] by the numerical finite element method.

In the process of computer design the following values were used as the input data:

– hot gas temperature $T_G$ = (300; 400; 500) °C;

– gas velocity in the heat exchanger $v$ = (1; 1.5; 2) m/s;

– heat-absorbing surface area $S_R$ = (0.025; 0.045; 0.07; 0,09) m$^2$;

– thermal conductivity of the hot heat exchanger material $\lambda_r$ = 140 W/m·K;

– thermal conductivity of thermoelectric material $\lambda_m$ = 1.4 W/m·K.

In so doing, it was considered that heat sinks are at the outlet of combustion products from the heat exchanger and at places of location of modules, and thermal adiabatic isolation conditions are imposed at the rest of the boundaries.

Fig. 10 shows computer designed dependences of the module hot side temperature $T_h$ on the

area of heat-absorbing surface $S_R$ at hot gas temperature $T_G$ within 500 – 300 °C.

From the data presented in Fig. 10 it is seen that in the case of undeveloped area of the heat-absorbing surface ($S_R \sim 0.025$ m$^2$) at $T_G = 400$ °C, $T_h$ approaches the optimal value and makes 290 °C. The increase in heat exchange area leads to the rise in temperature $T_h$ and at $S_R = 0.09$ m$^2$ the necessary temperature level of 330 °C is achieved on the hot side of module.

From the data presented in Fig. 10 it is seen that in the case of undeveloped area of the heat-absorbing surface ($S_R \sim 0.025$ m$^2$) at $T_G = 400$ °C, $T_h$ approaches the optimal value and makes 290 °C. The increase in heat exchange area leads to the rise in temperature $T_h$ and at $S_R = 0.09$ m$^2$ the necessary temperature level of 330 °C is achieved on the hot side of module.

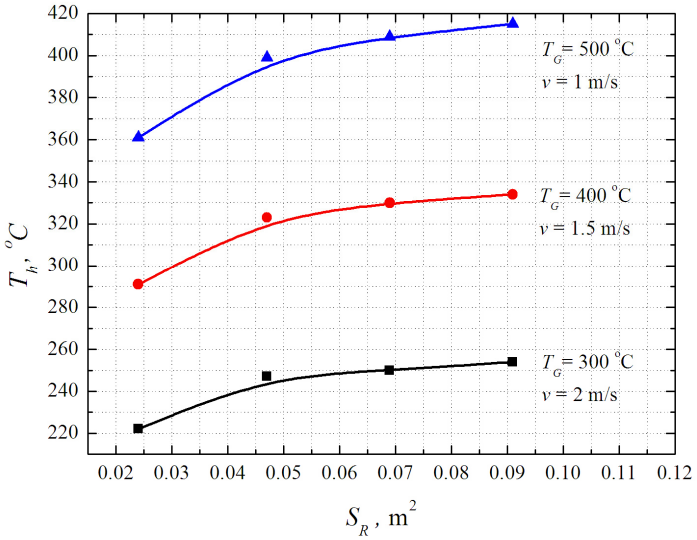


*Fig. 10. Dependence of the module hot side temperature $T_h$ on the area of the heat-absorbing surface $S_R$ of heat exchanger.*

Fig. 11 shows temperature distribution in the "hot heat exchanger-thermoelectric modules" system, Fig. 12 – finite element method mesh.

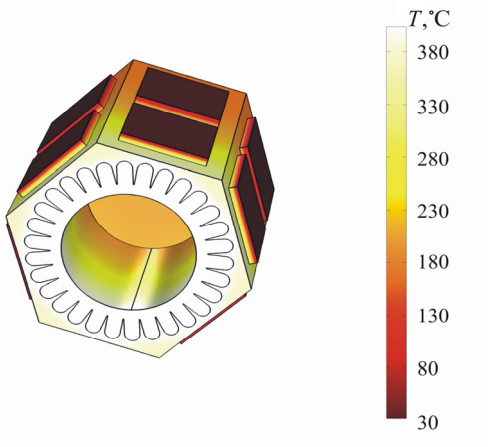


*Fig. 11. Temperature distribution in "hot heat exchanger-thermoelectric modules" system $T_G = 400$ °C, $S_R = 0.09$ m.$^2$*

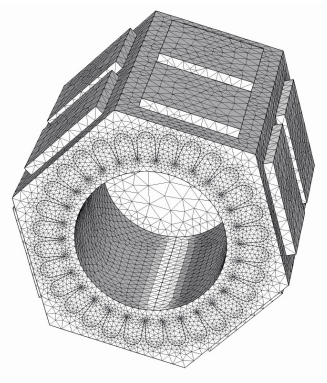

*Fig. 12. Finite element method mesh.*

Note that computer model of the heater is a somewhat simplified version of a physical model. To avoid awkward calculations aimed at determining heat flows due to radiation and convection and

heat losses with combustion products, we consider that heat transfer process occurs due to passing through the heat exchanger of gas flow with known inlet temperature $T_G$ So, as is evident from Fig. 11, as the gases flow to heat sink, $T_G$ is reduced, which results in the reduction of temperature $T_h$ from 330 to 250 °C. However, as long as in a real design the source of heat is directly in the heat exchanger, it can be considered that the hot side temperature of modules is equal.

Similar calculations to determine $T_G$ at constant $S_R = 0.09$ m$^2$ and $g_n = 180$ g/h show that to assure the hot side thermopile temperature 280 °C, the temperature of hot gases in the heat exchanger must be 350 °C. In this case air delivery velocity must be 1.2 m/s.

## Calculation of the cold heat exchanger

For quick heating of automobile engine it is necessary to assure maximum transfer of thermal power from the modules to the cold heat carrier. On the other hand, to assure the efficient operation of modules, it is important to create such conditions whereby the difference in heat carrier temperature at the inlet to and outlet of heat exchangers would be minimal. With this aim, at the present simulation stage the effective channel area of cold heatexchangers and optimal consumption of li -quid heat carrier were determined. The coldheat exchanger simulation was done by finite element method with the use of "Comsol Multiphysics" application software package.

In the process of computer design the following values were used as the input data:

– cold heat carrier temperature at inlet to cold heat exchanger $T_{in} = 30$ °C;

– thermal power removed from the modules $Q_4 = 1.4$ kW;

– heat carrier consumption $g_T = (0.25; 0.5; 0.7)$ m$^3$/h;

– channel area of the cold heat exchanger $S_c = (10 – 70)$ cm$^2$;

– thermal conductivity of cold heat exchanger material $\lambda_{r1} = 105$ W/m·K;

– heat carrier heat capacity $c_{pT} = 3151$ J/kg·K;

– heat carrier thermal conductivity $\lambda_T = 0.34$ W/m·K.

In the design, heat sink was assigned at points of heat carrier outlet from the heat exchanger, and adiabatic thermal insulation conditions were imposed at the rest of the boundaries.

Fig. 13 shows a dependence of thermal power $Q_5$ removed from thermoelectric modules to aut omobile engine on the total area of channels $S_c$ of the cold heat exchangers with different heat carrier consumption.

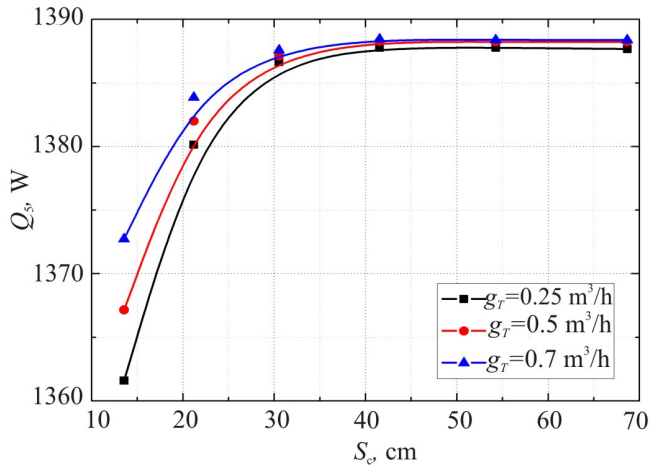


*Fig. 13. Dependence of thermal power $Q_5$ on the channel area $S_c$ of the cold heat exchangers.*

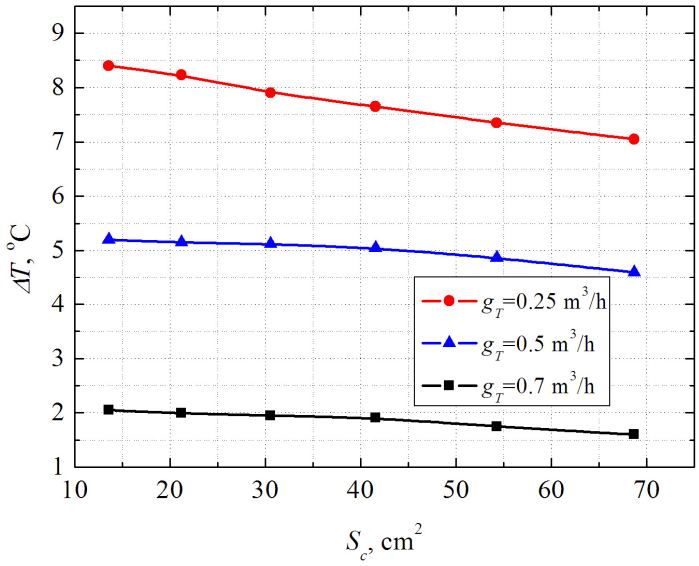


*Fig. 14. Dependence of heat carrier temperature difference ΔT between the inlet to and outlet of the cold heat exchangers on the channel area $S_c$.*

From the analysis of data represented in Fig. 13 it follows that for complete transfer of thermal power from the modules to engine the area of channels in the cold heat exchangers must be at least 40 cm$^2$. With such channel area $Q_5$ is practically independent of heat carrier consumption, which in turn allows reducing the losses of the output electric power of the heater on power supply to circulation pump. However, as follows from Fig. 14, heat carrier consumption must be 0.7 m$^3$/h. In this case heat carrier temperature difference between the inlet to and outlet from the heat exchangers is minimal and equal to ~ 2 °C.

Fig. 15 and Fig. 16 show temperature distribution and finite element method mesh for the cold heat exchanger:

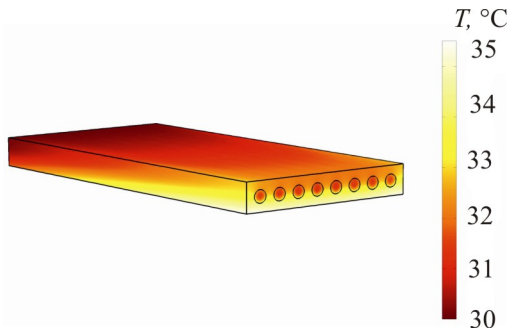


*Fig. 15. Temperature distribution in the cold heat exchanger. $S_c$ = 40 cm$^2$. $g_T$ = 0.7 m$^3$/h.*

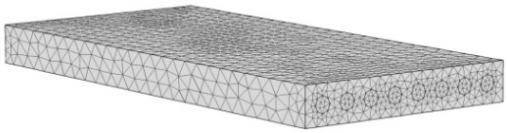

*Fig. 16. Finite element method mesh.*

According to (6), the amount of heat that must be spent on heating of engine with heat capacity 0.462 kJ/(kg K) (engine material – steel) and mass 200 kg from 0 °C to 30 °C will make ~ 2.8 MJ. Taking

into account that total thermal power removed from the thermopile by heat carrier with temperature 30 – 70 °C is ~ 1.39 kW (Fig. 17), start heating of engine requires ~ 40 min.

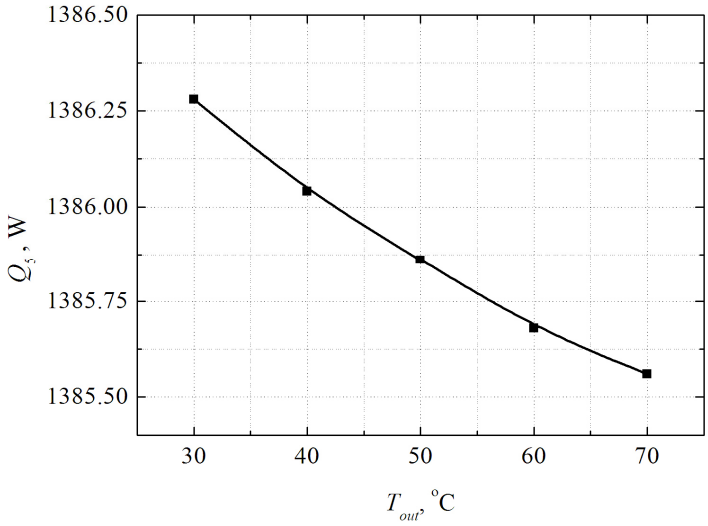


*Fig. 17. Dependence of thermal power $Q_5$, removed by heat carrier from heat carrier temperature $T_{out}$ at the outlet of the cold heat exchangers.*

Under real conditions the time of engine heating will be longer which is related to heat losses due to engine heat exchange with the environment, losses of heat transfer along cooling circuit, as well as due to the availability of hydraulic resistances in "heater-engine" system.

## Conclusions

1. It is established that the output electric power of the heater 90 – 70 W is attained through use of 12 modules "ALTEC-1061" with the hot and cold side temperatures 330 – 280 °C and 30 – 70 °C, respectively. With the heater efficiency within 3 – 3.5 %, to attain such electric power, it is necessary to spend ~ 2.3 – 2.5 kW of heat, which corresponds to fuel consumption 180 – 220 g/hour.
2. It is shown that the necessary temperature level on the hot side of thermopile is attained at gas temperature in the hot heat exchanger in the range of 400 – 350 °C, the velocity of air delivery to combustion chamber 1.5 – 1.2 m/s and the area of the heat-absorbing surface of the hot heat exchanger 0.09 $m^2$.
3. It is established that total thermal power transferred from thermopile to heat carrier is ~ 1.39 kW. With the heat carrier consumption 0.7 $m^3$/h and channel area of the cold heat exchangers 40 $cm^2$ both complete transfer of thermal power from heat carrier to automobile engine and minimal temperature difference of heat carrier between the inlet to and outlet from the heat exchangers is assured. Under these conditions, at heat carrier temperature 30 – 70 °C the start heating of engine from 0 °C to 30 °C requires ~ 40 min.

The author would like to express their gratitude to academician L.I. Anatychuk for the subject and the idea of the research and to junior research fellow R.M. Mochernyuk for the helpful advice on computer simulation.

## References

1. http://azbukadvs.ru/ holodnyj-pusk/ 1254 – osobennosti – puska – dizelnogo - dvigatelja-v-uslovijah-otricatelnyh-temperatur.html

2. V.S.Naiman, *All about Starting Pre-Heaters* (Moscow: ACT, 2007), p. 213.
3. http://autosiga.ru/gidronik/175-akkumulyator-sovmestnaya-rabota-akkumulyatora-i-predpuskovogo-podogrevatelya
4. V.Ya.Mykhailovsky, M.V.Maksymuk, Automobile Operating Conditions at Low Temperatures. The Necessity of Applying Heaters and the Rationality of Using Thermal Generators for their Work, *J.Thermoelectricity* 3, 20 – 31 (2015).
5. V.Ya.Mykhailovsky, M.V.Maksymuk, Rational Powers of Thermal Generators for Starting Pre-Heaters of Vehicles, *J.Thermoelectricity* 4, 69 – 77 (2015).
6. *Patent UA № 72304*, InCl: F01N 5/00; H01L35/00. Automobile Heater with Thermoelectric Power Source /L.I.Anatychuk, V.Ya.Mykhailovsky. Publ.10.08.2012, Bul. № 15, Application u2012 02055 of 23.02.2012.
7. http://www.webasto.com.ua.
8. http://www.inst.cv.ua
9. L.I.Anatychuk, V.Ya.Mykhailovsky, Gas-Fuelled Two-Sectional Thermoelectric Generator, *J.Thermoelectricity* 1, 76 – 86 (2008).
10. www.comsol.com

Submitted 16.02.2016.

**I.A. Konstantynovych[1, 2], O.V. Rendigevich[2]**

[1]Institute of Thermoelectricity, 1, Nauky str.,
Chernivtsi, 58029, Ukraine;
[2]Yu.Fedkovych Chernivtsi National University
2, Kotsyubinsky str., Chernivtsi,
58012 Ukraine

*I.A. Konstantynovych*

*O.V. Rendigevich*

# ON THE EFFICIENCY OF GYROTROPIC THERMOELEMENTS IN GENERATION MODE

*In this paper, analytical and numerical methods were used to study the basic relations for the calculation of optimal characteristics of gyrotropic thermoelements in electric energy generation mode. The InSb, InAs and $Bi_2Te_3$ thermoelectric materials for gyrotropic thermoelements were examined. Computer simulation was performed for InSb material and temperature distributions in various-shaped gyrotropic thermoelements were found. The temperature dependences of efficiency for gyroptropic thermoelements of optimal, rectangular and annular shapes were obtained.*

**Key words:** gyrotropic thermoelement, magnetic field, thermoelectric material, figure of merit, efficiency.

## Introduction

It is known that thermoelectric devices and systems developed on their basis are widely used in power engineering, refrigeration and measurement technology [1 – 3]. The main achievements of thermoelectricity in the field of instrument engineering were exactly based on the physics of thermocouple thermoelements. However, the upcoming trend of thermoelectricity development is devising of new types of thermoelements, for instance, based on gyrotropic media, and improving the efficiency of the existing ones. The properties of gyrotropic thermoelements are investigated in a series of papers [1 – 16].

Gyrotropic thermoelements offer a number of attractive features:

- absence of internal junctions, assuring their reliability and ease of manufacture;
- possibility of junction-free connection of rings into a spatial spiral structure for buildup of the necessary voltages;
- possibility of efficiency increase due to the effect of temperature and magnetic fields, particularly with their use in measurement technology.

Therefore, the relevance of the paper lies in the necessity to increase the efficiency and reliability of thermoelectric power converters based on gyrotropic thermoelements for their further use in instrument engineering.

*The purpose* of the paper is to estimate the efficiency of gyrotropic thermoelements in electric energy generation mode.

## Mathematical model

Thermal conductivity equation for the homogeneous gyrotropic medium is given below [1]:

$$\kappa\Delta T + \rho_0 j^2 + 2\alpha_B\left(j_y\frac{\partial T}{\partial x} - j_x\frac{\partial T}{\partial y}\right) = 0, \qquad (1)$$

where $\kappa$ is thermal conductivity of gyrotropic medium; $\rho_0$ is electric resistivity; $j$ is modulus of electric current density vector; $j_x, j_y$ are projections of vector $\mathbf{j}$ in Cartesian coordinate system; $\alpha_B = Q_\perp B$ is the asymmetric part of thermoEMF tensor which in the gyrotropic medium is of the form

$$\alpha = \begin{pmatrix} \alpha_0 & \alpha_B & 0 \\ -\alpha_B & \alpha_0 & 0 \\ 0 & 0 & \alpha_\perp \end{pmatrix}, \tag{2}$$

where $Q_\perp$ is the Nernst-Ettingshausen coefficient.

With regard to the system axial symmetry, Eq. (1) will be written in a polar coordinate system

$$\kappa \Delta T + \rho_0 j^2 + 2Q_\perp B \left( j_\varphi \frac{\partial T}{\partial r} - \frac{j_r}{r} \frac{\partial T}{\partial \varphi} \right) = 0, \tag{3}$$

where $j_\varphi$ is azimuth and radial components of current density vector $\mathbf{j}$, $r_1 \le r \le r_2$ is thermoelement radius.

## Computer simulation results

For the construction of computer model of gyrotropic thermoelements of rectangular, spiral and optimal shapes the Comsol Multiphysics application software package was used [17].

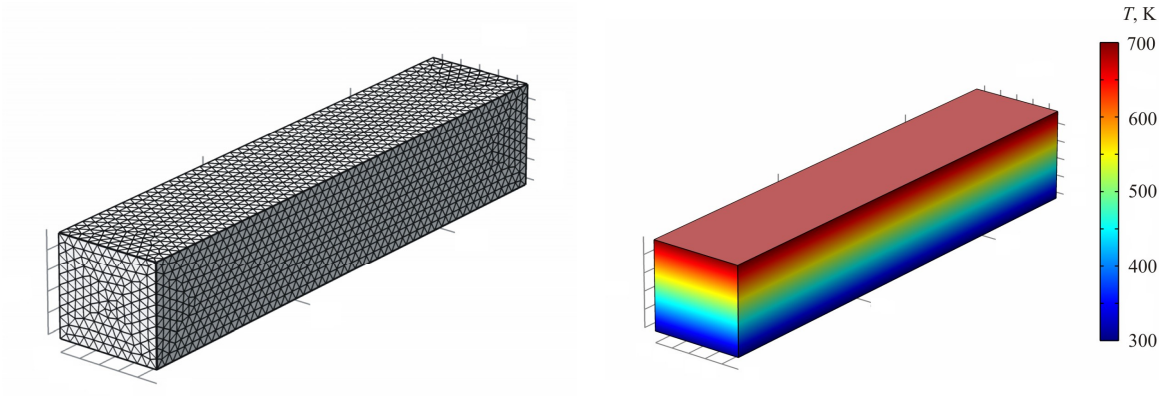


*a)* *b)*

*Fig. 1. Three-dimensional models of finite element method mesh (a) and temperature distribution (b) in gyrotropic rectangular-shaped thermoelement.*

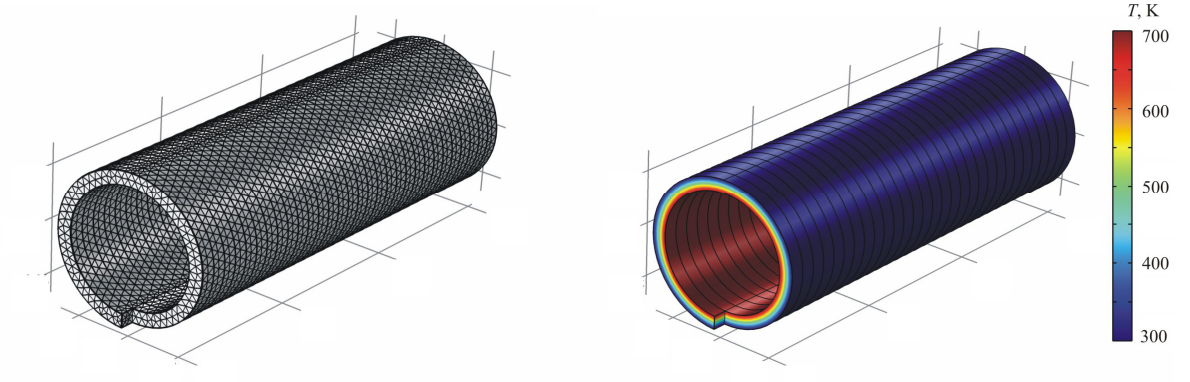


*a)* *b)*

*Fig. 2. Three-dimensional models of finite element method mesh (a) and temperature distribution (b) in a gyrotropic spiral thermoelement.*

Calculation of temperature distributions in gyrotropic thermoelements was done by finite element method [18]. By means of computer simulation the temperature distributions in various-shaped gyrotropic thermoelements were determined for *InSb* material in the temperature range of 300 – 700 K and magnetic field with induction $B = 1$ T. Fig. 1 shows three-dimensional models of finite element method mesh (*a*) and temperature distribution (*b*) in rectangular-shaped gyrotropic thermoelement (the Nernst-Ettingshausen thermoelement).

Fig. 2 shows three-dimensional models of finite element method mesh (*a*) and temperature distribution (*b*) in spiral gyrotropic thermoelement.

Fig. 3 shows three-dimensional models of finite element method mesh (*a*) and temperature distribution (*b*) in optimal-shaped gyrotropic thermoelement.

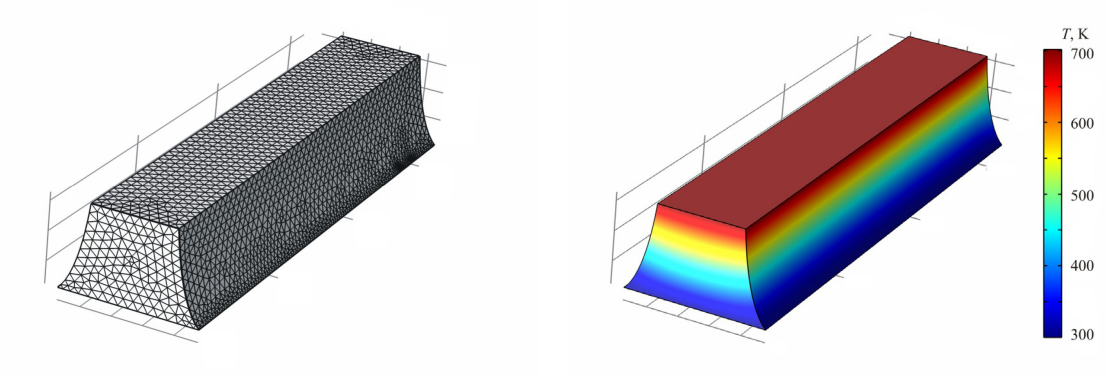


*a)* *b)*

*Fig. 3. Three-dimensional models of finite element method mesh (a) and temperature distribution (b) in optimal-shaped gyrotropic thermoelement.*

## Efficiency calculation

It is known that the efficiency of optimal-shaped gyrotropic thermoelement [2] is determined as follows:

$$\eta_1 = \eta_k \frac{1}{1+\dfrac{2M_H\left(1+M_H\right)}{T_2 Z_H}}, \tag{4}$$

where $M_H = \sqrt{1 - Z_H \overline{T}}$, $Z_H$ is thermomagnetic figure of merit, $T_2$ is the hot side temperature, $\eta_k$ is the Carnot cycle efficiency, $\overline{T}$ is the average temperature.

The efficiency of rectangular-shaped gyrotropic thermoelement is given below [1]:

$$\eta_2 = \frac{\eta_k}{\dfrac{4}{Z_H T_2} - \dfrac{2T_1}{T_2} - \dfrac{1}{2}\eta_k}, \tag{5}$$

where $T_1$ is the cold side temperature.

For the annular gyrotropic thermoelement the efficiency is as follows [3]:

$$\eta_3 = Z_H \frac{\Delta T}{4}. \tag{6}$$

Fig. 4 shows the temperature dependences of figure of merit for *InSb*, *InAs* and $Bi_2Te_3$ thermoelectric materials. It is seen that the best material for the manufacture of generator gyrotropic thermoelements is *InSb*, which is in agreement with experimental results presented in [1].

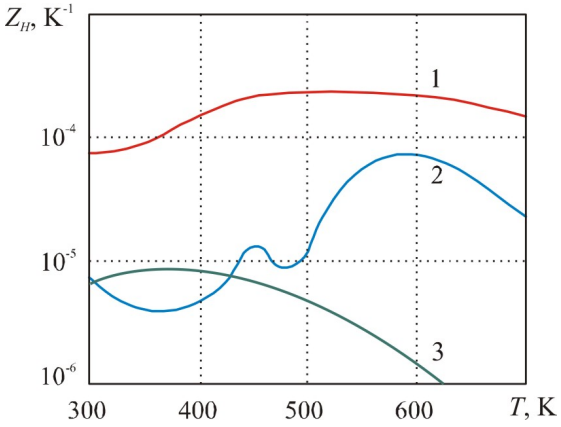


*Fig. 4. Temperature dependences of figure of merit of thermoelectric materials for gyrotropic thermoelements (1 – InSb, 2 – InAs, 3 – $Bi_2Te_3$).*

For the calculations *InSb* material was selected in the temperature range of 300 – 700 K. Various-shaped gyrotropic thermoelements were exposed to magnetic field with induction 1 T. According to calculated results, the dependences of efficiency on the hot side temperature of thermoelement $T_2$ were constructed at the constant cold side $T_1$ = 300 K for *InSb* (Fig. 5).

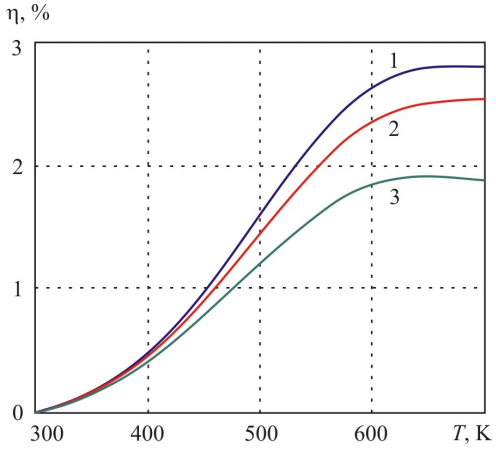


*Fig. 5. Temperature dependence of efficiency for various-shaped gyrotropic thermoelements (1 – optimal-shaped, 2 – rectangular-shaped, 3 – annular-shaped).*

From Fig. 5 it is seen that at temperature difference between the hold and cold side 400 K and magnetic field induction 1 T for an optimal-shaped gyrotropic thermoelement maximum efficiency value is about 2.8 %, which is less than in thermocouple elements based on $Bi_2Te_3$ and *PbTe*. However, gyrotropic thermoelements are characterize ed by increased reliability and possibility of high voltages build-up due to junction-free connection into a spatial spiral structure which makes such thermoelements promising for use in measurement and defense technology. Also, such thermoelements can be used for the manufacture of high-sensitive temperature and heat flux sensors.

## Conclusions

1. Parameters of thermoelectric materials (*InSb*, *InAs* and $Bi_2Te_3$) for gyrotropic thermoelements

were compared. It was established that the best material for the manufacture of generator gyrotropic thermoelements is *InSb* whose average figure of merit value in the temperature range of 400 – 600 K is $4 \cdot 10^4$ $K^{-1}$.

2. With the aid of computer simulation the distributions of temperature in the working medium of gyrotropic thermoelements of rectangular, spiral and optimal shapes for thermoelectric material *InSb* were determined.
3. The temperature dependences of efficiency for various-shaped gyrotropic thermoelements were determined. It was established that maximum efficiency value of optimal-shaped gyrotropic thermoelement for *InSb* material in the temperature range of 300 – 700 K and magnetic induction 1 T is 2.8 %.

## References

1. L.I.Anatychuk, *Thermoelements and Thermoelectric Devices* (Kyiv: Naukova Dumka, 1979), 766 p.
2. A.G.Samoiloivich, *Thermoelectric and Thermomagnetic Energy Conversion Methods* (Chernivtsi: Ruta, 2006), 226 p.
3. L.I.Anatychuk, *Thermoelectricity, Vol.2, Thermoelectric Power Converters* (Kyiv, Chernivtsi: Naukova Dumka, 2003), 386 p.
4. A.G.Samoilovich, L.L.Korenblit, Current Status of Theory of Thermoelectric and Thermomagnetic Effects in Semiconductors, *Advances in Physical Sciences* **49**(2), 243 –272 (1953).
5. H.Nakamura, K.Ikeda, and S.Yamaguchi, Transport Coefficients of *InSb* in a Strong Magnetic Field, *Proc. of XVI-th International Conference on Thermoelectrics* ( Dresden, Germany, 1997), P. 142 – 146.
6. L.I.Anatychuk, O.J.Luste, Ya.G.Fedoruk, and S.M.Shinkaruk, Eddy Thermoelectric Currents in a Gyrotropic Medium with a Radial Temperature Distribution, *J.Thermoelectricity* 1, 19 – 24 (2004).
7. O.J.Luste, Ya.G.Fedoruk, Gyrotropic Thermoelement in the Inhomogeneous Magnetic Field, *J.Thermoelectricity* 1, 16 – 22 (2006).
8. O.J.Luste, Ya.G.Fedoruk, Optimization of Materials for Gyrotropic Thermoelements, *J.Thermoelectricity* 4, 21 – 26 (2008).
9. Z.F.Agayev, D.G.Arasli, and S.A.Aliyev, Thermomagnetic Converter of IR Radiation, *Problemy Energetiki* 3, 12 – 21 (2003).
10. S.A.Nemov, V.I.Proshin, G.L.Tarantasov, R.V.Parfenyev, D.V.Shamshur, and A.V.Chernyayev, Transverse Nernst-Ettingshausen Effect, Resonance Scattering and Supercoductivity in *SnTe*: In, *Physics of the Solid State* **51**(1), 461 – 464 (2009).
11. T.G.Harman, J.M.Honig, *Thermoelectric and Thermomagnetic Effects and Applications* (New York, Mc. Graw – Hill, 1967), 377 p.
12. H.Nakamura, K.Ikeda, and S.Yamaguchi, Transport Coefficients of InSb in a Strong Magnetic Field, *Research Report. NIFS Series*, Nagoya, Japan (1998), 23 p.
13. Hiroaki Nakamura, Kazuaki Ikeda, and Satarou Yamaguchi, Transport Coefficients of *InSb* in a Strong Magnetic Field, *Proc.of XVI International Conference on Thermoelectrics* (Dresden, Germany, August 26 – 29, 1997), P. 142 – 146.
14. P.I.Baranskii, G.P.Haidar, Anisotropy of Thermoelectric Properties of Multi-Valley Semiconductors of Cubic Symmetry under the Influence of External Directional Effects, *J.Thermoelectricity* 1, 13 (2014).

15. H.J.Goldsmid, E.H.Volckmann, Galvanomagnetic and Thermoelectric Measurements on Polycrystalline $Bi_{88}Sb_{12}$, *Proceedings of XVI Internatial Conference on Thermoelectrics* (Dresden, Germany, August 26 – 29, 1997), P. 142 – 146.
16. L.I.Anatychuk, L.N.Vikhor, Low-Temperature Thermoelectric Cooling under Optimal Legs Inhomogeneity in the Optimal Nonuniform Magnetic Field, *Proc.of XVI International Conference on Thermoelectrics* (Dresden, Germany, 1997), P. 397 – 400.

Submitted 10.02.2016.

*V.V. Antonyuk*

**V.V. Antonyuk, I.M. Skrypskyi**

Institute of Thermoelectricity of the
NAS and MES of Ukraine,
1, Nauky Str., Chernivtsi, 58029, Ukraine

*I.M. Skrypskyi*

# IMPROVED RELIABILITY CONTACT CONNECTING STRUCTURES FOR BISMUTH TELLURIDE BASED THERMOELECTRIC MATERIALS

*A method for preparation of thin multilayer contact structures based on generator thermoelectric material is developed and their antidiffusion properties are studied. It is shown that maximum dynamic stability of thermoelectric devices is observed in the case when alloys of iron subgroup metals with phosphorous and tungsten having amorphous structure are used as antidiffusion layers.*

*It is established that contact structures proposed here allow minimization of the negative effect of inconsistency between thermal expansion coefficients of thermoelectric material and antidiffusion films which increases considerably the service life of thermoelectric devices.*

**Key words:** thermoelectric material, bismuth telluride, anti-diffusion layers, multi-layer films, nickel-tungsten alloy.

## Introduction

Solid-state thermoelectric energy converters offer a number of essential advantages over traditional electric generators and are finding ever widening application. So far, however, conversion efficiency provided by thermoelectric plants is lower compared to generators of traditional design. Moreover, current status of thermoelectric converters production is characterized by unjustifiably high consumption of thermoelectric material (TEM) and the resulting high cost [1].

One of the factors restricting wide application of thermoelectric converters is insufficient reliability of contact and connecting structures of thermoelements. In the field, thermoelectric and connecting materials must have mutual physical and chemical stability, which, on the one hand, assures their long-term operation, and, on the other hand, creates a reserve for increasing conversion efficiency due to operating temperature rise.

There are various methods of thermoelements connection: soldering, melt loading, joint pressing of thermoelectric legs and connecting material, thermal, magnetron, ion cluster sputtering of connecting materials in vacuum or inert gas, galvanic or chemical deposition of connecting material.

Of primary importance is selection of connecting materials that are in direct contact to semiconductor legs. The elements of iron subgroup, *Ni*, *Co*, *Fe,* are chemically inert to semiconductor material, have satisfactory anti-diffusion properties, good solder wettability, their linear expansion coefficients are close to that of thermoelectric material [2].

The methods of chemical and galvanic deposition of metals on semiconductors enables one to avoid the difficulties related to thermal processing of thermoelements in soldering, pressing, plasma deposition, melt loading, as long as galvanic processes proceed at low temperatures, are easy to operate, do not require costly equipment and make possible efficient control of the thickness of deposited layers.

A promising way of solving this problem is to create contact and connecting layers with preassigned properties and technologies of their connection to thermoelectric materials with attainment of ultimately low values of contact resistances [3].

Of critical importance for the technological properties of electrolytic coatings with metals and alloys is deposit structure. The structure of some or other electrolytic coating can be estimated no only during X-ray and metallographic studies, but also by the results of polarization measurements.

The galvanic method of alloys preparation is not new. However, systematic studies of general properties of electrolytic deposition of alloys began comparatively recently. Practical significance of these works lies in the fact that they expand considerably the range of galvanic coatings, and in many cases coatings based on alloys posses valuable properties, not typical of the metals of which this alloy is composed. Galvanic coating with alloys is related to a series of specific difficulties. Thus, there must be more precise control of such process parameters as current density on electrodes, concentration of ions in case of deposited metals. In many cases alloy deposition is done by galvanothermic method, which lies in alternate deposition of thin layers of each metal and subsequent thermal processing of products during which metals mutually diffuse, forming an alloy of variable composition. This method has not become as popular as galvanic one [4].

## Experimental

Experimental works were carried out for the deposition of anti-diffusion layers on bismuth telluride based TEM samples prepared by consecutive application of thin (1.5 – 3 μm) layers of nickel subgroup metals and their alloys with other metals.

On the discs of thermoelectric material synthesized at Institute of Thermoelectricity after their surface prefinishing by the method adopted at ITE the following coatings were deposited:

1. TEM | *SnNi*(10 μm) | *SnBi*(4 μm) – for *n*- and *p*-type discs;
2. TEM | *NiW*(3 μm) | *SnNi*(10 μm) | *SnBi*(4 μm) – for *n*-type discs;
3. TEM |*Fe*(3 μm) | *NiW*(3 μm) | *SnNi*(10 μm) | *SnBi*(4 μm) – for *p*-type discs;
4. TEM | $Co_{chem.}$(3 μm) | *SnNi*(10 μm) | *SnBi*(4 μm) – for *n*- and *p*-type discs

The coatings were deposited from electrolytes under conditions described in [5 – 7].

*Table*

*Change in the characteristics of thermoelectric devices*

| Legs coating composition | Annealing time, h | Δ*R*, Ω | Δ*W*, W | Δη, % |
|---|---|---|---|---|
| TEM \| *NiW*(3 μm) \| *SnNi*(10 μm) \| *SnBi* (4 μm) – for *n*-type discs; TEM \| *Fe*(3 μm) \| *NiW*(3 μm) \| *SnNi* (10 μm) \| *SnBi*(4 μm) – for *p*-type discs | 50 | 0.003 | 0.9 | 0.18 |
| | 100 | 0.014 | 0.67 | 0.01 |
| | 200 | 0.026 | 0.59 | - 0.1 |
| | 300 | 0.043 | 0.39 | - 0.25 |
| TEM \| $Co_{chem.}$(3 μm) \| *SnNi*(10 μm) \| *SnBi* (4 μm) – for *n*- and *p*-type discs | 50 | 0.003 | - 0.05 | - 0.19 |
| | 100 | 0.014 | - 0.42 | - 0.28 |
| | 200 | 0.107 | - 0.58 | - 0.56 |
| | 300 | 1.58 | - 1.10 | - 0.86 |
| TEM \| *SnNi*(10 μm) \| *SnBi*(4 μm) – for *n*- and *p*-type discs | 50 | 0.05 | - 0.33 | - 0.24 |
| | 100 | 0.19 | - 0.55 | - 0.63 |

Using wire instrument with deposited abrasive, the metalized TEM discs were cut into legs of which thermoelectric devices were assembled and their most important parameters were measured – resistance $R$, power $W$, efficiency $\eta$. The devices were annealed at 200 °C, and repeated measurements of parameters were performed at specific time intervals.

## Discussion of the results

As is evident from Table 1, the multilayer combined films of iron, nickel-tungsten, nickel-tin and tin-bismuth alloys applied on TEM discs improve considerably the life and reliability of thermoelectric devices.

In the authors' opinion, it is due to the following factors:

1. Both iron and nickel-tungsten alloy are much more passive in the reactions with thermoelectric material components as compared to other coatings under study – cobalt and nickel-tin alloy. In their properties, these alloys belong to heat-resistant alloys due to the content of tungsten and iron. According to the results of investigation of diffusion processes [8], the contact of cobalt to bismuth and antimony telluride is damaged with formation of reactive-diffusion layer of cobalt telluride and cobalt antimonide solid solution. The thickness of this layer is increased with time and operating temperature rise. The specific feature of this layer is low mechanical durability. For given cross-section of legs, attainment by the layer of its critical thickness is accompanied by the damage of contact die to arising thermal stresses, reducing considerably their life stability [9].
2. Nickel-tungsten films, unlike purely nickel or cobalt ones, have X-ray amorphous structure and, accordingly, lower internal stresses. And although nickel-tin alloy deposited under these conditions is also X-ray amorphous, its components at elevated temperatures react much more actively with thermoelectric material components than iron and tungsten. The adhesion strength of coatings under study is 17 – 20 MPa for *n*-type samples and 15 – 17 MPa for *p*-type samples.
3. Forming anti-diffusion coatings of the thin layers of different metals or their alloys, we overlap pores, cracks and other defects that are always available in galvanic films, with a layer of other metal or alloy, which improves considerably the anti-diffusion properties as compared to single metal film.

## Conclusions

1 To minimize the negative effect of such factors as inconsistency between linear expansion coefficients of TEM and contact antidiffusion structures, internal stresses of coating itself leading to considerable reduction of the dynamic stability of contact structures, it was proposed to use as antidiffusion layers chemically or electrodeposited thin (up to 3 μm) multilayer films of metals and their alloys.

2 It was established that maximum dynamic stability of composite contact and connecting structures based on chemically or electrodeposited thin multilayer films of metals and their alloys is observed in the case when such coatings employ iron subgroup metals and their galvanic alloys with tungsten.

3 The deposition potential of each metal separately is more negative than the potential whereby alloy is formed (with formation of solid solution the potential energy of its components is reduced). This difference can be so great that metal ions are discharged on the cathode whose

deposition in pure form from aqueous solutions is impossible. This is exemplified by the electrolyte deposition of tungsten alloys with nickel, iron and other metals, whereas purely tungsten coatings can be obtained only from the melts.

## References

1. L.I.Anatychuk, *Thermoelements and Thermoelectric Devices: Reference Book* (Kyiv: Naukova Dumka, 1979), 768 p.
2. Alfred D., Dec K., *Pat. USA 4654224* InCl: HOIL35/34 Method of Manufacturing a Thermoelectric Element, Published. 31/03/1987.
3. L.I.Anatychuk, V.A.Semenyuk, *Optimal Control of the Properties of Thermoelectric Materials and Devices* (Chernivtsi:Prut, 1992), 264 p.
4. Ya.V.Vainer, M.A.Dasoyan, *Technology of Electrochemical Coatings* (Moscow: Mashgiz, 1962), 347p.
5. S.A.Vishenkov, *Chemical and Electrochemical Methods for Metals Coatings Deposition* (Moscow: Mashinostroyeniye, 1975), 312 p.
6. G.A.Sadakov, *Galvanoplastics* (Moscow: Mashinostroyeniye, 1987), 288 p.
7. V.M.Fedosyuk, M.M.Malyush, L.B.Sosnovskaya et al., *Pat. RU 2 446 390* C1, InCl C 25 D 3/56 Electrolyte and Method for Protective Coating with Nickel-Tungsten Alloy, № 95105857/02; Filed 14.04.1995; Publ. 27.07.1998.
8. V.M.Sokolova, L.D.Dudkin, L.I.Petrova, and N.Kh.Abrikosov, Study of Diffusion Processes in Low-Temperature Thermoelements, *Applied Solar Energy* 1, 18 – 21 (1978).
9. V.M.Sokolova, L.D.Dudkin, V.A.Mazur, Calculation of Life Stability of Low Temperature Thermopiles, *Applied Solar Energy* 5, 7 – 10 (1978).

Submitted 14.01.2016.

**L.I. Anatychuk[1, 2], O.I. Ivaschuk[3], R.R. Kobylianskyi[1, 2], I.D. Postevka[3], V.Yu. Bodiaka[3], I.Ya. Gushul[3]**

[1]Institute of Thermoelectricity, 1, Nauky str., Chernivtsi, 58029, Ukraine;
[2]Yu. Fedkovych Chernivtsi National University,
2, Kotsiubynskyi str., Chernivtsi, 58012, Ukraine;
[3]Higher state educational institution of Ukraine "Bukovinian State Medical University",
2, Theatre sq.,Chernivtsi, 58002, Ukraine

# THERMOELECTRIC DEVICE FOR TEMPERATURE AND HEAT FLUX DENSITY MEASUREMENT "ALTEC-10008"

*This paper presents the design, operating principle and specifications of thermoelectric device developed for temperature and heat flux density measurement which involves connection to personal computer for saving, processing and visualization of measurement results in real-time mode.*
*The results of experimental research on heat release of implanted breast neoplasm of trial rat as a function of neoplasm progression stage are presented. It is established that the results obtained can be used for development of a method for early diagnostics of breast cancer.*
***Key words:*** thermoelectric sensor, temperature, heat flux density, breast cancer, diagnostics of oncologic diseases.

## Introduction

For the investigation of local human heat release much promise is held by semiconductor thermoelectric heat flux sensors [1 – 11] which combine miniature size, high sensitivity, parameter stability in a wide operating temperature range and are matched with state-of-the-art recording equipment [12 – 17]. The use of such sensors enables one to get high locality and precision of heat flux metering. This, in turn, provides insight into characteristics of objects under study and their detailed analysis for the purpose of early detection of human organism inflammatory processes and oncologic diseases.

An important factor in the investigation of human heat fluxes with the aid of thermoelectric sensors is precision and speed of signal recording. Early developments of signal recorders [3 – 9] have a relatively high measurement error, large overall dimensions, low speed and no self-contained power supplies. Further developments in this direction resulted in creation of modern electronic recorders with processing of information from thermoelectric heat flux sensors [18 – 20] which have internal memory for saving of measurement results and self-contained power supplies. However, the disadvantages of such devices are the impossibility of connection of several thermoelectric sensors, the absence of simultaneous temperature and heat flux density measurement and the absence of real-time connection to personal computer for processing, saving and visualization of measurement results. Moreover, the data on correlation between heat release and the level of health is still insufficient [21 – 27].

Therefore, *the purpose of this work* is development of a multi-channel thermoelectric device for temperature and heat flux density measurement and investigation with its help of heat release of implanted breast neoplasm of trial rat depending on neoplasm progression stage.

## Device design and specifications

Thermoelectric device for temperature and heat flux measurement "ALTEC - 10008" was developed at the Institute of Thermoelectricity of the National Academy of Sciences and Ministry of Education and Science of Ukraine under the agreement on cooperation with Bukovinian State Medical University of the Ministry of Public Health of Ukraine. The device is intended for a simultaneous measurement of temperature and heat flux density on human body surface by contact method, allowing early diagnostics of inflammatory processes and oncologic diseases. Device appearance and specifications are presented in Fig. 1 and Table 1, respectively.

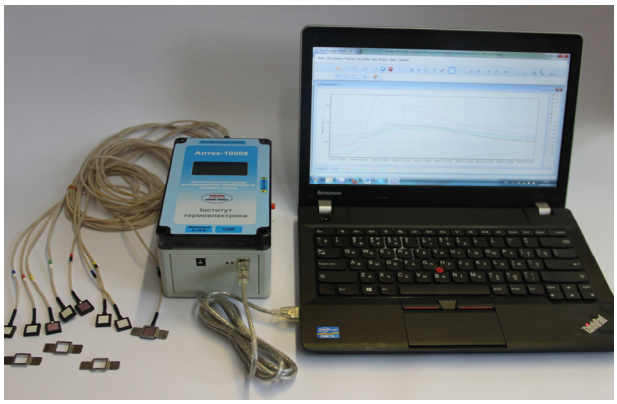

*Fig. 1. Appearance of thermoelectric device for temperature and heat flux density measurement "ALTEC-10008".*

*Table 1.*

*Thermoelectric device specifications*

| № | Device specifications, measurement unit | Value |
|---|---|---|
| 1. | Number of probes, pcs. | 8 |
| 2. | Probe dimensions, mm | 14 × 14 × 3 |
| 3. | Probe configuration | Temperature sensor, heat flux sensor |
| 4. | Temperature sensor type | Thermistor |
| 5. | Temperature sensor dimensions, mm | 2.2 × 2 × 0.7 |
| 6. | Heat flux sensor type | Thermocouple thermopile |
| 7. | Thermopile dimensions, mm | 10 × 10 × 3 |
| 8. | The length of probe connecting wires, m | 1.5 |
| 9. | Electronic recorder type | TRITON 9004TC A |
| 10. | Temperature measurement range, °C | 0 ÷ + 50 |
| 11. | Temperature measurement accuracy, °C | 0.05 |
| 12. | Heat flux density measurement range, W/cm$^2$ | $5 \cdot 10^{-5} \div 10^{-1}$ |
| 13. | Electronic recorder speed, s | 3 ÷ 5 |
| 14. | Electronic recorder supply:<br>a) mains AC/DC-adapter, V<br>b) three galvanic elements AA, V | <br>220/5<br>4.5 |
| 15. | Possibility of real-time display of measurement results on electronic recorder | + |
| 16. | Possibility of real-time display of measurement results on personal computer | + |
| 17. | Possibility of real-time saving measurement results on microSD memory card | + |

The device is composed of electronic control unit and 8 identical thermoelectric probes. Electronic control unit is a 16-channel microprocessor module for electric signal recording based on Triton-9004TCA recorder. Device can be powered in two ways: three galvanic elements of the type AA (4.5 V) or external power supply of voltage 5 V (mains AC/DC-adapter (220/5 V), USB-port of personal computer or laptop). With a simultaneous connection to device of external power supply and galvanic elements, the latter are recharged.

The device is fully-autonomous, i.e. measurement results are shown on display in real-time mode and saved on microSD memory card with given time interval. Moreover, for convenience of processing and analysis of measurement results the device involves data transfer through USB interface to personal computer by means of specially elaborated software program.

Thermoelectric probe comprises self-contained temperature sensor (thermistor) and thermocouple heat flux sensor. The thermoelectric probe is schematically shown in Fig. 2.

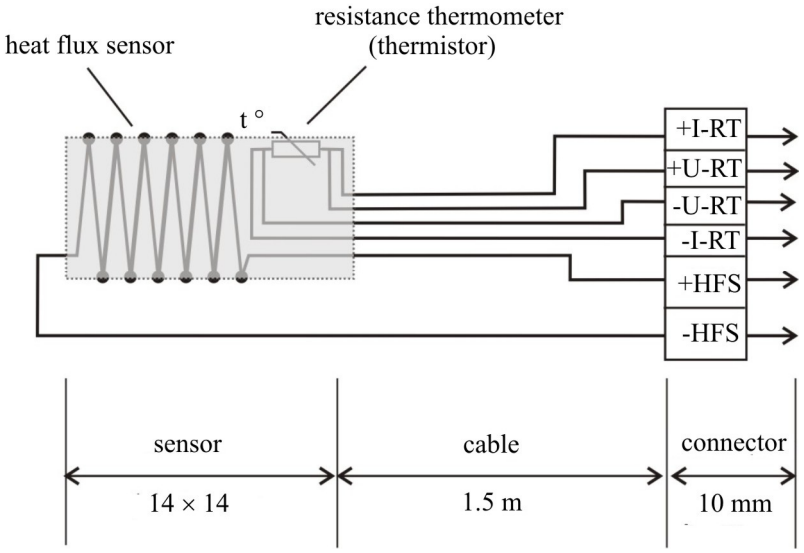


*Fig. 2. Schematic of thermoelectric probe.*

Heat flux sensor is a tightly packed thermopile of thermocouple elements made of high-performance semiconductor materials based on *Bi – Te* [1]. The intervals between thermocouple elements are filled with epoxy compound, and thermopile working surfaces are hermetically sealed by ceramic plates. Full hermetic state of thermoelectric probes allows their thorough disinfection. For convenient replacement of thermoelectric probe it is connected to electronic control unit. Thermoelectric probes are fastened to object under study by means of frames with the lobes made of food grade stainless steel.

## Experiment description

The experiment was carried out on 48 pubertal nonlinear rats of average age, of weight at least 180 g, female sex that had never been pregnant.

All trial animals were divided into two groups – comparative and main. The main group comprised 32 rats which were implanted with Geren's carcinoma in the area of location of the abdominal mammary gland by injection of cell suspension (Fig. 3).

*Fig. 3. Neoplasm of left abdominal mammary gland of trial rat (10-th day after injection of Geren's carcinoma cell suspension).*

Geren's carcinoma cell suspension was prepared by elimination of the latter from the other animal. The carcinoma was minced to fragments of size from 0.05 to 1.0 mm, with elimination of connective tissue elements. Also, cleaning in phycolous gradient was performed, in an effort to remove cell debris, elements of blood, mucus, connective tissue cells and large fragments. For transplantation a specimen of daily cells culture in culture medium was used, with their content $4 \cdot 10^8$ in 1 ml.

The main group was divided into two subgroups. In the first subgroup of animals, temperature and heat flux sensor was arranged in the projection of pathologically unchanged tissues of the abdominal mammary gland, in the second group – in the projection of carcinoma. The comparative group comprised 16 intact animals for which temperature and heat flux sensor was arranged in the projection of the abdominal mammary gland tissue.

For the purpose of measurement of heat flux from the abdominal mammary gland, the animal was fixed lying on its back. Heat flux sensor was fixed to skin by means of two simple interrupted stitches, the said area having been preliminarily shaved and treated with 70 % alcohol (Fig. 4).

*Fig. 4. Arrangement and fixation by simple interrupted stitches of thermoelectric temperature and heat flux sensors in the projection of the abdominal and inguinal mammary glands tumor.*

Temperature and heat flux density on the skin surface of mammary gland of trial rats was measured for 5 minutes, from the $8^{th}$ to $16^{th}$ day after tumor implantation. Said dates of experimental

investigations are caused by the size of implanted neoplasm, as well as by the beginning of destructive processes in the latter. In the course of experimental investigations air temperature in the room was within 20 ÷ 21 ºC. For the comparative group animals, temperature and heat flux density measurement was performed with thermoelectric sensor arranged horizontally on the skin in the projection of the abdominal mammary gland.

The experiment was carried out in the vivarium of Bukovinian State Medical University in conformity with the national requirements of "General ethical principles of animal experimentation" (Ukraine, 2011) that are consistent with provisions of "European Convention for the Protection of Vertebrate Animals used for Experimental and other Scientific Purposes" (Strasbourg, 1985).

Mercy killing of laboratory rats was done according to ethical standards and effective recommendations in heavy sedation state by injection of excess amount of drug in conformity with the law of Ukraine № 3447-1 of 21.02.2006 "On the protection of animals from cruelty".

## Experimental results

In Table 2 are listed the results of experimental studies on heat flux density of trial rat mammary gland. The results obtained point to definitely lower values of heat flux density for the main group animals during the whole observation period. The figures of heat flux density for the animals of the first subgroup of the main group are definitely higher than the figures of the second subgroup during the entire investigation period. In both subgroups of the main group there is a definite reduction of heat flux density after the $8^{th}$ to $10^{th}$ day of observation.

*Table 2.*

*Dynamics of heat flux density of trial rat mammary neoplasm depending on the term after tumor implantation (M ± m), mW*

| Term after tumor implantation | Animal group | | |
|---|---|---|---|
| | The main group $n = 32$ | | Comparative group $n = 16$ |
| | Первая подгруппа | Вторая подгруппа | |
| the $8^{th}$ to $10^{th}$ day | 19.26 ± 0.31<br>$p < 0.001$ | 15.07 ± 0.30<br>$p < 0.001$; $p_1 < 0.001$ | 28.99 ± 0.60 |
| the $11^{th}$ to $13^{th}$ day | 17.93 ± 0.31<br>$p < 0.001$* | 13.08 ± 0.26<br>$p < 0.001$; $p_1 < 0.001$* | |
| the $14^{th}$ to $16^{th}$ day | 13.65 ± 0.32<br>$p < 0.001$* | 9.17 ± 0.38<br>$p < 0.001$; $p_1 < 0.001$* | |

Notes: $n$ – number of observations; $p$ – with respect to comparative group; $p_1$ – with respect to the first subgroup of the main group; * – reliable on the $8^{th}$ to $10^{th}$ day of observation.

Evaluating the results of experimental studies on skin surface temperature in the projection of trial rat mammary gland, one should note definitely lower temperature values for the main group animals during the whole observation period (Table 3). The skin surface temperature in the projection of mammary gland for animals of the first subgroup of the main group is definitely higher than for animals of the second subgroup. There is a definite reduction of skin surface temperature in the projection of mammary gland for the main group animals during the whole investigation period with a reliable difference on the $14^{th}$ to $16^{th}$ day.

*Table 3.*

*Dynamics of skin surface temperature of trial rat mammary neoplasm depending on the term after tumor implantation (M ± m), ºC*

| Term after tumor implantation | Animal group | | |
|---|---|---|---|
| | The main group $n = 32$ | | Comparative group $n = 16$ |
| | The first subgroup | The first subgroup | |
| the 8th to 10th day | 25.45 ± 0.58<br>$p < 0.001$ | 22.90 ± 0.31<br>$p < 0.001$; $p_1 < 0.001$ | 31.50 ± 0.63 |
| the 11th to 13th day | 24.98 ± 0.42<br>$p < 0.001$ | 22.33 ± 0.36<br>$p < 0.001$; $p_1 < 0.001$ | |
| the 14th to 16th day | 24.11 ± 0.30<br>$p < 0.001$* | 21.72 ± 0.40<br>$p < 0.001$; $p_1 < 0.001$* | |

Notes: $n$ – number of observations; $p$ – with respect to comparative group; $p_1$ – with respect to the first subgroup of the main group; * – reliable on the 8th to 10th day of observation.

Summarizing the results of experimental investigations, it should be noted that in the case of malignant state of trial rat mammary gland one can observe definitely lower mode and median values of temperature and heat flux density as compared to intact animals. The said figures are definitely lower in tumorous mammary gland compared to intact one in the organism of the same animal. Progression of mammary gland tumor is characterized by a definite reduction of the mode and median values of heat flux density and skin surface temperature, though the latter is characterized by less pronounced changes, as testified by unreliable difference on the 11th to 13th day of observation.

Thus, heat flux density and skin surface temperature in the projection of mammary gland malignant neoplasm have definitely lower values decreasing with the latter growth. The results obtained can be used for the development of a method for early detection of breast cancer. Introduction to medical practice of the thermoelectric device for temperature and heat flux density measurement "Altec-10008" will yield a simple and cheap method for early detection of inflammatory processes and oncologic diseases.

## Conclusions

1. A multi-channel thermoelectric device was developed and manufactured for a simultaneous contact measurement of temperature and heat flux density of human body surface which involves connection to personal computer for saving, processing and visualization of measurement results in real-time mode.
2. It was experimentally established that the value of heat flux density and skin surface temperature of tumorous mammary gland is lower compared to intact one and is reduced with neoplasm growth. The results obtained can be used for the development of a method for early detection of breast cancer.
3. The proposed device is promising for the monitoring of temperature and thermal state of human organism, enabling early detection of inflammatory processes, oncologic diseases and express diagnostics during mass preventive examination of patients.

## References

1. L.I.Anatychuk, *Thermoelements and Thermoelectric Devices: Reference Book* (Kyiv:Naukova Dumka, 1979), 768 p.
2. O.A.Geraschenko, *Foundations of Heat Flux Measurement* (Kyiv: Naukova Dumka, 1971), p.192.
3. L.I.Anatychuk, N.G.Lozinsky, P.D.Mykytyuk and Yu.Yu.Rozver, Thermoelectric Semiconductor Heat Meter, *Instruments and Experimental Techniques* **5**, 236 (1983).
4. L.I.Anatychuk, L.P.Bulat, D.D.Gutsal and A.P.Myagkota, Thermoelectric Heat Meter, *Instruments and Experimental Techniques* **4**, 248 (1989).
5. R.B.Ladyka, D.N.Moskal and V.D.Didukh, Semiconductor Heat Meters in Arthropathy Diagnostics and Treatment, *Meditsinskaya Tekhnika* **6**, 34 – 35 (1992).
6. R.B.Ladyka, O.N.Dakalyuk, L.P.Bulat and A.P.Myagkota, Use of Semiconductor Heat Meters in the Diagnostics and Treatment, *Meditsinskaya Tekhnika* **6**, 36 – 37 (1996).
7. B.M.Demchuk, L.Ya.Kushneryk, and I.M.Rublenyk, Thermoelectric Sensors for Orthopedics, *J.Thermoelectricity* **4**, 80 – 85 (2002).
8. A.A.Ascheulov, A.V.Klepikovskyi, L.Ya.Kushneryk, A.O.Rarenko, and V.I.Cherchenko, Patent of Ukraine № 53104 A, Sensor for Preliminary Diagnostics of Inflammatory Processes in Mammary Glands, Yu.Fedkovych Chernivtsi Nastional University, Application № u2002031955; Filed 12.03.2002; Publ. 15.01.2003, Bul. № 1.
9. A.A.Ascheulov, L.Ya.Kushneryk, Thermoelectric Device for Medico-Biological Express-Diagnostics, *Tekhnologiya i Konstruirovaniye v Elektronnoi Apparature* **4**, 38 – 39 (2004).
10. B.M.Demchuk, R.R.Kobylyansky, and A.V.Prybyla, Primary Thermoelectric Converters Based on Semiconductor Materials for Gradient Het Meters, *The 31-st International and 10-th European Conference on Thermoelectrics* (2012, Aalborg, Denmark), P. 277.
11. L.I.Anatychuk, R.R.Kobylyanskii, Thermoelectric Converters for Gradient Heat Meters, *Proceedings of XIII Interstate Workshop "Thermoelectrics and Their Applications"* (Saint-Petersburg, November 13 – 14, 2012), pp. 440 – 444.
12. L.I.Anatychuk, R.R.Kobylyanskii, *Patent of Ukraine № 71619*, Thermoelectric Medical Heat Meter, Application № u 2011 14007; filed 28.11.11; publ. 25.07.12, Bul. № 14.
13. L.I.Anatychuk, R.R.Kobylyanskii, *Patent of Ukraine № 72032*, Thermoelectric Sensor for Temperature and Heat Flux Measurement, Application № u 2011 14005; filed 28.11.11; publ. 10.08.12, Bul. № 15.
14. P.D.Mykytyuk, R.R.Kobylyanskii, and T.V.Slepenyuk, *Patent of Ukraine № 73037*, Thermoelectric Medical Device, Application № u 2012 01922; filed 20.02.12; publ. 10.09.12, Bul. № 17.
15. L.I.Anatychuk, R.R.Kobylyanskii, *Patent of Ukraine № 78619*, Method for Determination of Heat Flux Density, Application № u 2012 11018; filed 21.09.12; publ. 25.03.13, Bul. № 6.
16. L.I.Anatychuk, *Patent of Ukraine № 79929,* Thermoelectric Converter of Heat flux for Gradient Heat Meters, Application № 2012 11857; filed 15.10.12; publ. 13.05.13, Bul. № 9.
17. L.I.Anatychuk, R.R.Kobylianskyi, and I.A.Konstantinovich, Calibration of Thermoelectric Heat Flux Sensors, *Proc. of XV International Research and Practical Conference "Current Information and Electronic Technologies", Vol.2* (Odessa, Ukraine, May 26 – 30, 2014), P. 30 – 31.
18. V.S.Gischuk, Electronic Recorder of Signals from Human Heat Flux Sensors, *J.Thermoelectricity* 4, 105 – 108 (2012).
19. V.S.Gischuk, Electronic Recorder with Processing Signals from Heat Flux Thermoelectric Sensor, *J.Thermoelectricity* 1, 82 – 86 (2013).

20. V.S.Gischuk, Modernized Device for Human Heat Flux Measurement, *J.Thermoelectricity* 2, 91 – 95 (2013).
21. L.I.Anatychuk, R.R.Kobylianskyi, Research into the Effect of Thermoelectric Heat Meter on Human Heat Release Measurement, *J.Thermoelectricity* 4, 60 – 66 (2012).
22. L.I.Anatychuk, R.R.Kobylyanskii, 3D-Model for Determination of Thermoelectric Heat Meter Effect on the Accuracy of Human Heat Release Measurement, *Scientific Bulletin of Chernivtsi University: Collected Scientific Works. Physics. Electronics,* ***2****, issue 1* (Chernivtsi: Chernivtsi National University, 2012), p. 15 – 20.
23. L.I.Anatychuk, R.R.Kobylianskyi, Computer Design of Thermoelectric Heat Meter Readings under Real-Service Conditions, *J.Thermoelectrucity* 1, 53 – 60 (2013).
24. L.I.Anatychuk, R.G.Giba, and R.R.Kobylianskyi, Some Peculiarities of Using Medical Heat Meters in the Investigation of Local Human Heat Release, *J.Thermoelectricity* 2, 67 – 73 (2013).
25. O.I.Ivaschuk, I.K.Morar, R.R.Kobylianskyi, L.V.Nepelyak, and V.D.Deley, The Role of Abdominal cavity Heat Flux in the Monitoring of Acute Destructive Pancreatis, *Collection of Abstracts of Research and Practical Conference "Highlights of Surgery"* (Chernivtsi, Ukraine, 2013), P. 254 – 259.
26. L.I.Anatychuk, R.R.Kobylianskyi, and I.A.Konstantinovich, The Impact of a Thermoelectric Supply on the Accuracy of Temperature and Heat Flux Measurement, *J.Thermoelectricity* 6, 53 – 61 (2013).
27. R.R.Kobylianskyi, V.V.Boichuk, The Use of Thermoelectric Heat Meters in Medical Diagnostics, *Scientific Bulletin of Chernivtsi University: Collected Scientific Works. Physics. Electronics,* ***4****, issue 1* (Chernivtsi: Chernivtsi National University, 2015), p. 90 – 96.

Submitted 26.02.2016.

**L.I. Anatychuk[1, 2], M.V. Havrylyuk[1], V.V. Lysko[1], V.A. Tyumentsev[1]**

[1]Institute of Thermoelectricity of the NAS and MES of Ukraine, 1,
Nauky str., Chernivtsi, 58029, Ukraine
[2]Yu. Fedkovych Chernivtsi National University
2, Kotsyubinsky str., Chernivtsi, 58000 Ukraine

# AUTOMATED MEASURING SYSTEM "ALTEC-10003" FOR THE DETERMINATION OF THERMOELECTRIC PROPERTIES OF MATERIAL INGOTS

*The results of development of automated system "ALTEC-10003" intended for automation of the process of measuring the properties of thermoelectric material shaped as rods and data processing are presented. Control unit comprises a multi-channel analog-digital converter, measuring probes travel system, thermal control system and power supplies for measuring unit components. Measurement process control, processing and display of the results are done with the aid of computer to which measuring unit is connected via standard USB channel. The results are displayed as plots and tables. Examples of using the elaborated measuring system control to determine the distributions of material thermoelectric properties in the rods, as well as the analysis of precision and reproducibility of the results are presented.*

**Key words:** electric conductivity, thermoEMF, thermal conductivity, error, thermoelectric material, automation.

## Introduction

*General characterization of the problem.*

Bismuth compounds ($Bi_2Te_3$, $Bi_2Se_3$, $Bi_2Sb_3$) and their solid solutions remain the best materials used in thermoelectric modules for refrigeration. The widely accepted methods for obtaining such thermoelectric materials under industrial conditions are zone recrystallization and extrusion [1]. In the former case, due to segregation of impurities in the process of growth and other factors, the resulting material is inhomogeneous, especially on the rod ends. The extruded material is characterized by considerable distortions of homogeneity at the beginning of a rod, when process conditions are not stable yet.

Therefore, of paramount importance in the manufacture of modules is quality control of thermoelectric material. In this connection, one of the most important tasks when creating quality control equipment is its speed and independence of human factors. For this purpose, full automation of measurement processes is helpful.

*Analysis of the literature.* The choice of material with the required properties under laboratory conditions is generally done by measuring the distributions of electric conductivity and thermoEMF along the ingot.

The measurement of electric conductivity is based on a two-probe measurement method whereby current is passed through the end surfaces of the ingot, and the electric potential on its surface is measured by two mobile probes with a known distance between them [2, 3]. The electric conductivity is calculated by the values of current and potential difference between the probes with

regard to geometrical dimensions (cross-section area of the ingot and the distance between the probes). This method is generally accepted for the investigation of semiconductor material rods (international standard SEMI MF397-02 «Test Method for Resistivity of Silicon Bars Using a Two-Point Probe»).

The measurement of the Seebeck coefficient is based on the hot probe method [4]. One of the two probes is heated relative to the other, and thermoEMF is created between them at contact to ingot. The Seebeck coefficient is calculated as the ratio between the generated thermoEMF and temperature difference between the probes.

To increase the efficiency of express measurements, the electric conductivity and thermoEMF are measured in a single cycle, with one lowering of probes, one of them being heated (Fig. 1). To eliminate thermoEMF in the calculation of electric conductivity, measurements are made with two current directions or on a sign-variable rectangular current meander.

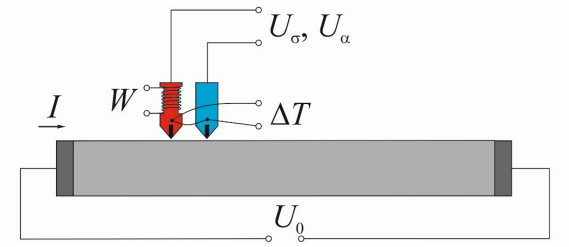


*Fig. 1. Schematic for measuring electric conductivity and thermoEMF of ingots.*

At the Institute of Thermoelectricity of the NAS and MES of Ukraine, a series of investigations were performed aimed at creating high-precision methods and equipment for measuring the properties of thermoelectric material ingots. These investigations resulted in new physical methods for reducing measurement errors and equipment on their basis for precise measurement of electric conductivity and thermoEMF of materials shaped as ingots [5 – 9]. The following errors of the developed equipment were achieved: electric conductivity – up to 1 %, thermoEMF – to 1.5 %. Also, a procedure for measuring thermal conductivity of ingots under dynamic conditions was created.

For an ingot 300 mm long at a step of 10 mm with the four ingot rotation angles it is necessary to perform over one hundred measurements. When positioning the probes and measuring in manual mode, full measurement cycle may require up to four hours. Moreover, in this case human errors in operator's work are possible when positioning the probes, taking device readings, calculating, plotting of graphs, etc.

Therefore, of particular importance in the development of such equipment is automation of measurement process, which allows not only avoiding human errors, but also increasing considerably measurement speed. Moreover, automation contributes to identity of measurement conditions, hence to measurement precision increase.

*The purpose of the work* is creation of measurement and probe travel control system for automation of processes of determination of thermoelectric properties of materials, processing and display of their results.

## Description of measuring equipment design

The basic specifications in the development of automated measuring equipment were as follows: ingot length – 50 – 400 mm, their diameter – 6 – 30 mm; minimum discreteness of

coordinate measurement along the ingot axis – 0.1 mm; minimum discreteness of ingot rotation angle measurement – 1 degree. The installation must be operated by computer which sets measuring tasks, the necessary calculations and their averaging, builds the plots, fills in the tables, saves and prints the results.

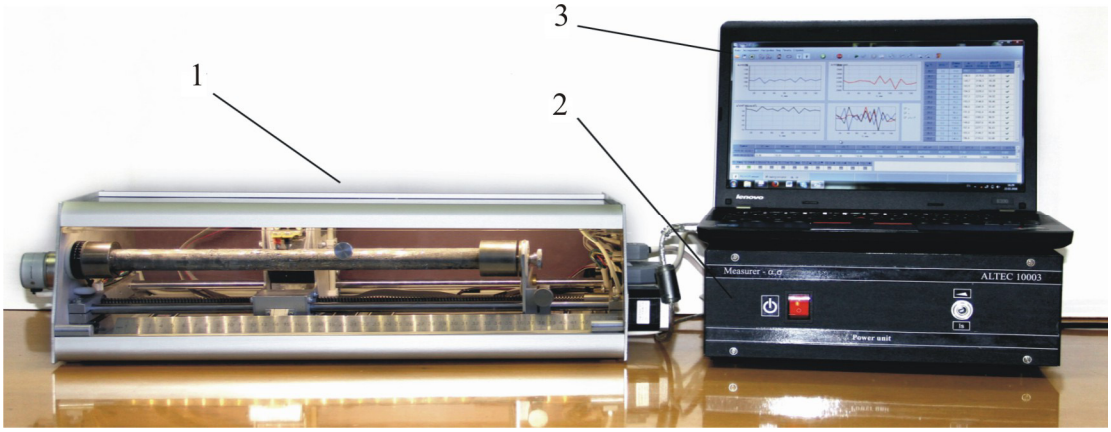


*Fig. 2. Installation for measuring thermoelectric parameters of semiconductor material rods "ALTEC-10003".*
*1 – measuring unit (rod holder); 2 – control unit;*
*3 – computer with software support.*

The design requires constant distance between the probes, hot probe temperatures, probes hold-down force to sample, equal time of measuring thermoEMF and time of current supply when measuring electric conductivity. To assure equal temperature conditions of measurement, the installation unit involves thermal stabilization system adapted to heating 5 – 10 degrees above room temperature.

The whole measurement process is controlled by high-level computer programs working together with low-level microprograms of control unit AD converter.

The appearance of "ALTEC-10003" installation is given in Fig. 2. It is composed of three units, namely measuring – rod holder, control unit and computer. Its block-diagram is shown in Fig. 3.

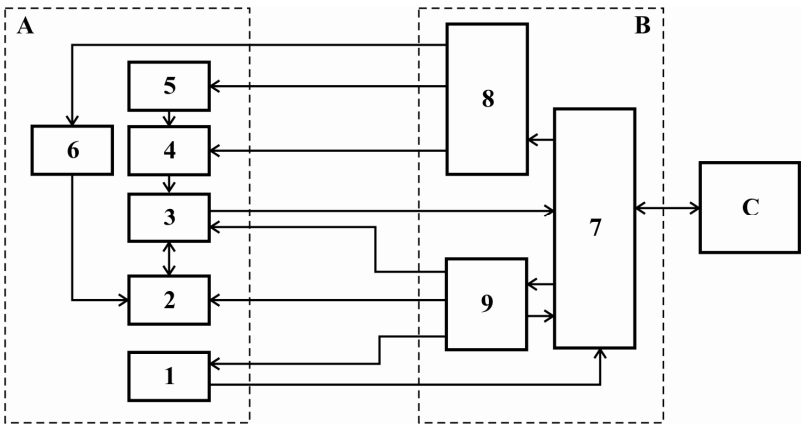


*Fig. 3. Block-diagram of installation "ALTEC-10003" for measuring thermoelectric properties of material rods. A – measuring unit, B – control unit, C – computer;*
*1 – housing thermostat, 2 – thermoelectric material rod, 3 – measuring probes,*
*4 – probe travel mechanism, 5 – carriage travel mechanism, 6 – rod rotation mechanism,*
*7 – microcontroller with embedded AD converter; 8 – power supplies and drivers of step motors,*
*9 – measuring unit.*

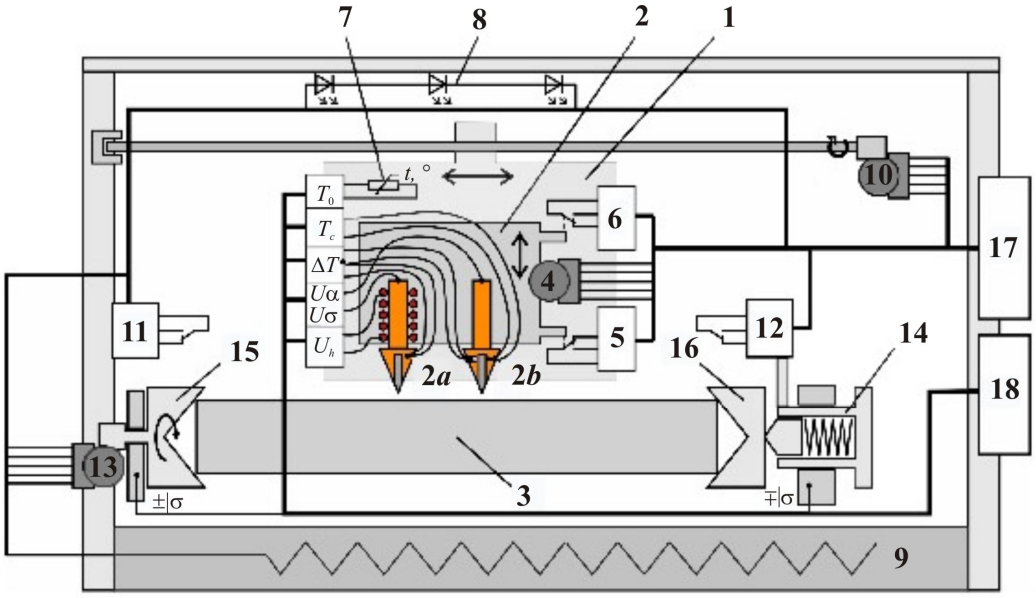


*Fig. 4. Functional diagram of measuring unit of installation "ALTEC-10003".*
*1 – mobile carriage, 2 – measuring unit, 2a – "hot" probe, 2в – "cold" probe,*
*3 – thermoelectric material rod, 4 – step motor of probe lifting and lowering mechanism,*
*5, 6 – limit switches of the up and down positions of probes, 7 – ambient temperature sensor,*
*8 – LED backlight of measuring unit, 9 –heater of measuring unit case,*
*10 – step motor of mechanism for longitudinal travel of carriage, 11, 12 – limit switches*
*of mechanism for longitudinal travel of carriage, 13 – step motor of rod rotation mechanism,*
*14 – rod pressure and fixation mechanism, 15, 16 – cone-shaped current leads,*
*17, 18 – sockets for connection of measuring unit to measurement control unit.*

The main unit in the installation is measuring unit which performs the whole process of primary measurement and consists of rod holder and measuring probes. Its functional diagram is shown in Fig. 4.

Measuring unit is arranged in aluminum housing with a front transparent hinged cover which besides being a structural component performs the function of thermostat. Its bottom accommodates heating elements making it possible to maintain air temperature inside the housing at a level of 300 K. When measuring, thermoelectric material rod is installed into a holder that consists of two coaxial current leads one of which (the right one) is mobile along the rod axis and has hold-down and fixation members.

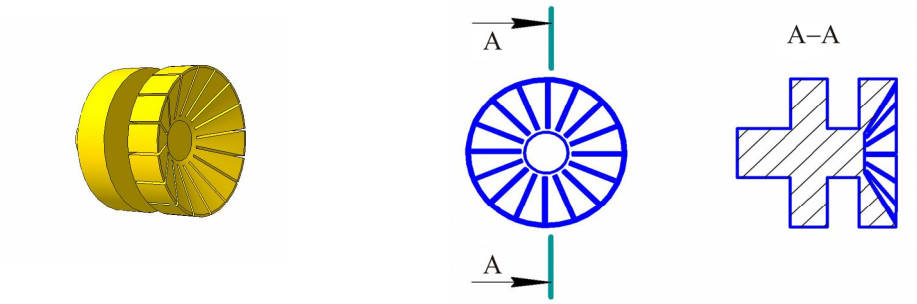


*Fig. 5. Appearance and design of current leads.*

For self-centering of the rods current leads are made in the form of cut cones (Fig. 5). They have radial grooves which divide hold-down surface into 16 sector parts assuring contact to the real

shape of rod ends. This provides for at least 16 points of electric contact for each rod end with current leads. Mounted on the side walls of the housing are means for longitudinal travel of measuring probes and rotation of the rod itself about its axis.

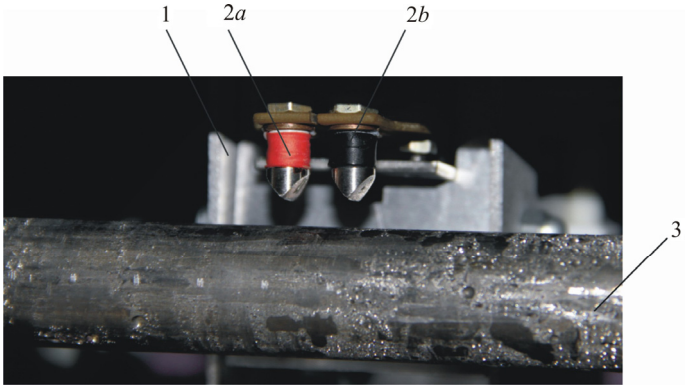


*Fig. 6. Measuring unit.*
*1 – mobile carriage, 2a – "hot" probe, 2b – "cold" probe, 3 – ingot.*

Measuring unit is mounted on a mobile carriage (Fig. 6). It accommodates measuring head with two probes. The head is designed to perform electric and temperature measurements and has two rigidly fixed knife-edged probes: one with heating – "hot probe" (2*a*), the other without heating – "cold probe" (2*b*). To reduce the errors in temperature measurement of rod surface contact zone, the probes are made of high thermal conductivity material (copper). For greater durability the probes have embedded knife-edged tungsten plates.

Also, the carriage has probe lifting and lowering mechanism consisting of step motor with a reducer and limit switches of the up and down probe positions.

Automation of measurement process is done by control unit which controls travel of probes in measuring unit, provides for stabilized voltages and currents to electric circuit elements of measuring unit. The voltages and thermoEMF are measured with the aid of an 8-channel 24-digit A/D converter that transfers measured voltages via USB interface to computer. Control unit comprises measuring unit, microcontroller unit and power unit. Power unit components for control of step motors are composed of three identical drivers of stem motors assuring travel of measuring probes in the horizontal and vertical directions and rod rotation.


*Fig. 7. Main window of measurement control program "SThEM-3".*

The installation is controlled by computer with "SThEM-3" (Semiconductor ThermoElectric Material) software, developed jointly with "Tereks" Scientific Industrial Enterprise (Kyiv, Ukraine). The program allows online measurement, processing of measured result, displaying data in the form of plots and tables, saving them in computer, exporting to MS Excel, and printing-out.

Measurement control program "SThEM-3" has a standard structure adopted in Windows operational system. The main window of the program is shown in Fig. 7. It comprises means for control of measurement process (call buttons of experiment control box, on/off indicators of current through the sample, power supply to hot probe heater, etc), the area of plotting measured results, the tables with measured values and calculated values of rod properties. Also displayed is information on the rod entered by operator himself.

The software allows working in "manual" and "automatic" modes.

In "manual" mode the user can install the probes at any point of the rod under study, perform the measurements and calculations with reference to the rod coordinates. In "manual" mode one can also determine the thermal conductivity of the rod. For this purpose, a special device shown in Fig. 8 must be placed on one of the rod ends.

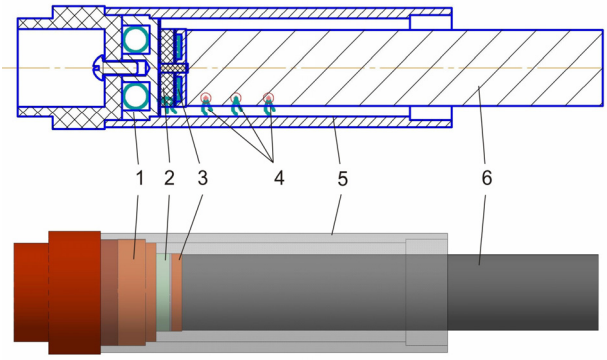


*Fig. 8. Design of device for measuring thermal conductivity.*

The device is composed of sample reference heater 3, thermoelectric material rod 6 with installed thermocouple probes 4. To reduce thermal losses and assure reproduction of equal thermal conditions when measuring, the device is provided with screen heater 1, differential "null-thermocouple" 2 and screen tube 5.

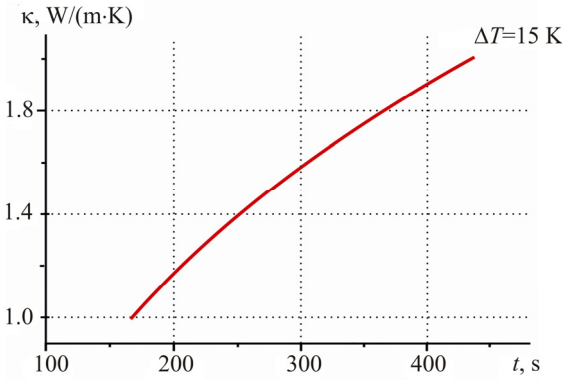


*Fig. 9. Calibration dependence for determination of thermal conductivity.*

Calibration dependence obtained by computer simulation for this device design is given in Fig. 9.

In "automatic" mode the user shapes the task as a table of coordinates according to which the installation automatically performs a set of measurements in this cyclogram, calculates electrophysical parameters of material with reference to the rod coordinates.

The calculated result is tabulated, and a plot of the value versus measurement coordinate is built simultaneously. In the table, one can average the results for all rotation angles, save and print out the tables and the plots.

It is worth mentioning that the hardware and software parts of the installation are developed with the possibility of measurements both on the rods and flat samples of any size, for instance, discs. All one has to do is to change sample holder and set the appropriate coefficients in the program.

## Experimental studies on automated equipment "ALTEC-10003" to measure the properties of thermoelectric material ingots.

Jointly with State enterprise "Bukovinastandartmetrologiya", the program and procedure of metrological certification of installation "ALTEC-10003" was developed and approved. It was established that a relative error in the measurement of electric conductivity is not more than 0.5 %, in the measurement of thermoEMF – not more than 1 %, which corresponds to expected values obtained by means of computer simulation.

Also, the speed and productivity of equipment was determined. It was established that one measurement takes 20 sec. Accordingly, measurement of a rod 30 cm long with its four rotation angles and step 10 mm will require 40 min.

*Table*

*Comparing thermal conductivity values measured on the installation "ALTEC-10003" to thermal conductivity values measured by the absolute method on the installation "ALTEC-10001"*

| Rod № | Thermal conductivity value measured on the installation "ALTEC-10003", κ, W/(m*K) | Thermal conductivity value measured on the installation "ALTEC-10001", $\kappa_0$, W/(m*K) | Deviation, % |
|---|---|---|---|
| *n*-type $Bi_2Te_3 - Sb_2Te_3$ | | | |
| 1 | 1.8 | 1.93 | 7.0 |
| 2 | 1.4 | 1.54 | 9.1 |
| 3 | 1.6 | 1.74 | 8.0 |
| *p*-type $Bi_2Te_3 - Sb_2Te_3$ | | | |
| 4 | 1.6 | 1.77 | 9.6 |
| 5 | 1.7 | 1.85 | 8.0 |
| 6 | 1.8 | 1.93 | 6.7 |

Also, investigations of error in measuring thermal conductivity were performed. For this purpose, thermal conductivity values obtained when measuring on the rods were compared to thermal conductivity values of samples cut of the same rods and measured on the installation "ALTEC-10001" by the absolute method. The results of comparison are listed in Table.

As can be seen from the table, the error in measuring thermal conductivity on the installation "ALTEC-10003" is different from the measurements by the absolute method by 7 – 10 %.

System automated measurements of rods are useful for the optimization of composition and production conditions of thermoelectric materials.

The use of such equipment is particularly attractive under production conditions. A single insta-

llation "ALTEC-10003" can realize quality control of nearly 1500 kg of thermoelectric material per year. The introduction of such control allows not only eliminating rejected rods from modules fabrication technology. Determination of $\alpha^2\sigma$ along the rods makes it possible to find reliably and with minimum losses the places of low-quality material on their ends that must be eliminated. The topography of $\alpha^2\sigma$ allows also determination of places on the rods where material quality is high, average or reduced. With regard to equal electric conductivity values such rejecting allows choosing thermoelectric material for the modules of enhanced, average and reduced quality. In so doing, the modules of enhanced quality must have better parameters than those made without using automated quality control.

The use of automated system "ALTEC-10003" under production conditions has proved its efficiency. Investigations were performed in "ALTEC-M" company. Typical dependences of rod properties are given in Fig. 10. In the figure, one can see ingot part 1 with maximum value $\alpha^2\sigma$, part 2 with the values $\alpha^2\sigma$ corresponding to averaged quality values of non-rejected modules, part 3 with the values $\alpha^2\sigma$ somewhat lower than the averaged and part 4 with the unsatisfactory values $\alpha^2\sigma$. The latter are eliminated from the technological process of modules manufacture. This quality distribution of material provides for manufacture of modules with the values $\Delta T_{max}$ 75 – 73 K from ingot part 1, 72 – 70 K from part 2 and 69 – 68 K from part 3.

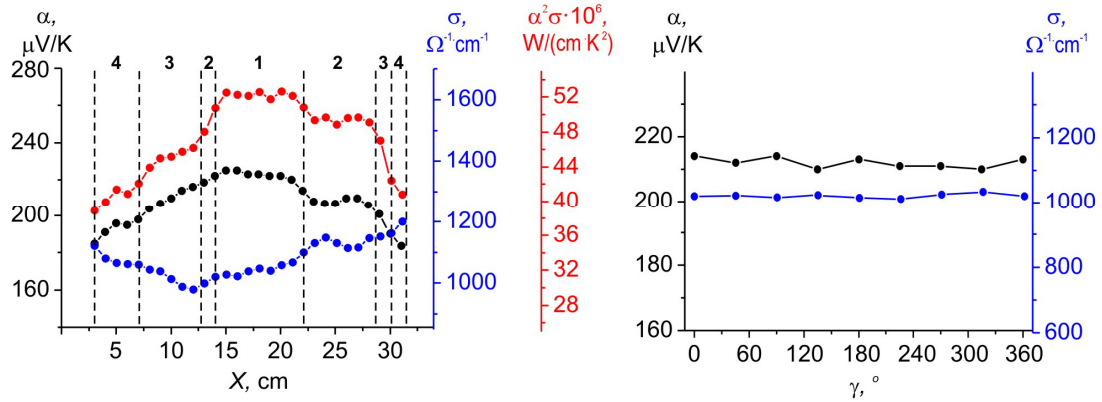


*a)* *b)*

*Fig. 10. Distributions of the Seebeck coefficient and electric conductivity in the n-type thermoelectric material based on $Bi_2Te_3$ – $Sb_2Te_3$, solid solution prepared by vertical zone melting method (a – along the length X of the rod, b – along the angle of rotation γ of the rod).*

Thus, the use of automated measurements in the industrial manufacture of modules allows getting modules of enhanced quality and rejecting low-quality material.

## Conclusions

1. State metrological certification of automated measuring complex "ALTEC-10003" has established that a relative error in the measurement of electric conductivity is not more than 0.5 % and not more than 1 % in the measurement of thermoEMF, which corresponds to the values obtained by means of computer simulation.
2. By comparing the results of measuring thermal conductivity of thermoelectric material ingots on the installation "ALTEC-10003" to thermal conductivity values of samples cut of these ingots and measured on the installation "ALTEC-10001" by the absolute method it was

established that the error of thermal conductivity determination by the developed device lies within 7 – 10 %.

3. The efficiency of using measuring complex "ALTEC-10003" under production conditions has been confirmed. It has been established that introduction of automated control of material quality allows not only withdrawing low-quality material from the technological process of modules manufacture , but also getting modules of enhanced quality with $\Delta T_{max}$ about 2 – 4 K higher.

## References

1. B.M.Goltsman, V.A. Kudinov, and I.A.Smirnov, *Semiconductor Thermoelectric Materials Based on $Bi_2Te_3$* (Moscow: Nauka, 1972), 320 p.
2. A.O.Yepremyan, V.M.Arutunyan, and A.I.Vaganayn, Figure of Merit of Modern Semiconductor Thermoelectric Materials, *International Scientific Journal for Alternative Energy and Ecology* 5, 7 – 18 (2015).
3. L.I.Anatychuk, *Thermoelements and Thermoelectric Devices* (Kyiv: Naukova Dumka, 1978), 768 p.
4. A.S.Okhotin, A.S.Pushkarsky, R.P,Borovikova, and V.A.Simonov, *Methods for Measuring Characteristics of Thermoelectric Materials and Converters* (Moscow: Nauka, 1974), 167p.
5. L.I.Anatychuk, V.T.Dimitraschuk, O.J.Luste, and A.P.Melnik, Probe Method for Determination of Thermoemf of Epitaxial Films, *Instruments and Experimental Techniques* 2, 239 – 240 (1971).
6. V.V.Razinkov, Equipment for Measuring Parameters of Thermoelectric Material Ingots, *J.Thermoelectricity* 4, 70 – 79 (2002).
7. L.I.Anatychuk, V.V.Lysko, High Precision Method for Measuring the Electric Conductivity of Thermoelectric Material Rods, *J.Thermoelectricity* **1**, 70 – 75 (2008).
8. L.I.Anatychuk, N.V.Havrylyuk, and V.V.Lysko, Methods and Equipment for Quality Control of Thermoelectric Materials, J.Electronic Materials 41(6), 1680-1685 (2012).
9. L.I.Anatychuk, M.V.Havrylyuk, V.V.Lysko, and V.A.Tyumentsev, Automated Equipment for Measurement of Properties of Thermoelectric Material Rods, *J.Thermoelectricity* 4, 83 – 88 (2015).
10. L.I.Anatychuk, V.V.Lysko, *Patent of Ukraine №38470*, InCl G01R 27/00, Filed 11.08.2008, Publ. 12.01.2009, Bul. №1.

Submitted 10.02.2016.

## ARTICLE PREPARATION RULES

The article shall conform to the journal profile. The article content shall be legible, concise and have no repetitions.

The article shall be submitted to the editorial board in electronic version.

The text shall be typed in text editor not lower than MS Word 6.0/7.0.

Page setup: "mirror margins"- top margin – 2.5 cm, bottom margin – 2.0 cm, inside – 2.0 cm, outside– 3.0 cm, from the edge to page header – 1.27 cm, page footer – 1.27 cm.

Graphic materials, pictures shall be submitted in color or, as an exception, black and white, in .opj or .cdr formats, .jpg or .tif formats being also permissible. According to author's choice, the tables and partially the text can be also in color.

The article shall be submitted in English on A4 paper sheets; the number of pages shall not exceed 12. By agreement with the editorial board, the number of pages can be increased.

**To accelerate publication of the article, please adhere to the following rules:**

- the authors' initials and names are arranged in the centre of the first page at the distance of 1 cm from the page header, font Times New Roman, size 12 pt, line spacing 1.2;
- the name of organization, address (street, city, postal code, country) – indent 1 cm below the authors' initials and names, font Times New Roman, size 11 pt, line spacing 1.2, center alignment;
- the title of the article is arranged 1 cm below the name of organization, in capital letters, semi-bold, font New Roman, size 12 pt, line spacing 1.2, center alignment. The title of the article shall be concrete and possibly concise;
- the abstract is arranged 1 cm below the title of the article, font Times New Roman, size 10 pt, in italics, line spacing 1.2 ,center alignment;
- key words are arranged below the abstract, font Times New Roman, size 10 pt, line spacing 1.2, justified alignment. The title "Key words" – font Times New Roman, size 10 pt, semi-bold;
- the main text of the article is arranged 1 cm below the abstract, indent 1 cm, font Times New Roman. size 11 pt, line spacing 1.2, justified alignment;
- formulae are typed in formula editor, fonts Symbol, Times New Roman. Font size is "normal" – 12 pt, "large index" – 7 pt, "small index" – 5 pt, "large symbol" – 18 pt, "small symbol" – 12 pt). The formula is arranged in the text, centre aligned and shall not occupy more than 5/6 of the line width, formulae are numbered in round brackets right;
- dimensions of all quantities used in the article are represented in the International System of Units (SI) with the explication of the symbols employed;
- figures are arranged in the text. The figures and pictures shall be clear and contrast; the plot axes – parallel to sheet edges, thus eliminating possible displacement of angles in scaling;
- tables are arranged in the text. The width of the table shall be 1 cm less than the line width. Above the table its ordinary number is indicated, right alignment. Continuous table numbering throughout the text. The title of the table is arranged below its number, center alignment;
- references should appear at the end of the manuscript. References within the text should be enclosed in square brackets. References should be numbered in order of first appearance in the text. Examples of various reference types are given below.

– L.I. Anatychuk, *Thermoelements and Thermoelectric Devices: Handbook* (Kyiv: Naukova Dumka, 1979), p.766. (Book)
– T.M. Tritt, Thermoelectric Phenomena, Materials, and Applications, *Annual Review of Materials Research* **41**, 433 (2011). (Journal paper)
– U. Ghoshal, *Proceedings of the XXI International Conference on Thermoelectrics* (N.Y., USA, 2002), p. 540. (Proceedings Conference)

**The article should be supplemented by:**

• letter from the organization where the work was performed or from the authors of the work applying for the publication of the article;

• information on the author (authors): last name and initials; full name and postal address of the institution where the author works; academic degree; position; telephone number; E-mail;

• author's (authors') photo in color or, as an exception, in black and white. With the number of authors more than two their photos are not given;

• author's application to the following effect:

We, the undersigned authors, … transfer to the founders and editors of "Journal of Thermoelectricity" the right to publish the article…in Ukrainian, Russian and English. This is to confirm that the present publication does not violate the copyright of other persons or organizations.

Date Signatures